Construction of functional and robust cobalt phthalocyanines modified electrodes for the electrocatalytic detection of metal-based and pharmaceutically derived pollutants

by

Danica Moodley

Submitted in the fulfilment of the requirements for the degree of
Master of Science
in the School of Chemistry and Physics at the
University of KwaZulu-Natal

Supervisor: Prof. Irvin N. Booysen
Co-supervisor: Dr. Allen Mambanda

As the candidate's supervisor, I hereby approve this dissertation for submission:

Supervisor signature: [redacted] Date: 04/04/2024

Co-supervisor signature: [redacted] Date: 04/04/2024

Table of contents

Abstract

Water pollution has become a detrimental global concern in a world that continues to grow through industrialisation, population, and demand in sales from agricultural and pharmaceutical industries. It is therefore imperative for innovative methods of continuous water monitoring to be implemented to avoid the harsh effects that pollution poses to human, animal and environmental preservation. Advances from traditional analytical methods have been made to combat associated drawbacks such as tedious sample preparation, high maintenance costs, and lack of mobility. Electrochemical sensors can be used for the analysis of a vast range of water pollutants while offering on-site, simple analysis and inexpensive fabrication. Metallophthalocyanines have been utilised extensively as electrode modifiers due to their excellent redox properties and stability which can be fine-tuned by alteration of the metal centre and substituents. In addition, thes3e alterations improve selectivity, solubility and immobilisation onto electrode substrates. This research is aimed at the application of gold electrodes modified with CoPc-cou nanoconjugates and CoPc-cou electrospun nanofibers (ENFs) for the electrocatalytic detection of pollutants, paraquat and mercury, in real water samples.

Experimental chapter one explores the optimization and application of a gold-modified electrode, CoPc-cou-f-MWCNTs/3-HT|Au, for the electrocatalytic detection of a water pollutant, paraquat (PQ). It was fabricated via a sequential modification procedure entailing the formation of self-assembled monolayers (SAMs) of a nanocomposite comprising of a coumarin tetra-substituted cobalt phthalocyanine (CoPc-cou) and carboxylic acid functionalized multiwalled carbon nanotubes (f-MWCNTs). This was followed by the in-situ immobilization of poly(3-hexylthiophene) ([3-HT]n) through electropolymerisation to render the chemically modified electrode (CME). Subsequently, the CME illustrated enhanced sensitivity towards PQ compared to the bare or CoPc-cou-f-MWCNTs modified electrodes. The CoPc-cou-f-MWCNTs/3-HT|Au electrode displayed a linear PQ detection range of 0.193 – 1000 μM with a limit of

detection (LOD) and limit of quantification (LOQ) of 0.193 µM and 0.584 µM, respectively. Comparison between calibration curves for the modified electrode and HPLC-MS illustrates that the former method has a lower but comparable calibration sensitivity for PQ. In addition, this CME could electrocatalytically distinguish PQ within a real water sample collected from the Durban lagoon. Furthermore, the direct recovery of PQ in the lagoon water by the modified Au electrode was found to be 86%, which is lower than the calculated value of 97% obtained by HPLC-MS after rigorous solid-phase microextraction of the analyte. However, the lower percentage recovery could be rationalized by the interference studies.

In experimental chapter two fabricated electrospun nanofibers containing CoPc-cou, polyaniline (PANI) and poly-vinyl alcohol (PVA) were used to modify a gold substrate which was subsequently immobilised using a 5% Nafion solution affording the CoPc-cou-ENFs-Nf|Au modified electrode. Comparison of the chemically modified electrode with the bare and other modified electrodes under optimised conditions displayed superior detection of mercury (Hg(II)) attaining a linear range of 10 – 3000 µM and an LOD and LOQ of 0.14 µM and 0.46 µM, respectively. This can be attributed to the affinity between Hg(II) and the mercaptocoumarin substituent (Hg-S) as well as the higher surface area occupied by the ENFs resulting in an increased number of active sites. Furthermore, the chemically modified electrode exhibit selectivity and sensitivity in an interference sample containing multiple heavy metals (Pb^{2+}, Cd^{2+} and Hg^{2+}). A good percentage recovery of 96% was attained when the CoPc-cou-ENFs-Nf|Au electrode was applied to a real water sample which was comparable to a percentage recovery of 98% which was attained using the ICP-OES to analyse the same water samples.

Keywords: 3-hexdylthiophene, carbon nanotubes, cobalt phthalocyanines, differential pulse anodic stripping voltammetry, electrospun nanofibers, mercaptocoumarin, mercury, Nafion, paraquat, polyaniline, polyvinyl alcohol.

Preface

The experimental work described in this dissertation was carried out in the School of Chemistry and Physics at the University of KwaZulu-Natal, Pietermaritzburg, from January 2021 to November 2023, under the supervision of Prof. Irvin Noel Booysen and co-supervision of Dr. Allen Mambanda. These studies represent original work by the author and have not otherwise been submitted in any form for any degree or diploma to any tertiary institution. Where use has been made of the work of others, it is duly acknowledged in the text.

Declaration 1 - Plagiarism

I, Danica Moodley, declare that:

1. The research reported in this dissertation, except where otherwise indicated, is my original research.

2. This dissertation has not been submitted for any degree or examination at any other university.

3. This dissertation does not contain any other persons' data, pictures, graphs or other information, unless specifically acknowledged as being sourced from other persons'.

4. This dissertation does not contain any other persons' writing, unless specifically acknowledged as being sourced from other researchers. Where other written sources have been quoted, then:

   a. Their words have been re-written but the general information attributed to them has been referenced.

   b. Where their exact words have been used, then their writing has been placed in italics and inside quotation marks and referenced.

5. This dissertation does not contain text, graphics or tables copied and pasted from the internet, unless specifically acknowledged, and the source being detailed in the dissertation and in the References section.

Signed: 

Declaration 2 - Publications

Manuscripts published:

1. **Moodley, D.,** Nocanda, X., Nelson, P., Mambanda, A., Booysen, I.N., **2023**, Construction of a Functional and Robust Cobalt(II) Phthalocyanine-Modified Electrode for the Electrocatalytic Detection of Paraquat, *ChemElectroChem*, 10, e202300427, https://doi.org/10.1002/celc.202300427.

The following manuscript is currently under preparation:

1. Moodley, D., Mambanda, A., Booysen, I.N., Immobilization of cobalt phthalocyanine-imbedded electrospun nanofibers on a gold electrode for the electrocatalytic detection of mercury(II)

Signed: [redacted] Date: 04/03/2024

Supervisors:

Prof. I. N. Booysen

Signed: [redacted] Date: 04/04/2024

Dr. A. Mambanda

Signed: [redacted] Date: 04/03/2024

Data availability

All data collected during this research study can be found at the following links:

Chapter 3:

https://drive.google.com/drive/folders/1dIT4ySVjN8Hgi2Tyq3yXY8s_7Hom4g3_?usp=sharing

Chapter 4:

https://drive.google.com/drive/folders/1yiLyRejclhD4jkjlLCZ4hjNLEsMEwuTk?usp=sharing

Acknowledgements

There have been so many people during the completion of my Masters Degree who have had such a huge impact on my life. To put into words all the gratitude and appreciation I have towards everyone for all they have done for me would be near impossible.

I would like to thank my supervisors Prof. Booysen and Dr. Mambanda. Having to be an integral part of the start of any individual's career is no easy task. You have shaped me into a person that I can be proud of and in the process equipped me with attributes I will carry throughout my career. Not only are you supervisors to me but you both are individuals I admire, respect and aspire to be like one day. Thank you for all the time and effort you have invested in this research and me.

To my parents, I will forever be indebted to you for all the love, support, advice and comfort you have given me throughout my life, especially through the past years when I needed your support and guidance the most. Without you by my side, none of this would have been possible. I owe all my successes to you. I would like to thank my sisters, nephews, brother-in-law and my partner for all the laughs and much-needed breaks along the way. You are the people I look towards when everything gets too much as it always does and you never fail to get me through it. You inspire me, keep me motivated and always remind me of my dreams. There is so much more to say and thank you for individually but I'll leave it at that, you all mean the world to me. I love you all.

I would like to thank our research group members: Siyabonga Shoba, Tariro Mapapiro, Daniel Makhanyane, Phakamani Dlamini, Mongezi Majebe, Sanam Maikoo and those who have ventured off Kevin Kantize, Patrick Mangundu, Vuyelwa Ngwena and Shabaaz Abdullah. You have been my support system, offering an understanding of all the issues we face and advice both academically and personally. I am so grateful to have met each and every one of you.

My deep gratitude to the technicians and staff at UKZN who have provided me with all the help you could offer. You have always greeted me with such friendliness and always lifted my spirits with every interaction we had. I would like to thank the University of Kwa-Zulu Natal for the opportunity to enabling me to complete this research through the facilities and resources provided. Furthermore, I would like to thank the National Research Foundation for funding this research and making it a possible for me to complete.

Lastly but most importantly, I would like to give my utmost thanks, gratitude, and appreciation to God. I have knelt before you countless times asking for guidance, strength, perseverance, motivation and focus and you have answered my prayers every single time. The amount of overflowing love I have for you in my heart could never be expressed. Thank you, God, for all your blessings over my life.

CHAPTER ONE

Introduction

1.1 General background

Heavy metal contamination, predominantly occurs through emissions and effluent outflows originating from a multitude of industries such as the mining and agricultural industries in addition to human activities such as incorrect disposal of waste forming landfills and sewage discharges.[1] These metals are of major concern to the provision of safe water sources due to their persistence and thus accumulation in the environment and water bodies.[2] At the heart of the problem, our ever-growing population increases the risks of pollution being a threat to the eco-balance of aquatic ecosystems. This is due to the increase in demand for water resulting in an inadequate distribution of potable water. In addition, there is a larger demand for other resources which requires industries to produce higher outputs in turn leading to increased pollution.[3]

Heavy metals such as Hg, As, Pb, Cr(IV), Cd and the majority of the late transition metal elements[4] can be exposed to humans through either ingestion of food or contaminated water, which would lead to detrimental health effects even at trace levels.[5] Documented side effects experienced from heavy metal contamination include brain and kidney damage (due to Pb-poisoning), lung damage and fragile bones (ascribed to Cd-poisoning), the damaging of blood vessels (as a result of As-poisoning) but with continued heavy metal exposure, these side effects can eventually lead to death.[6]

In particular, mercury poses great risks to global environmental pollution due to the spread of the contamination through water sources.[7] The major sources of mercury pollution in South Africa come from the combustion of coal, incineration of waste and chlor-alkali production. Mercury-containing solutions and powder residues generally leach into water bodies and result in contaminated water bodies.[8] In addition, mercury is

known to cause nervous system damage in adults and impede neurological development in infants.[9] Despite the known health risks that increased levels of these persistent pollutants, there remains a significant delay in awareness and insufficient data available on the extent of pollution in various water bodies.

Due to the exponential rate of pollution, water resources must be consistently monitored to prevent the use of contaminated water bodies. Particularly in South Africa, the scarcity of water leads to many people relying on alternate sources of water to compete daily activities.[10] Wastewater treatment plants (WWTP) are useful for the removal of the majority of the pollutants present in the water. However, the process of removal requires chemicals which are harmful to the environment and expensive without any guarantee that all pollutants will be removed at the end of the process, especially persistent heavy metal pollutants.[11] To monitor the efficiency of these WWTPs, specialized analytical instrumentation that is highly selective and sensitive is required.

There are a wide variety of laboratory-based analytical methods to analyse these water sample which include atomic spectroscopic techniques such as atomic adsorption spectroscopy (AAS), inductively coupled plasma-optical emission spectroscopy (ICP-OES), inductively coupled plasma-mass spectroscopy (ICP-MS) and X-ray fluorescence spectroscopy (XRF).[12] These methods are proven to detect trace levels of heavy metals and have been utilized for many years accurately and reliably. These methods, however, are associated with high processing costs, require skilled technicians to operate, are involved with complicated pre-treatment steps and are not suitable for on-site analysis.[13] Electrochemical sensing has gained much attention as it is a competitive alternative to traditional methods and is associated with the advantages of being highly sensitive with a rapid response time, it is a low-cost method and is easy to use.[14] A good electrochemical sensor is considered to have excellent stability, be robust and have good sensitivity and selectivity towards its target analyte. Surface modification of the commercially available electrode can contribute to enhancing these properties.

1.2. Aims and motivation

Metallophthalocyanines (MPcs) are proven electrocatalysts on conductive substrates due to their adaptive electrochemical properties based on the alteration of the redox active metal centers they accommodate as well as the delocalized electron density within their Pc rings which is dependent on the electronic effects of the substituents.[15, 16] For this reason, MPcs was chosen to be utilized in this research study as electrocatalysts on a bare gold working electrode for the electrocatalytic detection of a metal-based pollutant, mercury and a pesticide, paraquat.

Coumarin has been specifically chosen as peripheral substituent on the CoPc core as there has been increasing emphasizes on enhancing the selectivity of electrodes modified with CoPcs. Recent literature illustrated that polymer including coumarin fluorescent chromophores can reproducibly photochemically detect heavy metal pollutants such as mercury in real water samples.[17] In addition, a study by Ngororabanga *et al.* produced a fluorescent sensor using a coumarin-triazole polymer with good sensitivity and selectivity for Hg detection, further motivating the use of coumarin for mercury detection in this research.[18] Although the mechanism of interaction between coumarin photochemical or electrochemical sensors is often not established, it is theoretically deduced that sulphur atoms on the coumarin group or the coumarin ketonic and ester oxygen atom bonds the heavy metal cations.[19] While MPcs offer substantially superior electrochemical detection of target analytes they are still associated with drawbacks such as surface fouling of electrode substrates.

Therefore, this research study sought to address these shortcomings by incorporating network structures (*viz.* carbon nanotubes) and polymeric constituents (*viz.* electrospun nanofibers) to improve the stability and electrocatalytic activities of chemically modified electrodes. Consequently, this research study utilizes nanoconjugates which combine the redox properties of MPcs which are enhanced when conjugated with ENFs and MWCNTs to render selective, sensitive and accurate electrochemical sensors of mercury and paraquat in real surface water samples.

The primary aims of this research were:

- Fabrication and characterisation of electrospun nanofibers containing CoPc-cou
- Modification of gold electrodes with CoPc-cou-*f*-MWCNTs and CoPc-cou-ENFs nanoconjugates.
- Electrochemical, spectroscopic and morphological characterisation of the modified electrodes.
- Optimisation of instrumental parameters for the accurate detection of the CMEs towards target analytes.
- Determination of the applicability, accuracy and sensitivity of the modified electrodes towards desired analytes.
- Confirm reproducibility, stability and selectivity of the modified electrodes.
- Application of the modified gold electrodes to real water, complex samples under optimised parameters.
- Analyse real water samples using ICP-MS and ICP-OES after appropriate sample preparation and under optimal method parameters.
- Comparison of electrochemical sensor results with those of traditional analytical techniques to validate electrochemical sensors as a suitable alternative.

1.3. Literature survey

1.3.1. Metallophthalocyanines

The serendipitous discovery of phthalocyanines (Pcs) was made in 1907.[20] Their metallated analogs, metallophthalocyanines (MPcs) (**Figure 1.1**) were later discovered in the 1930s by Linstead *et al.*[21] This led to an upsurge in research conducted on MPcs to determine their physical and chemical properties as well as potential applications. As a metallocyclic compound containing highly conjugated 18π electrons, Pcs can form stable unsubstituted or substituted complexes with 70 different metal elements.[22] In fact, the structural diversity and the high stability of MPcs make them an attractive choice for a

variety of applications.[23] More specifically, these macrocyclic metal complexes have been utilized as conventional dyes, fuel cells, Langmuir-Blodgett (LM) films, photodynamic therapy (PDT) and chemical sensors.[24]

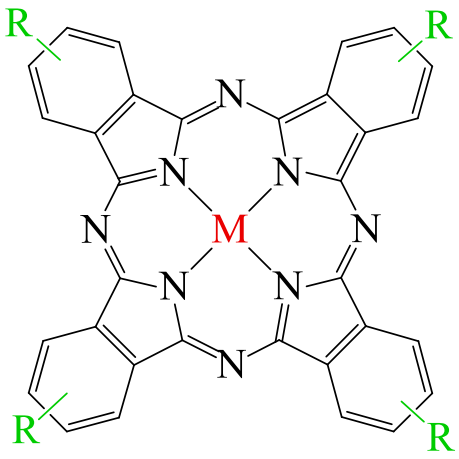

Figure 1.1: *General structure of metallophthalocyanines.*

1.3.1.1. Influence of substituents on the redox properties of MPcs

While MPcs are highly impressive with numerous advantageous properties, they do have some drawbacks such as limited solubility in aqueous and organic media.[25] Fortunately, this can be improved through the modification and alteration of MPcs substituents on their peripheral and non-peripheral sites which in turn fine-tunes the electrochemical properties of these diverse complexes. For example, Akinbulu *et al.* showed that the addition of substituents to either the peripheral or non-peripheral sites influences key properties such as the rate of electron transfer as well as the intensity of the characteristic *Q*-band of MPcs.[26]

Different substituents affect the electrocatalytic behaviour of MPcs by either withdrawing or donating electrons into and out of the Pc ring and ultimately altering the current density at the electrode surface. Electron donating groups such as -RNH_2, ArS- and -R(OMe) stabilize lower oxidates states by donating electrons into the Pc ring and

towards the metal core. Conversely, electron-withdrawing groups such as halogen groups, -RCOOH and -NO_2 make oxidation of the metal centre easier as they draw electrons out of the Pc ring.[27] Furthermore, substituents can be chosen in line with the modification technique being used to form a robust modified electrode taking advantage of non-covalent or pre-associative interactions it could have with the electrode to aid in good adherence to the electrode surface and thus afford a reproducible stable electrode. Moreover, MPcs substituted with biologically active moieties expand the applicability of these metal complexes towards a wider range of target analytes as the combination provides specific and strong analyte-substituent interactions.[14]

1.3.1.2. Electrochemical properties of cobalt phthalocyanines

MPcs have superior chemical stability and excellent electron transfer properties which if affected by the alteration of the metal center.[14] In comparison to other MPcs, cobalt phthalocyanines have been recognized to be effective electrocatalysts used in the modification of electrochemical sensors to detection a variety of chemical pollutants.[11] The electrocatalytic behaviours of MPcs, and thus the modified electrode, is dictated by the redox properties (*i.e.* reduction and oxidation potentials) of the metal. Co(II) is a $3d^7$ ion ([Ar]$3d^7$) that is redox-active and can lose or gain an electron to form the Co(III) or Co(I) ions, respectively.[28] This happens when the redox process of the substrate occurs within the vicinity of the metal-based Co(II)/Co(III) or Co(II)/Co(I) process.[29] This was also demonstrated in a study conducted by Xu *et al.* which cobalt phthalocyanines for the electrochemical sensing of thiols which occur in the redox potential window of 0 – (-0.2) V which is in the vicinity of the reduction potential of Co(II)/Co(I).[30]

1.3.2. Applications of MPcs

1.3.2.1. MPcs as photosensitisers in PDT

Photodynamic Therapy (PDT) is used to treat cancer using photosensitizers that can produce singlet oxygen that kills tumorous cells. MPcs meet two main criteria as prospective PDT agents which include high photochemical stability and they can absorb light in a defined wavelength to render singlet excited MPc species which in turn interchange energies with triplet oxygen. The excellent physiochemical properties of MPCs enhance the yield and lifetime of the triplet oxygen thereby producing a higher concentration of singlet oxygen, which makes them an attractive option for use as photosensitizers.[31] Conjugation of MPcs with semi-conducting nanoparticles is known to increase the triplet quantum yield and life-time of the nanocomposite-based photosensitizers,[32] see **Figure 1.2**. A research study by Dube *et al.* shows that the use of Zn and Ir phthalocyanines in combination with gold nanoparticles significantly increased the yield of both singlet and triplet oxygen, with the additional benefit of decreasing fluorescence yield which is desirable during its application as photosensitizers in PDT.[33]

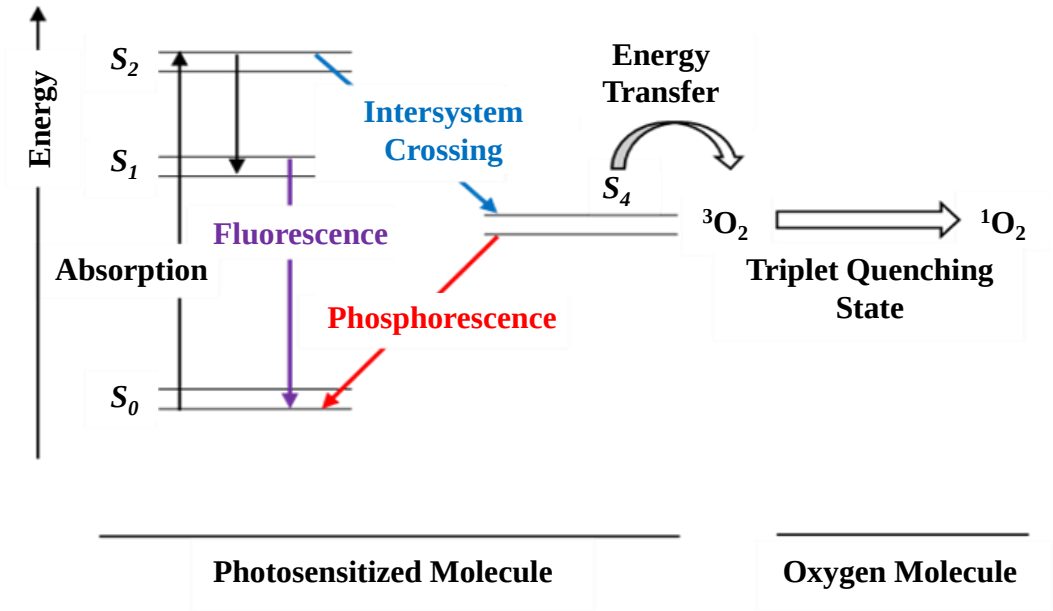

Figure 1.2: *Jablonski energy diagram depicting radiative and non-radiative pathways utilized in PDT.*

1.3.2.2. Fuel cells incorporating MPcs

Fuels cells are electrolytic cells that convert fuel sources to benign by-products and in the process generate electrical energy through chemical conversion[34] (**Figure 1.3**). The earlier generation of fuel cells comprised of solid-state platinum anode where the electrochemical oxidation of fuel sources (such as methanol) occurred. Despite the high activities of these in Pt-containing fuel cells, their widespread application is limited by expense where upscaling for industrial use is often not feasible and their domestic use in developing countries are essentially non-existent .[35] MPcs can be an appealing alternative due to their lower synthetic costs as well as their comparable critical charge transfer character aided by a careful design of their structures and nanoconjugation. Hebie *et al.* probed the use of MPcs for their applications in Proton Exchange Membrane (PEM) fuel cells as cathodic electrocatalysts. Evidentially, it was found that the use of carbon-supported metallophthalocyanines (FePc/C) afforded a significantly higher sensitivity towards the formation of OH^- while increasing the catalytic rate of oxygen reduction.[36]

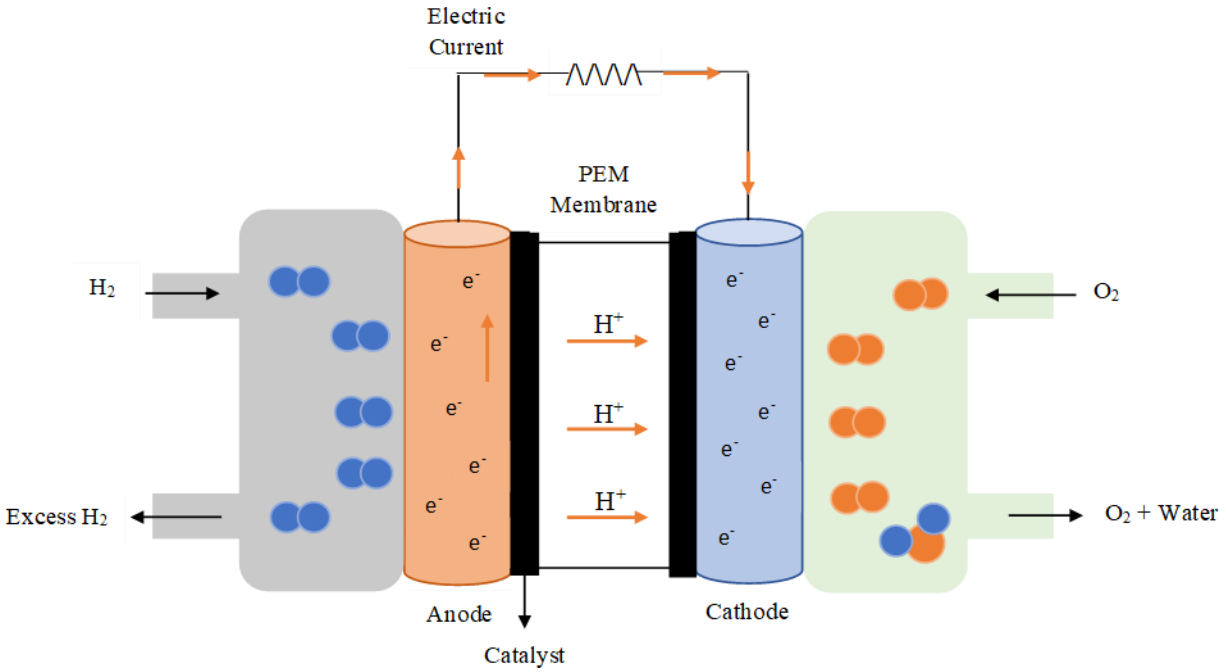

Figure 1.3: *Illustration of a proton exchange membrane (PEM) fuel cell.*

1.3.2.3. Significance of MPcs in electrochemical-based sensors

There are close correlations between the redox properties of MPcs and their electrocatalytic activities which in turn are also dependent on the potential on the redox potential window of the analyte.[37] Working electrodes modified with MPcs has served as chemosensors for various analytes such as bio-analytes for disease detection, carcinogenic aromatic polyphenols, pesticides and heavy metal cations.[38] Structural alterations of MPcs not only modulate their redox properties but also provide a means for harnessing different strategies for nanofabrication and electrode modification.[39]

It is well established that MPcs exhibit optimal electrocatalytic activities but challenges still remain to address their stabilities on various substrates and the propensities of MPc-based electrochemical sensors to suffer from surface fouling as well as improve their target specificity during analyte detection.[40] To address these apparent shortcomings, literature trends indicate that the covalent linking of MPcs to electrode surface affords more robust sensors with high electrocatalytic sensing reproducibility while the direct bonding between conductive nanomaterials and MPcs produces nanocomposite with larger effective surface areas on the electrode, leading to lower surface fouling.[41] The planarity of the MPc structure requires simple physical and electrochemical modification techniques which are cheap and produce robust modified sensors.[42] With respect to encouraging discriminate electrochemical sensing capabilities of MPc-based electrochemical sensors, the nature of the substituents is starting to play an increasing role in the mechanism of electrocatalytic selectivity.[26]

Ideally, a good electrocatalyst should increase the rate of transfer of electrons between the electrolyte and the electrode surface, lower the activation energy and be easily regenerated for reuse (repetitive use of the sensor without fouling the electrode surface).[43] Modified electrodes are capable of excellent reproducibility, stability and high interfacial currents when a potential is applied to them. This is attributed to their high conjugation which readily delocalise and thus significantly contribute to the electro catalysing effect during redox processes.

1.3.3. Current trends

1.3.3.1. Conductive polymeric hybrids of MPcs

Polymeric constituents offer an increase in surface area, increased porosity and active sites for interaction, low resistivity and a further enhanced rate of electron transfer.[44] Research is continuously evolving to improve existing methods and technology which is why nanofibers have gained popularity as electrocatalysts in recent years. This is due to their adaptability as multiple polymers can be combined to form fibres, their simplicity in design and formation as well as their capability for mass production.[45] The inclusion of nanofibers in the modification of electrochemical sensors enabled lower limits of detection and accuracy while maintaining fast response time and sensitivity. However, the stability of these modifying layers is short which motivates the use of nanofibers is conjunction with coating polymers.[46] Some of the conducting and coating polymers which have been used to successfully modify and enhance electrode sensing capabilities are polyaniline, 3-hexylthiophene and Nafion.[47-49]

1.3.3.2. MPc-based nanoconjugates

The primary goal of utilizing MPc nanocomposites on bare electrodes for electrocatalysis is to harness the favourable properties of both the metal complexes and the nano-confined materials. In particular, CNTs are expanded arrays of hexagonal lattice arranged sp^2 hybridized carbon atoms within open or close-ended tubes and upon applied potentials, the *pi*-conjugation within the CNTs can be delocalized. This electrical conductivity of the parent CNTs is inherent in their MPc-carbon nanotube composites where more rapid electron transfer behaviours of MPc-MWCNTs electrodes have been reported than MPc-modified electrodes.[50] In addition, the higher surface area of the MWCNTs leads to a nanocomposite-containing electrochemical sensor which is less prone to surface fouling due to a higher number of electro-active sites.[51] Another

favourable attribute of MPc-MWCNTs-based detectors from its nanomaterial is its mechanical strength which often leads to the chemically modified having more robustness. A recent study by Balogun *et al.* reported the various fabrication techniques and analyte detections in micro molar ranges using CoPc-MWCNT nanoconjugates.[52]

An emerging area in the development of electrochemical sensor design is the use of redox-active electrospun nanofibers and their hybrids as redox mediators on electrode surfaces. Gökçeören *et al.* demonstrated through their research that phthalocyanine-incorporated ENFs are an inexpensive practical alternative to traditional phthalocyanine-modified electrodes expanding the research field of nanoelectronics sensors.[53] More specifically, the ENFs offer high loading capacities of MPcs and the additive effect of the number of functional groups within a high molecular weight polymer chain or network structure can induce direct covalent bonding with the substrate, rendering high stability to the sensor. Therefore, nanocomposites containing MPcs and ENFs provide enhanced electrical conductivity and improved electrochemical properties in comparison to the constituents on their own.

CHAPTER TWO

Materials, reagents and instrumentation

2.1. Materials

Chemical reagents materials were sourced from commercial suppliers, including Merck-Sigma Aldrich and Capital Research Distributors (CRD) being the major supplier. Chemicals for syntheses included the following reagent-grade organic precursors: 4-nitrophthalonitrile, 7-mercapto-4-methylcoumarin and the metal precursor, cobalt(II) chloride as well as the basic catalysts potassium carbonate and 1,8-diazabicyclo[5.4.0]undec-7-ene (DBU). Furthermore, standard probes, analytical grade ferrocene, sodium sulphate, copper(II) sulphate, potassium ferricyanide and potassium hydroxide and lithium perchlorate were procured and used for electrochemical evaluations and analyses Pesticide analytical standards of paraquat (PQ), atrazine (ATR), triclopyr (TCP) were also purchased from Merck- Sigma Aldrich.

Bulk polymers including poly(vinyl) alcohol and perfluorinated resin solution containing Nafion (Nf) used for the formation of electrospun fibres (ENFs), were purchased from Sigma Aldrich and Capital Research Distributors. The monomers, aniline and 3-hexylthiophene carboxylic acid functionalized multiwalled carbon nanotubes *(f*-MWCNTs) were procured from Sigma Aldrich and Capital Research Distributors and used together with the repurposed ENFs as electrocatalytic composite conjugates for the modification of the electrodes. General consumables such as molecular sieves (4 Å), silicon dioxide (silica gel 60, 0.2-0.5 mm) used in column chromatography and silica plates (TLC Silica gel 60, F_{254}) used for thin layer chromatography were obtained from Merck-Sigma Aldrich. Metrohm polishing kits containing the aluminum oxide 90 (alumina) and Buehler felt pads were used to clean the electrodes were purchased from

Metrohm SA Furthermore, solid phase ion-exchange columns, Strata-X and Strata-X-C used real sample clean up and concentration were purchased from Phenomenex SA.

Phosphate buffered saline (PBS) tablets and analytical grade solvents were purchased from Merck-Sigma Aldrich. The reported metal complex, CoPc-cou was synthesised according to a previously reported method by Esenpınar *et al.*[54, 55] Dimethylformamide (DMF) used for synthesis and analysis was distilled as well as dried over molecular sieves. All other solvents were used without any further purification while. Ultrapure water was obtained from an ElgaPurelab Ultra system. All wastes generated during the electrochemical sensor modification were disposed of in designated waste containers according to laid down laboratory standard operating procedures (SOPs). Furthermore, all prepared mercury standards or fortified sample solutions during sensor evaluations and validation were carefully disposed of in separate dark, air-tight screw-capped glass containers which were quarantined in an isolated fume hood. The Hg waste solutions were then handed over to the waste stores technician who followed laid down laboratory SOPs for the proper handling and disposal of toxic waste samples from the School's transit store rooms for hazardous wastes.

Table 2.1: *List of commercially available chemicals used in synthesis and electrochemistry.*

Chemical	Purity
4-nitrophthalonitrile	99%
7-mercapto-4-methylcoumarin	99%
cobalt(II) chloride	97%
potassium carbonate	99.5%
1,8-diazabicyclo[5.4.0]undec-7-ene	98%
tetrabutylammonium tetrafluoroborate ($TBABF_4$)	99%
3-hexylthiophene	≥99%
lithium perchlorate	99.99%

ferrocene	98%
potassium ferricyanide	99%
sodium sulphate	≥99%
copper sulphate	≥99%
ferricyanide	99%
sodium hydroxide	≥98%
Paraquat	98%
atrazine	≥98%
triclopyr	≥98%
aniline	≥99.5%
poly(vinyl alcohol)	99%
mercury(II) sulfate	≥98%
perfluorinated resin solution containing Nafion	
carbon nanotube multiwalled, carboxylic acid functionalised	99.9%

2.2. *Instrumentation*

Characterisation data obtained for the CoPc-cou complex and 7-mecrcapto-4-methylcoumarin ligand has been confirmed by alignment with previously reported data.[54, 55] An Invenso Nanospinner Electrospinning instrument equipped with a Siemens Simatic HMI touch screen was used in conjunction with a Rocker 400 pump for the formation of electrospun nanofibers. Cyclic voltammetry, square wave voltammetry and electrochemical impedance spectroscopy were performed using an Autolab Potentiostat equipped with a three-electrode system: platinum working electrode, a pseudo Ag | AgCl reference electrode and a Pt counter electrode. Autolab Nova 1.7 software was used to operate the potentiostat and for data analysis. The working electrode surface was cleaned and regenerated, before and in between performing voltammetry scans, by polishing over an aqueous alumina slurry on Bühler and diamond polishing pads. A Specac optically transparent thin-layer electrochemical (OTTLE) cell was used to conduct

spectroelectrochemical experiments. Electrochemical solutions of the MPcs were prepared in anhydrous DMF containing 0.1 M $TBABF_4$ as a supporting electrolyte.

A Metrohm 827 pH meter calibrated with standard buffer solutions of pH 4 and 7 was used for sample pH. measurements Transmission electron microscopy (TEM) experiments were conducted using a JEOL 1400 microscope. Sample preparation included the dissolution of powdered samples at room temperature in ethanol followed by sonication of the samples for 15 mins before drying the TEM grids. Scanning electron Microscopy (SEM) images for the bare and modified electrodes were taken using a Zeiss EVO LS15 microscope operating under a high vacuum. Energy Dispersive X-ray analysis (EDX) spectra of the electrode modifiers were recorded using an Oxford X-MAX EDX detector under a high vacuum with an accelerating voltage of 20 kV to determine the elemental composition to corroborate SEM data.

Powder X-ray diffraction was conducted using a Rigaku Miniflex 600 diffractometer while Raman data was collected using a Renishaw inVia Raman microscope at a wavelength of 514 nm with and exposure time, objective and laser power of 20 seconds, X20 and 100% respectively. A Shimadzu LC-MS-2020 equipped with a Shim-pack guard column and a C18 Shim-pack GIST-HP (3 µm particle diameter) column (4.6 x 150 mm), was used to analyse real samples. In addition, a Shimadzu ICPE-9820 operating at a high-frequency power supply of 27 MHz and equipped with an Echelle polychromator and a semiconductor detector with a measurement range of 167- 800 nm and was used to conduct comparative analysis of real samples.

CHAPTER THREE

Construction of a Functional and Robust Cobalt(II) Phthalocyanine-Modified Electrode for the Electrocatalytic Detection of Paraquat

3.1. Introduction

Water pollution arising from accelerated industrialization and the lack of suitable water treatment is an escalating global concern. Impacting more than a third of the world's population, polluted water results in the lack of safe drinking water and poor sanitation in addition to having negative impacts on economic ventures.[56] Generally, the primary sources of pollution originate from domestic waste, industrial effluent, and untreated runoff from agricultural and mining industries among others.[57] A recent case of incidental pollution of the neighbourhood environment was an arson attack on an agricultural commodity warehouse in Cornubia, South Africa allegedly perpetrated by unknown protesters.[58] This unfortunate incident occurred on the 12th of July 2021. Consequently, the cocktails of toxic fumes and settleable solids from the combustion of the agricultural chemicals led to immediate and considerable pollution of the air, soil and water in a wide geographical area from the warehouse epicentre.[59] In addition, the adverse aftermath effect of the combusted chemicals was reported to have caused widespread loss of aquatic plants and animals within the Durban lagoon and beaches along the coastline which in turn led to the closure of these beaches for public use.[60, 61]

Numerous analytical techniques are currently available for the detection of pesticide-based pollutants. These include gas chromatography coupled with mass spectrometry (GC-MS), high-performance liquid chromatography coupled with mass

spectrometry (HPLC-MS), and liquid chromatography coupled with photodiode array (LC-PDA) detection.[62] However, these techniques require pre-extraction and pre-concentration steps which are generally time-consuming.[63] Furthermore, the analytical instrumentation is associated with high operating costs and requires highly skilled professionals to operate them.[64]

Electrochemical sensors are an attractive alternative as they are easy to use, relatively affordable and portable thereby allowing for real-time and on-site analysis.[65, 66] Currently, there is an upsurge in the research and development of chemically modified electrodes (CMEs) that can provide accurate and seamless detection of emerging environmental pollutants in water sources.[67, 68] Of particular interest are metallophthalocyanines (MPcs) which have been used as electrocatalysts for the modification of electrode surfaces due to their conductive and fascinating redox properties under applied potentials while retaining their structural integrity.[69] Electrocatalytic selectivity and robustness of MPc-based electrodes have been modulated through the choice of substituents covalently linked to the MPc core.[19]

Coumarin is a benzopyrone and a secondary metabolite found in many plants. It has been incorporated into various photoluminescence and electrochemical sensors of various water pollutants.[70] The general mechanism of its electrocatalytic selectivity is either through direct coordination of metal-based pollutants or complementary hydrogen-bonding interactions of organic analytes to coumarin core.[71, 72] Literature trends have shown that fine-tuning the sensing capabilities of coumarin-containing Schiff bases can improve their selectivity and sensitivity towards various analytes.[73]

Paraquat (PQ) is a pesticide widely used for crop protection to ensure high agricultural output. Due to its toxic effect on flora and fauna, its application and dissipation into the environment can cause a primary contamination effect on air, soil and water. Secondary contamination and poisoning of humans and animals can occur through the regular consumption of foods with high residual levels of PQ.[74] There have been reports on the PQ contamination of water bodies close to farms through dissipation

or unintentional spillages of this pesticide.[75] PQ is a severe neurotoxin which has been linked to the prognosis of Parkinson's Disease. Other studies have suggested some detrimental effects of PQ on the cardiovascular system.[76]

Given the primary contamination of PQ around the Cornubia suburb in Durban, Kwa-Zulu-Natal Province, Republic of South Africa (vide supra), we designed and fabricated a Au chemically modified electrode (CME) that can detect PQ in the water of multifarious sample matrices with good selectivity, high sensitivity and micromolar-level detection limits. The analytical performance of the CME towards PQ in spiked water samples (collected from Umhlanga Lagoon Beach, Durban) was comparable and slightly better than the conventional LC-PDA/MS method. The fabrication of this CME was initiated by the formation of a composite self-assembled monolayer (SAM) of a coumarin tetrasubstituted cobalt phthalocyanine (CoPc-cou) with multiwalled carbon nanotube conjugate (*f*-MWCNTs) onto a bare Au electrode. Thereafter, the resultant CME was further electropolymerized with 3-hexylthiophene to improve the stability and sensitivity of the SAM-modified electrode, refer to **Scheme 3.1**.

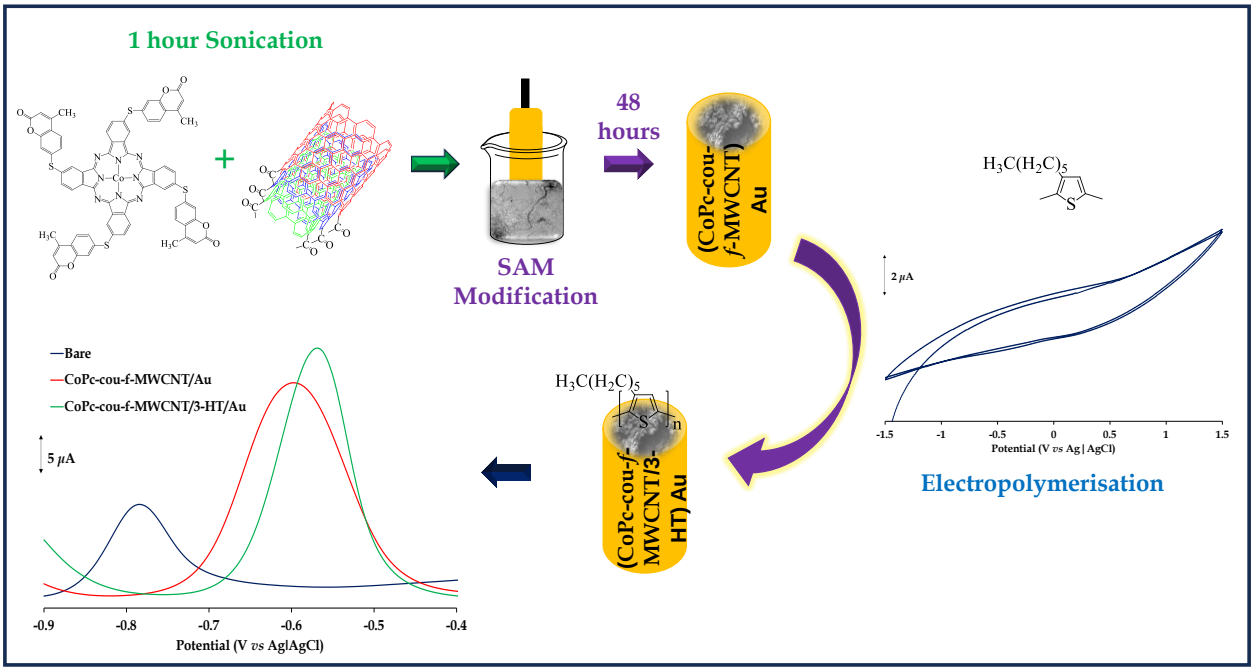

Scheme 3.1: *Illustration of the modification process for the CoPc-cou-f-MWCNT/3-HT|Au.*

3.2. Experimental

3.2.1. Materials and equipment

The following reagent-grade chemicals: 4-nitrophthalonitrile, 7-mercapto-4-methylcoumarin, cobalt(II) chloride, potassium carbonate, 1,8-diazabicyclo[5.4.0] undec-7-ene (DBU), 3-hexylthiophene (HT), lithium perchlorate and electrochemical grade tetrabutylammonium tetrafluoroborate (TBABF4) were purchased from Sigma Aldrich. Silicon dioxide (silica) used in column chromatography and silica plates used in thin layer chromatography were obtained from Merck SA. Aluminum oxide (alumina) utilized to polish the electrodes, was purchased from Metrohm SA. The ligand and CoPc-cou were synthesized and characterised according to previously reported methods.[54, 55]

Transmission electron microscopy (TEM) experiments were conducted using a JEOL 1400 microscope. Sample preparation included the dissolution of powdered samples at room temperature in ethanol followed by sonication of the samples for 15 mins before drying the TEM grids. Scanning electron Microscopy (SEM) images for the bare and modified electrodes were attained using a Zeiss EVO LS15 operating under a high vacuum. Energy Dispersive X-ray analysis (EDX) was carried out using an Oxford X-MAX EDX detector under a high vacuum with an accelerating voltage of 20 kV to determine the elemental composition to corroborate SEM data.

The nanoconjugate was characterized by Powder X-ray diffraction using a Rigaku Miniflex 600 diffractometer. A Shimadzu LC-MS-2020 with a Shim-pack GIST-HP 3 µm C18 column (4.6 x 150 mm), equipped with a Shim-pack guard column was used to conduct comparative real sample studies.

3.2.2. Electrochemical methods

All electrochemical experiments were done using an Autolab Potentiostat equipped with a three-electrode system: a gold (Au) working electrode, a pseudo

Ag/AgCl reference electrode and a Pt counter electrode. A hot solution of hydrogen peroxide and sulfuric acid in a 1:3 volume-to-volume ratio at 120 ºC, known as a Piranha solution, was used to clean the surface of the Au electrode. Thereafter, it was polished over an aqueous alumina slurry on Buhler and diamond polishing pads, respectively. In addition, the electrode was rinsed with ultra-pure water and anhydrous dimethyl formamide (DMF) and finally sonicated in DMF for 2 minutes.

3.2.3. Electrode modification

The nanoconjugate was formed by adding 1 mg of *f*-MWCNTs to 2 mL of a 2 mM solution of CoPc-S-cou in DMF before sonicating the solution for an hour. Thereafter, the bare Au electrode was immersed in the solution for 48 hours at room temperature to form the CoPc-cou-*f*-MWCNTs SAM-modified Au electrode. The modified electrode was thereafter rinsed using ultrapure water and DMF before electropolymerizing (3-HT)n on the CME using a previously reported method.[48] The modification process of the CoPc-cou-*f*-MWCNTs/3-HT | Au is illustrated in **Scheme 3.1**.

3.3. Results and discussion

3.3.1. Morphological characterisation

CoPc-*f*-MWCNTs composites are well known to be stabilized by direct covalent bonding occurring between the carboxylic acid functional groups of f-MWCNTs and the CoPc's central atom.[77, 78] These nanohybrids are reinforced by complementary hydrogen bonding and π -π stacking interactions. The surface morphology of the bare and modified electrodes was investigated via SEM, see **Figure 3.1**. Noticeably the bare electrode does not have a smooth surface but upon modification, significant alteration in the surface is observed. Furthermore, the SEM micrograph for the modified electrode surface displays a porous surface which can be attributed to aggregation of the metal complex which is

typical of MPcs. Therefore, it can be deduced that there is good surface coverage of the SAM-modified Au electrode as the texture of the bare gold sputtered electrode is no longer evident. Evidently, the elemental composition of the modified gold sputtered electrode, as indicated by EDX data consists of Au, Co, C, N, S and O, confirming the modification of the electrode surface by the CoPc-cou complex. This can be evaluated against **Figure 3.1 (D)**, displaying the presence of only Au on the gold-sputtered bare electrode. A SEM micrograph of the nanoconjugate immobilized via SAM formation on the Au-coated glass was also collected and it showed enhanced surface coverage attributed to the cylindrical shape of the MWCNTs, see **Figure 3.1 (C).**[79] No informative conclusions could be made from the EDX spectrum of the nanoconjugate-modified surface as it was dominated by the carbon peak.

TEM images of the CoPc-S-cou, *f*-MWCNTs and CoPc-S-cou-*f*-MWCNTs were collected (**Figure 3.2**) to confirm the formation of the nanoconjugate. Indicative to the SEM analysis, the CoPc-S-cou micrograph (**Figure 3.2 (A)**) illustrates clusters that are due to the MPc molecules experiencing significant aggregation due to the π – π stacking interactions existing between the molecules.[80, 81] Conversely, *f*-MWCNTs (**Figure 3.2 (B)**) appear as dispersed long strands with minimal overlapping. The nodal points which can be seen in **Figure 3.2 (C)**, are attributed to the linking between the CoPc-S-cou and the *f*-MWCNT thus confirming that the nanoconjugate had formed.[77]

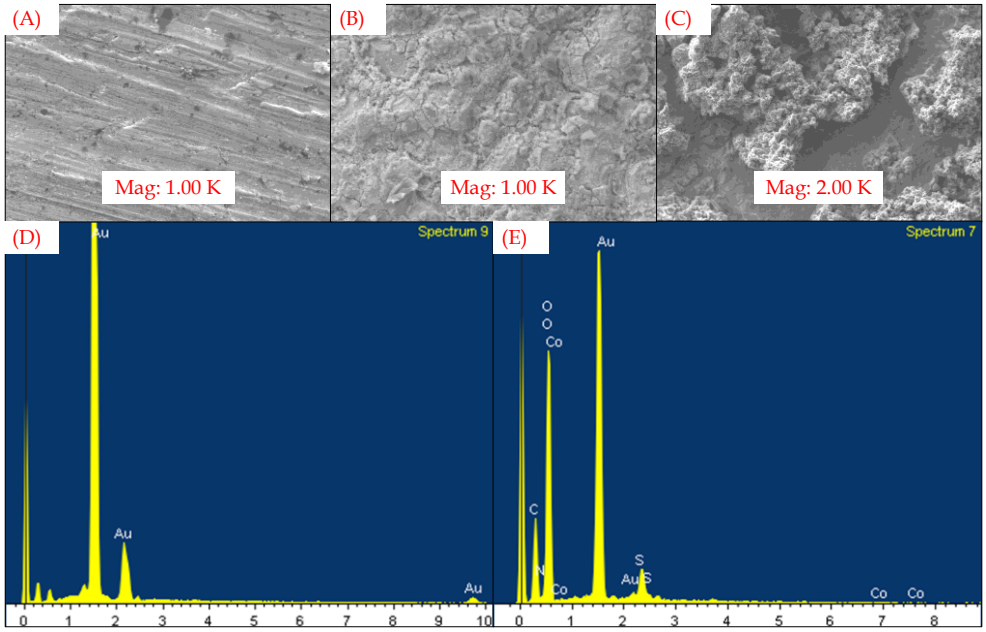

Figure 3.1: *SEM images of (A) Bare gold-sputtered glass and (B) SAM-CoPc-S-cou sputtered glass, (C) SAM-CoPc-cou-f-MWCNT. EDX spectra of (D) Bare gold-sputtered glass and (E) SAM-CoPc-S-cou sputtered glass.*

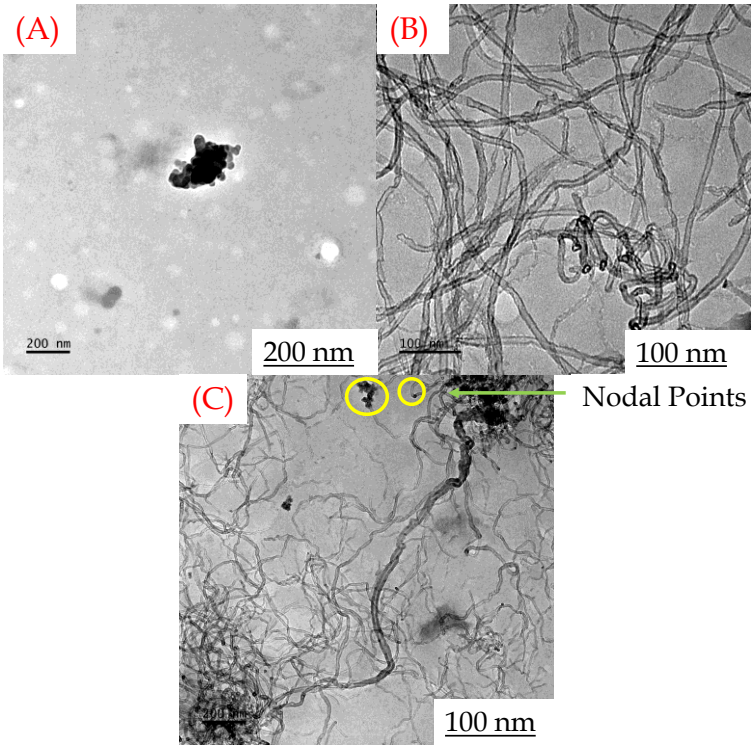

Figure 3.2: *TEM images of (A) CoPc-cou, (B) f-MWCNTs and (C) CoPc-cou-f-MWCNTs.*

X-ray diffraction (XRD) was employed to further characterize the nanoconjugate (**Figure 3.3**). Diffraction peaks for the nanoconjugate appear at 26º and 43º degrees which can be indexed to MWCNTs (002) and (100) planes. In addition, the peak at 13º can be attributed to the CoPc.[82] Furthermore, the broadness of the peaks indicates that the compound is amorphous.[83]

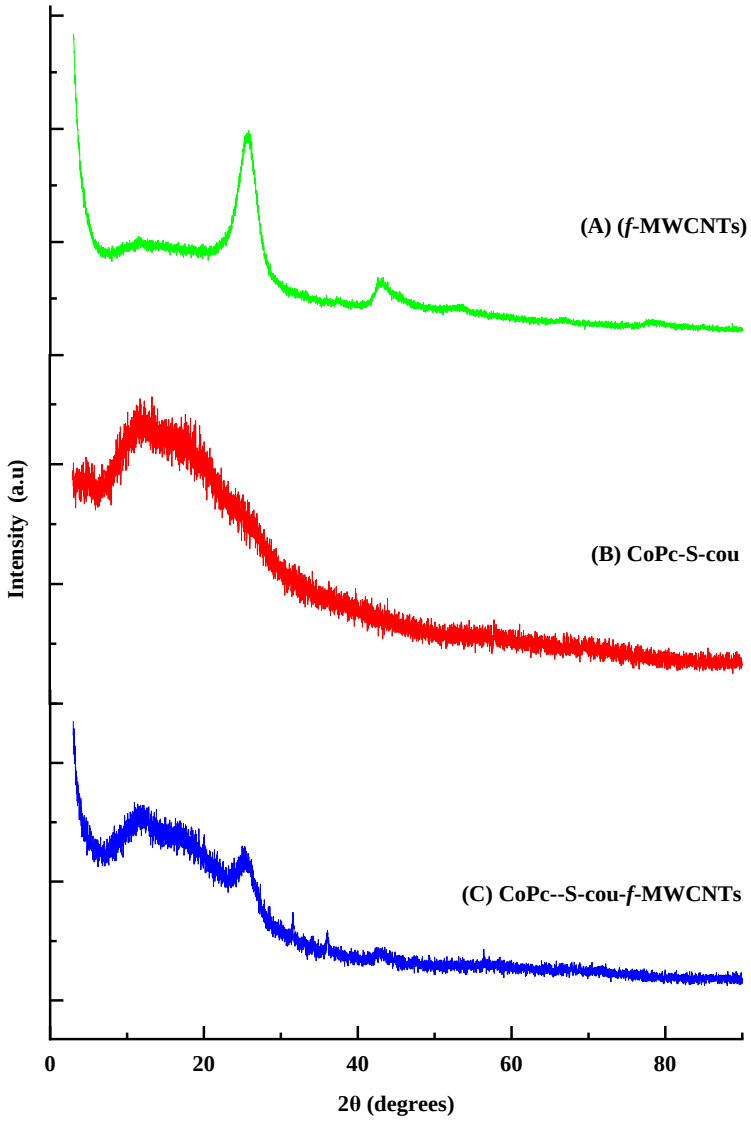

Figure 3.3: *XRD patterns of (A) f-MWCNTs, (B) CoPc-S-cou and (C) CoPc-S-cou-f-MWCNTs.*

3.3.2. Characterisation of modified electrode.

The intensities of the peaks for the SAM-CoPc-cou Au electrode when analysing a 1 mM solution of ferrocene in DMF are visibly lower than that of the bare electrode (**Figure 3.4**). This is expected as the formation of SAMs on the electrode surface would inhibit signal detection of the ferrocene by the gold surface. This indicates that the modified electrode is not sensitive towards ferrocene which is desirable as modification aims to ensure that the electrode is sensitive towards the target analyte whilst being insensitive towards other analytes. Furthermore, the peak-to-peak separation, $\Delta E_{(bare)}$ and $\Delta E_{(modified)}$ were calculated to be 0.29 and 0.25 V, respectively, which is an indication of faster electron transfer kinetics when using the modified electrode.

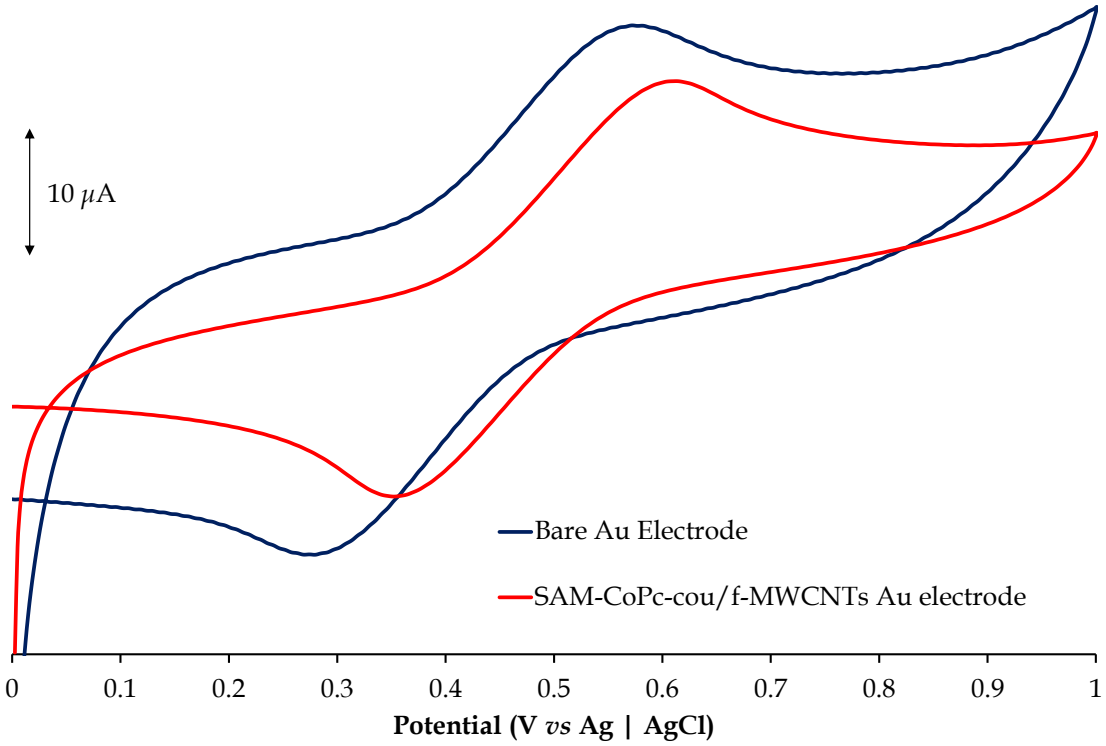

Figure 3.4: *Overlay CVs of the bare and CoPc-cou-f-MWCNTs | Au electrode in a 1 mM solution of ferrocene in DMF.*

Electrochemical techniques were then employed to characterize the CoPc-cou-f-MWCNTS|Au modified electrode. **Figure 5 (A)** displays cyclic voltammograms of a 1 mM Na_2SO_4 solution in a pH 4 buffer solution using the Au modified electrode and bare electrodes. The peak which appears at 0.976 V is a result of the redox reactions of the unmodified gold surface. The significant reduction in the peak potential infers impermeability which is a result of the electrode being modified. Furthermore, a comparison of CVs obtained using the bare and modified Au electrodes in a 1 mM solution of $CuSO_4$ in a pH 4 buffer solution displayed in **Figure 3.5 (B)** confirms SAM modification of the bare Au electrode. The Cu underpotential deposition at 0.069 V which easily formed on the gold electrode was significantly inhibited when the solution was analyzed using the modified electrode. The formation of the SAMs on the electrode is expected to decrease the intensity of the Cu peak as it restricts the interaction between gold and Cu.

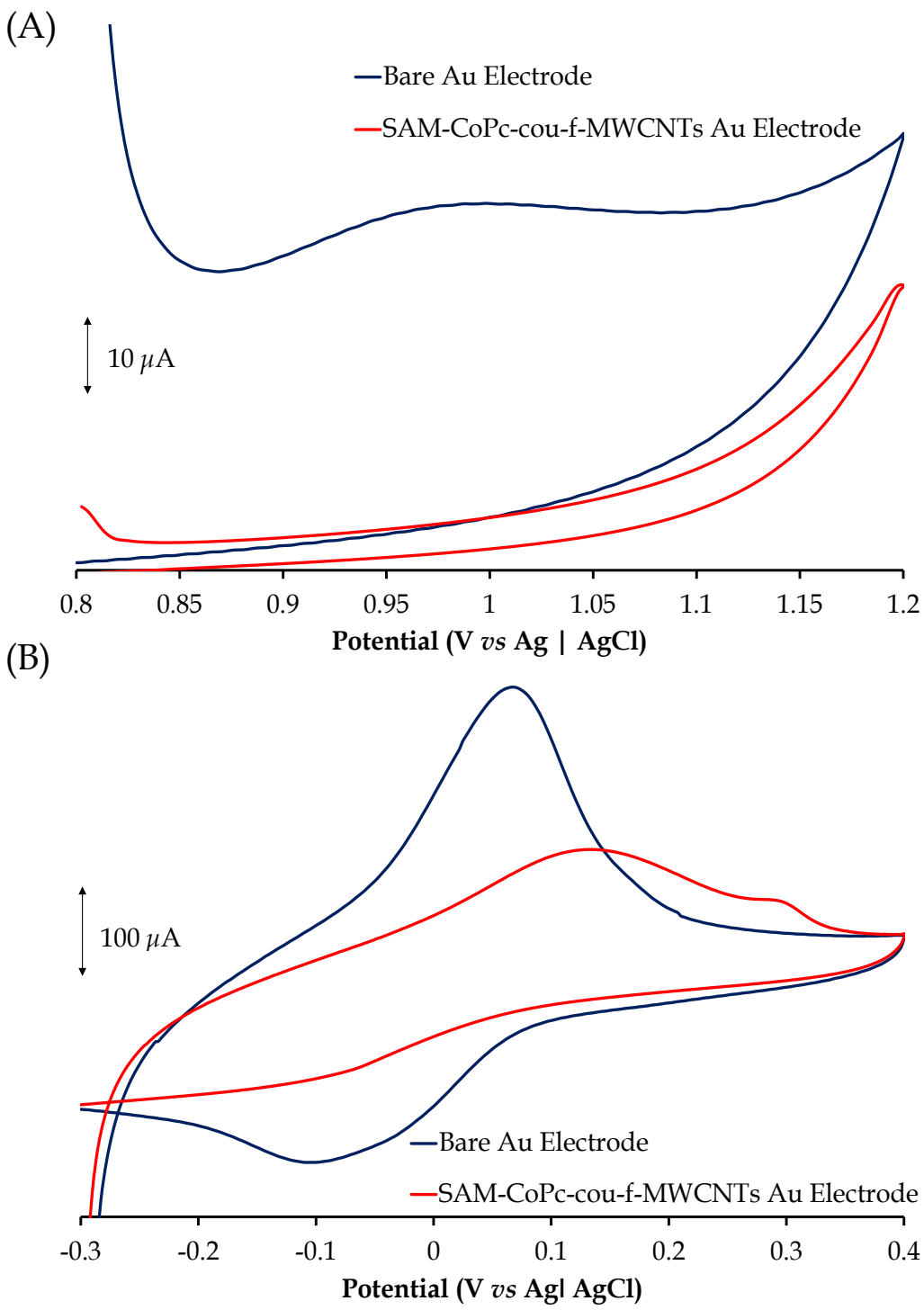

Figure 3.5: *Overlay CVs of the bare and CoPc-cou-f-MWCNTs | Au modified Au electrode in (A) 1 mM Na_2SO_4 and (B) 1 mM $CuSO_4$ in a pH 4 solution.*

The ion barrier factor (Γ_{IBF}), which is an indication of the compactness of the SAMs bonded to the unmodified electrode was calculated using the Na_2SO_4 redox probe. An ion barrier factor of 1 is considered an ideal ion-permeable film. This indicates the substrate has been completely covered by the formation of the SAM and no exposed sites on the surface are available to detect redox reactions occurring resulting in an impermeable film towards the redox probes. The ion barrier factor can be calculated using **Equation 3.1**,

$$\Gamma_{IBF} = 1 - \frac{I_{pa(SAM)}}{I_{pa(Bare)}} \quad (\mathbf{3.1})$$

where the peak currents of the bare and modified electrodes are compared. An ion barrier factor of 0.87 was calculated for the CoPc-cou-*f*-MWCNT|Au modified electrode, suggesting almost complete coverage of the gold surface by the SAM.

Potassium ferricyanide, $K_3[Fe(CN_6)]$ was used as a redox probe to determine the surface coverage and effective surface area of the modified electrode. **Figure 3.6 (A)** displays CVs at increasing scan rates conducted using the CoPc-cou-*f*-MWCNT|Au electrode in a 5 mM $K_3[Fe(CN_6)]$ in 0.1 M aqueous solution of KCl. To determine the effective surface area, the Randles-Sevcik equation (**Equation 3.2**) was applied[77]:

$$I_{pa}=2.69 \times 10^5 AD^{1/2}n^{3/2}v^{1/2}C \quad (\mathbf{3.2})$$

where A is the effective surface area, D is the diffusion coefficient of $K_3[Fe(CN_6)]$, n is the number of electrons transferred (n = 1), v is the scan rate and C is the bulk molar concentration of $K_3[Fe(CN_6)]$. The slope obtained from a plot of the oxidation peak current against the square root of the scan rates, shown in **Figure 3.6 (B)**, was used to determine the effective surface area of the modified electrode. Putting the values into **Equation 3.2** yielded an effective surface area of 2.42 cm^2. This is larger than the effective area of the bare electrode (0.071 cm^2) which translates to successful modification as well as the modified electrode having more active sites to interact with the target analyte than

the bare electrode.[77] The surface coverage was calculated using **Equation 3.3** and the effective surface area to further establish the extent of the modification.

$$\Gamma = \frac{Q}{nFA} \qquad (\mathbf{3.3})$$

The terms in the equation are as follows, Γ is the surface coverage, Q is the total charge under the peak, n is the number of electrons transferred, A is the effective surface area (cm^2) and F is the Faraday's constant. Surface coverage was found to be 2.42×10^{-10} mol cm^{-2} which is significantly higher than the typical surface coverage of 1×10^{-10} mol cm^{-2} for CoPc immobilized flat on an electrode surface.[84] However, this elevated surface coverage is characteristic of CMEs modified with CoPc carbon nanotube conjugates which can be associated with the nano-scaled dimensions of these composite materials.[85, 86]

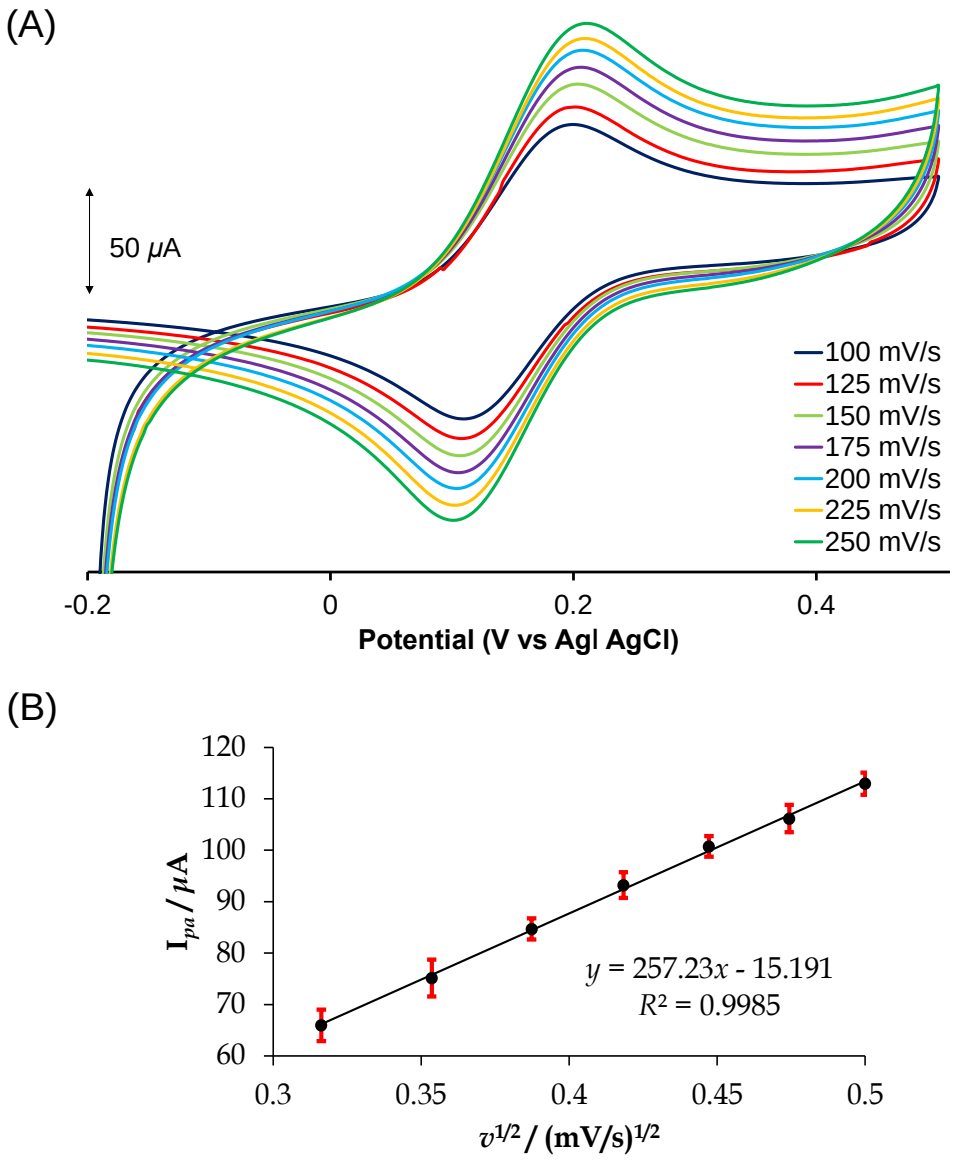

Figure 3.6: *(A) Overlay CVs in a 5 mM $K_3[Fe(CN_6)]$ in 0.1 M KCl solution at the CoPc-cou-f-MWCNTs | Au interface at increasing scan rates and (B) Plot of I_{pa} vs $v^{1/2}$.*

3.3.3. Stability studies

The stability of the chemically modified electrode in 1 mM PQ was investigated via repetitive cyclic voltammetry scans (10 cycles). The cumulative deposition of PQ on the electrode surface is evident in **Figure 3.7**, as the peak current increases with an

increase in the number of CV scans.[87, 88] This demonstrates the instability of the CV current responses for PQ when the potential of the modified electrode is cycled repeatedly due to the tenacious adsorption of PQ on its active sites.[63, 89] This could lead to systematic errors in the quantitative analysis of the PQ. In addition, CV is intrinsically less sensitive than most differential pulsed techniques such as DPV. Hence, DPV was chosen as the preferred method for further studies.

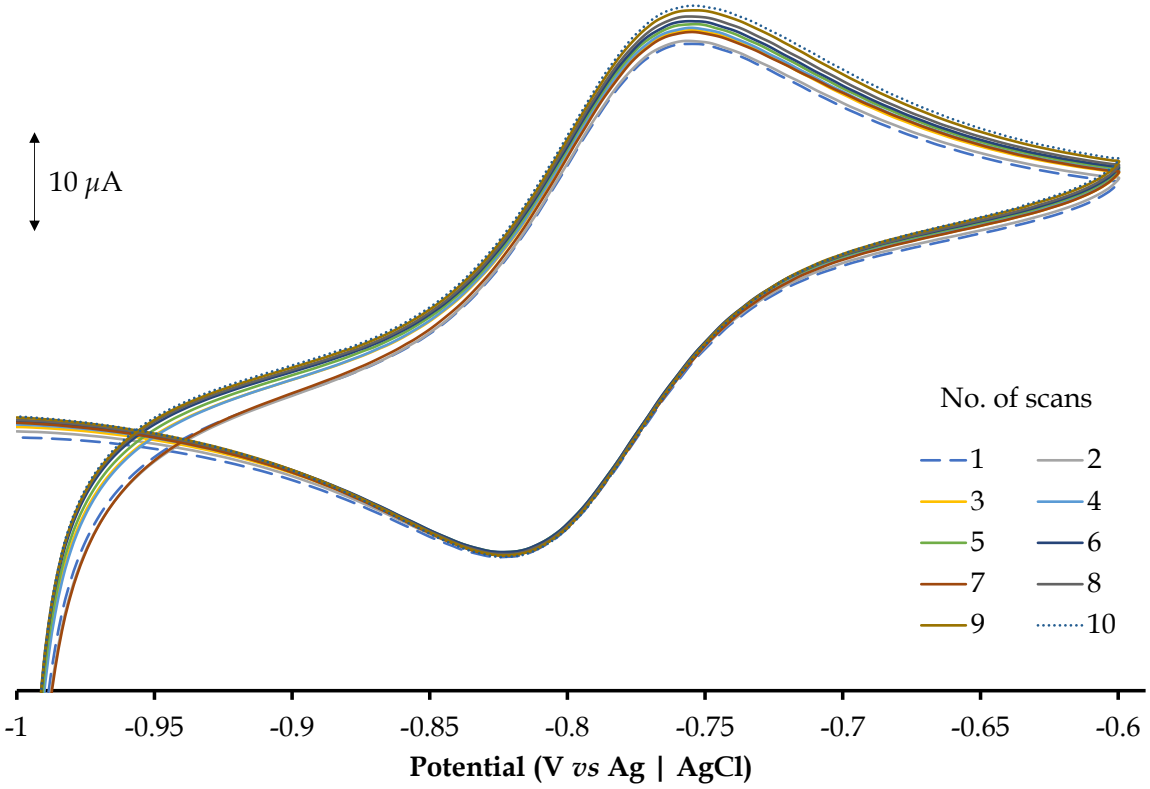

Figure 3.7: *Overlay of 10 CV cycles in a 1 mM PQ in 0.1 M NaOH solution at the CoPc-cou-f-MWCNTs | Au interface at a scan rate of 0.1 V.s^{-1}.*

Furthermore, the SEM images in **Figures 3.8 (A)** and **-(B)** illustrates the chemically modified electrodes before and after continuous CV cycles in 1 mM PQ. The alteration to the surface morphology of the modified electrode is due to adsorption of artifacts that

include PQ which is visually evident from the SEM image. In addition, the EDX spectra of the electrodes in **Figure 3.8 (C)** and **-(D)**, display a decrease in the elemental composition when comparing the CMEs before and after CV electrocatalytic studies. This further supports the use of DPV for further quantitative analyses since it can strip off the adsorbed PQ and hence renew the electrode surface in each analysis cycle.

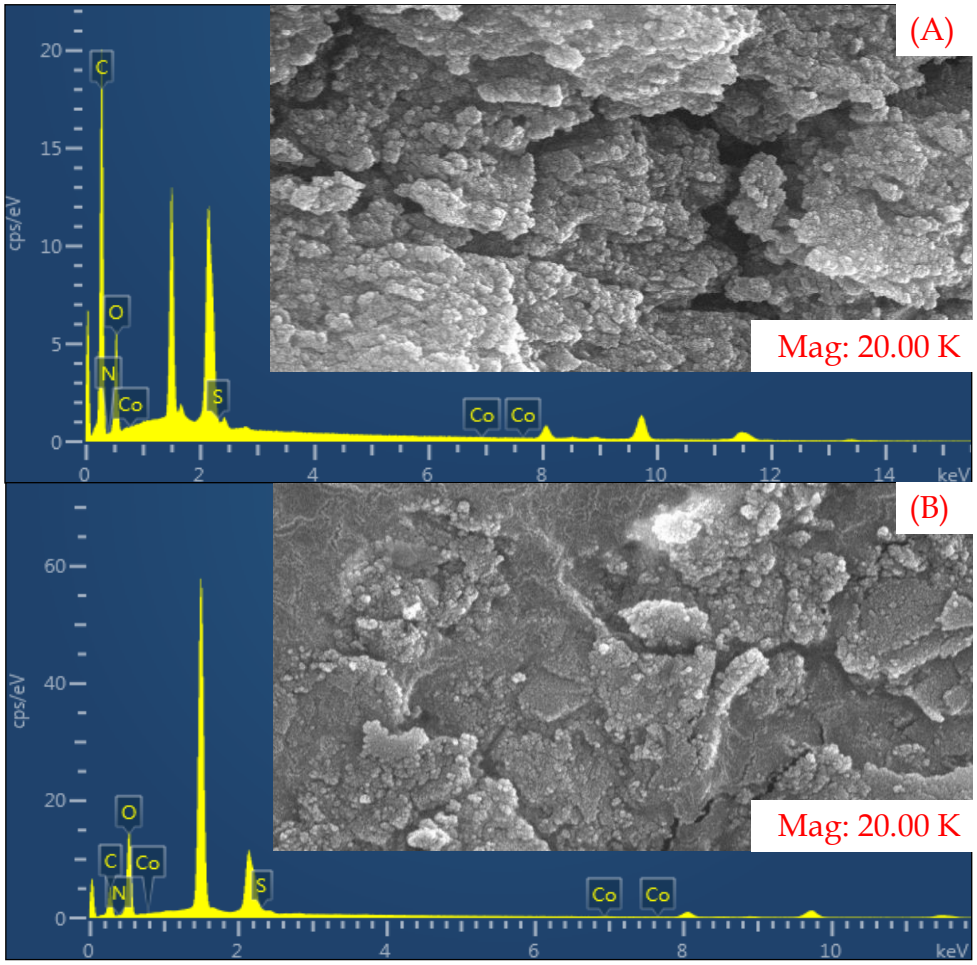

Figure 3.8: *SEM Images and EDX spectra of (A) modified electrode before PQ analysis and (B) modified electrode after PQ analysis.*

3.3.4. Interference studies

An important functional characteristic of a CME is its ability to selectively detect the analyte of interest in the presence of other pollutants. The structures of potential

interfering pesticides, triclopyr (TCP), and atrazine (ATR), together with the analyte, PQ are shown in **Figure 3.9**.

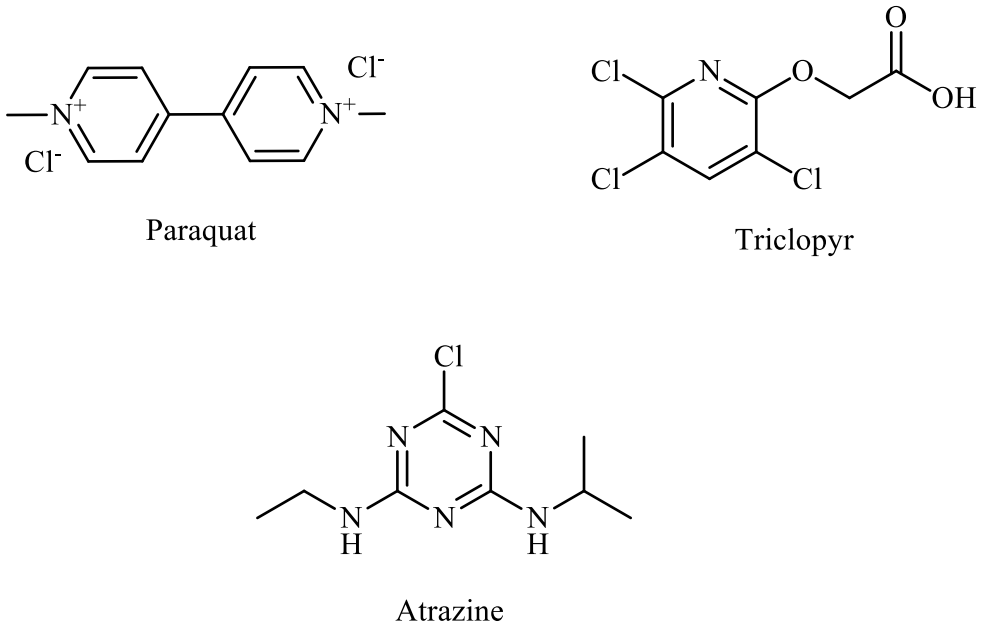

Figure 3.9: *Structures of paraquat (PQ), atrazine (ATR) and triclopyr (TCP) which were used in interference studies.*

Detection of PQ was conducted in the same potential window as those run for interferences to establish if the latter pesticides interfered with the detection of PQ as shown in **Figure 3.10**. The other two pesticides were chosen based on the list of agrochemicals that were housed at the torched Cornubia warehouse in large quantities.[90] The DPV current response of the CoPc-cou-*f*-MWCNT/3-HT | Au in 1 mM PQ displayed one well-defined intense peak for PQ at -0.58 V. However, the peak for PQ was broad between -0.78 V and -0.37 V while the current response peaks for PQ in the presence of 1 mM ATR and TCP were suppressed by 67%, refer to **Figure 3.10**. The electrocatalytic current for the DPV signals of PQ attained in a sample containing PQ was background corrected using the DPV attained in the buffer solution. The baseline triangulation

method was employed for a multifarious sample since a noticeable increase in the background current was observed in the presence of ATR and TCP.

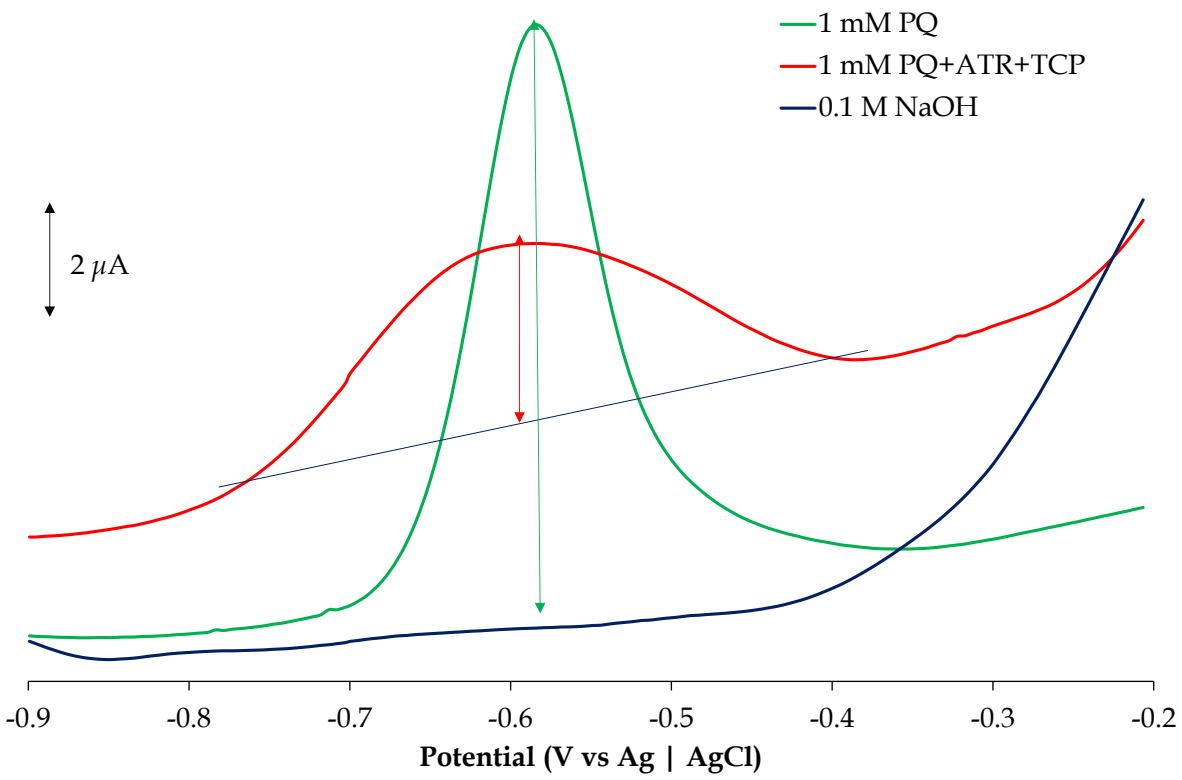

Figure 3.10: *Overlay of DPVs of 1 mM solutions in 0.1 M NaOH / 1:3 ACN:UPW of paraquat (PQ), atrazine (ATR) and triclopyr (TCP) at the CoPc-cou-f-MWCNT/3-HT | Au interface showing PQ signal suppression by interferents.*

3.3.4. Electrocatalytic detection of PQ

The differential pulse voltammetry (DPV) current responses of the bare and modified electrodes towards paraquat (PQ) were recorded in a 1 mM solution of PQ in 0.1 M NaOH to establish the electrocatalytic detection of the analyte by the latter CMEs (refer to **Figure 3.11**). As per literature trends, PQ undergoes a two-step reduction process at the Au electrodes as shown below[91, 92]:

$PQ(II) + e^- \rightarrow PQ(I)$

$PQ(II) + e^- \rightarrow PQ(I)$

However, due to extensive fouling at the electrode interface upon analysis of PQ, only 1 reduction peak was investigated as shown in **Figure 3.10**. To inspect the performance of the modified electrodes against the bare electrode, the peak current and potentials of the DPVs in **Figure 3.11** were compared and the data is shown in **Table 3.1**. The Ipa values for PQ using the bare electrode are significantly lower than those of the modified electrodes. Upon modification of the Au electrode with the CoPc-cou-*f*-MWCNTs, the affinity of the coumarin substituents of the CoPc towards PQ and the enhanced conductivity of the *f*-MWCNTs render a synergetic effect on the electrocatalysis of the composite modifier. This is evident from the increased peak intensity of the CME compared to the bare Au electrode. The fouling effects of PQ on the CoPc-cou-*f*-MWCNTs-modified Au electrode made it difficult to attain reproducible results, therefore an additional mediating film of poly(3-hexylthiophene) (3-HT) was necessary to provide stability to the modified electrode. The DPV current response of CoPc-cou-*f*-MWCNT/3-HT|Au is slightly higher and the peak is narrower, indicating enhanced sensitivity and better reduction stability was attained by the inclusion of the poly(3-hexylthiophene) in the ternary nanocomposite film of the Au electrode. In addition, the decrease in peak potential indicates that the CoPc-cou-*f*-MWCNT/3-HT|Au has faster electron transfer kinetics when compared to the bare electrode.

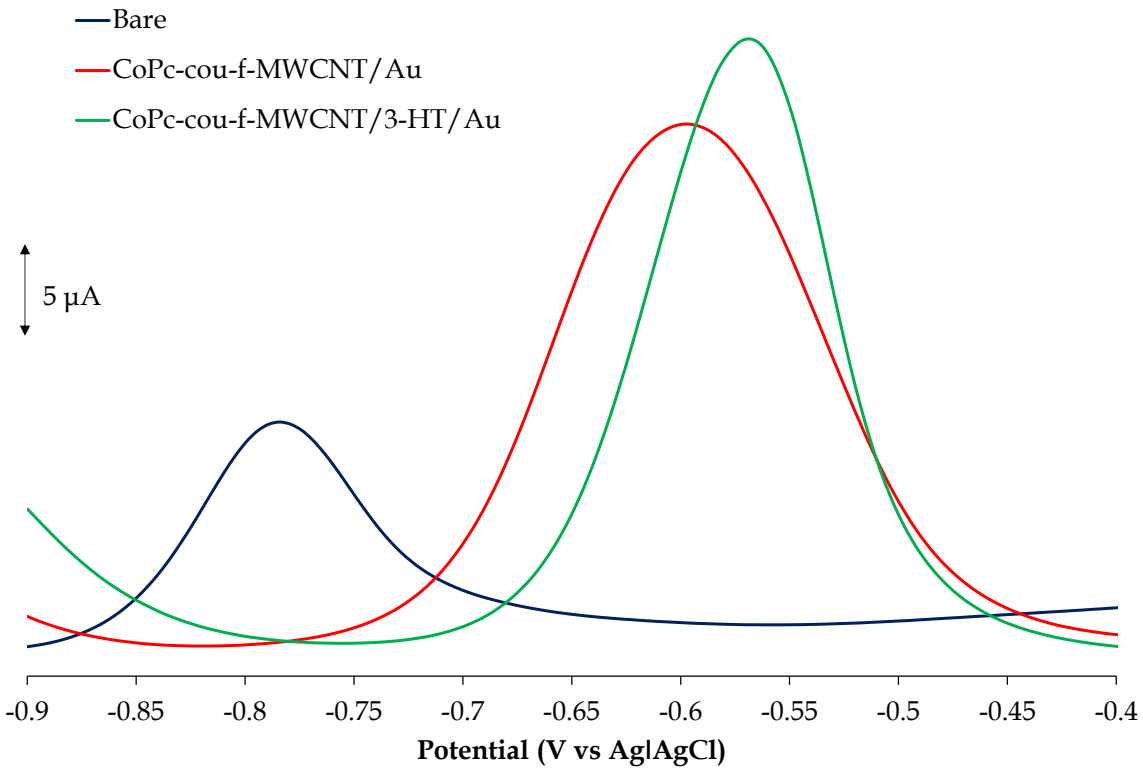

Figure 3.11: *Overlay of DPVs of 1 mM PQ in 0.1 M NaOH using the bare, CoPc-cou-f-MWCNT | Au and CoPc-cou-f-MWCNT/3-HT | Au.*

Table 3.1: *DPV Peak currents and redox potentials of 1 mM PQ using the bare and modified electrodes. The current has been background corrected against DPVs conducted in the electrolyte solution.*

Electrode	Potential (V)	Current (µA)
Bare Au	-0.78	14.2
CoPc-cou-*f*-MWCNT | Au	-0.60	27.7
CoPc-cou-*f*-MWCNT/3-HT | Au	-0.58	32.6

The effect of scan rate on the current response for a 1 mM PQ in 0.1 M NaOH solution was investigated within the range of 25 – 250 mV/s to gain an insight into the mechanism of PQ detection at the CoPc-cou-*f*-MWCNT/3-HT|Au surface, see **Figure 3.12 (A)**. It is evident that both diffusion and adsorption-controlled processes are occurring, deduced from the linear plots for peak current versus square root of scan rates, and scan rates, respectively (**Figures 3.12 (B) & (C)**). Furthermore, a slope of ca. 0.88 was obtained from a plot of the logarithm of peak currents (Log Ipa) and the logarithm of scan rates (Log v) (**Figure 3.12 (D)**) which is within the range of 0.5 and 1, thus corroborating that the mechanism is both diffusion and adsorption controlled.[93]

To further ascertain the charge transfer kinetics of the CoPc-cou-f-MWCNT/3-HT|Au towards PQ, the Tafel slopes were attained from a plot of Ep vs Log v, using the following equation[84],

$$E_p = \frac{2.3RT}{2(1-a)Fn_a} \text{Log } v + K \qquad (\mathbf{3.4})$$

The terms of **equation (3.4)** are defined as follows: α is the transfer coefficient, v is the scan rate, nα is the number of electrons in the rate-determining step and K is the intercept. The Tafel slope was calculated to be 61 mV/decade which is within the normal range of 30-120 mV/decade, indicating an electrode mechanism proceeding by a chemical reaction followed by a fast first-electron transfer as the rate-determining step.[94, 95]

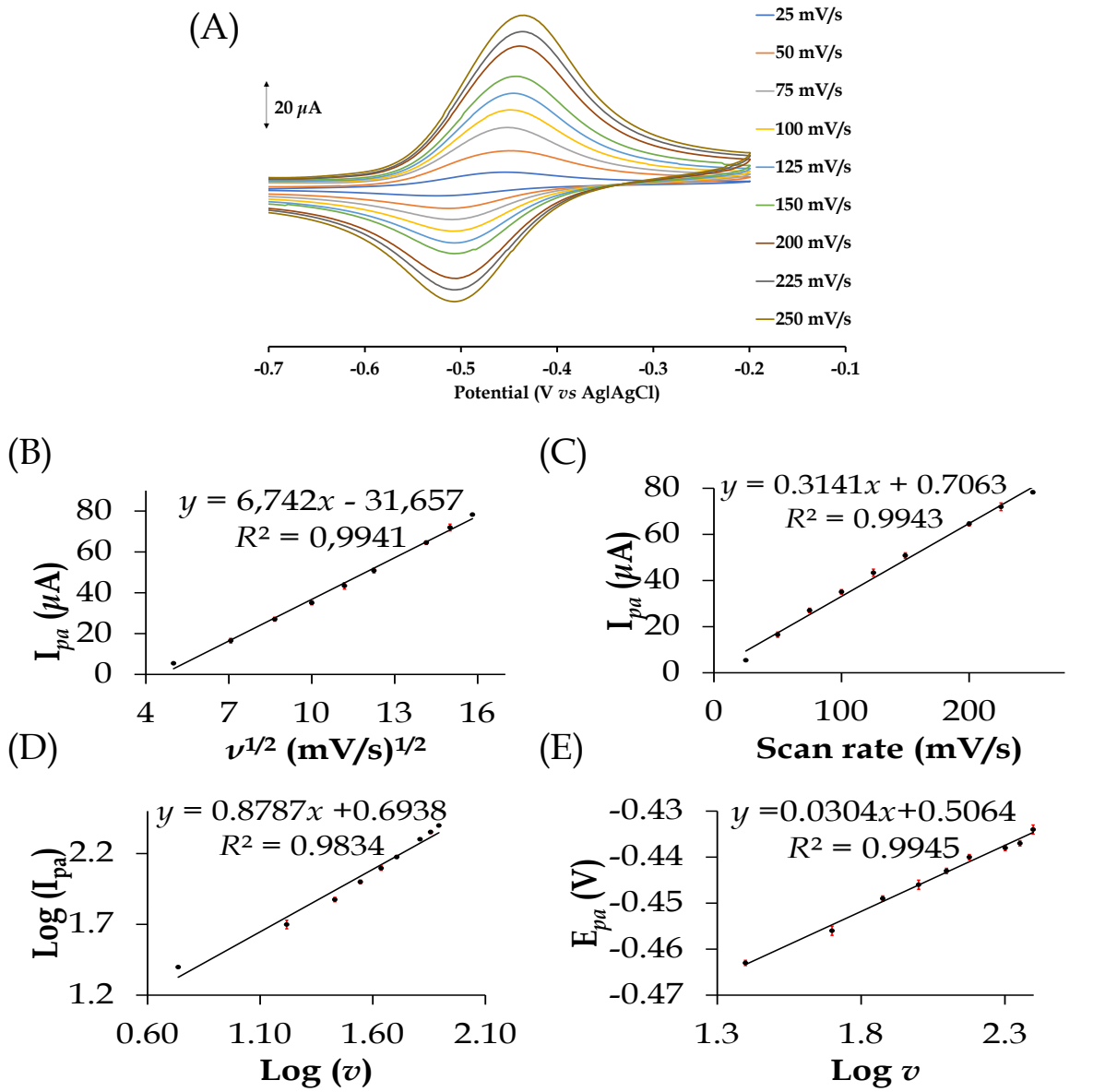

Figure 3.12: *(A) Overlay CVs of 1 mM PQ in 0.1 M NaOH at the CoPc-cou-f-MWCNT/3-HT|Au interface at increasing scan rates, (B) Plot of E_{pa} vs Log v, (C) Peak current vs scan rate, (D) Plot of log I_{pa} vs log v and (E) Plot of E_{pa} vs log v.*

The CMEs were assessed by DPV to determine their linear responses to PQ when its concentration was varied. The generated calibration curve had a calibration slope of 24.88 M^{-1} and a linear range of 100-1000 μM for the CoPc-cou-*f*-MWCNT/3-HT|Au electrode (**Figure 3.13**). Furthermore, the limit of detection (LOD) and limit of

quantification (LOQ) was calculated to be 0.193 μM and 0.584 μM, respectively. The linear range for detection of PQ by the CoPc-cou-*f*-MWCNT/3-HT|Au electrode is comparable to the biomass-derived electrochemical, chitosan-modified carbon paste electrode (Chit|CPE) which produced a superior linear range of detection width of 1200 μM, refer to **Table 3.2**. Furthermore, a comparable LOD was calculated from the calibration curve for the CoPc-cou-f-MWCNT/3-HT|Au electrode. Our CME electrocatalytically detected PQ in the spiked real water sample with high precision evident from the error bars as well as the R^2 value of 0.9959. Furthermore, the %RSD was calculated to be 4.04 % (value < 5%, N = 3).

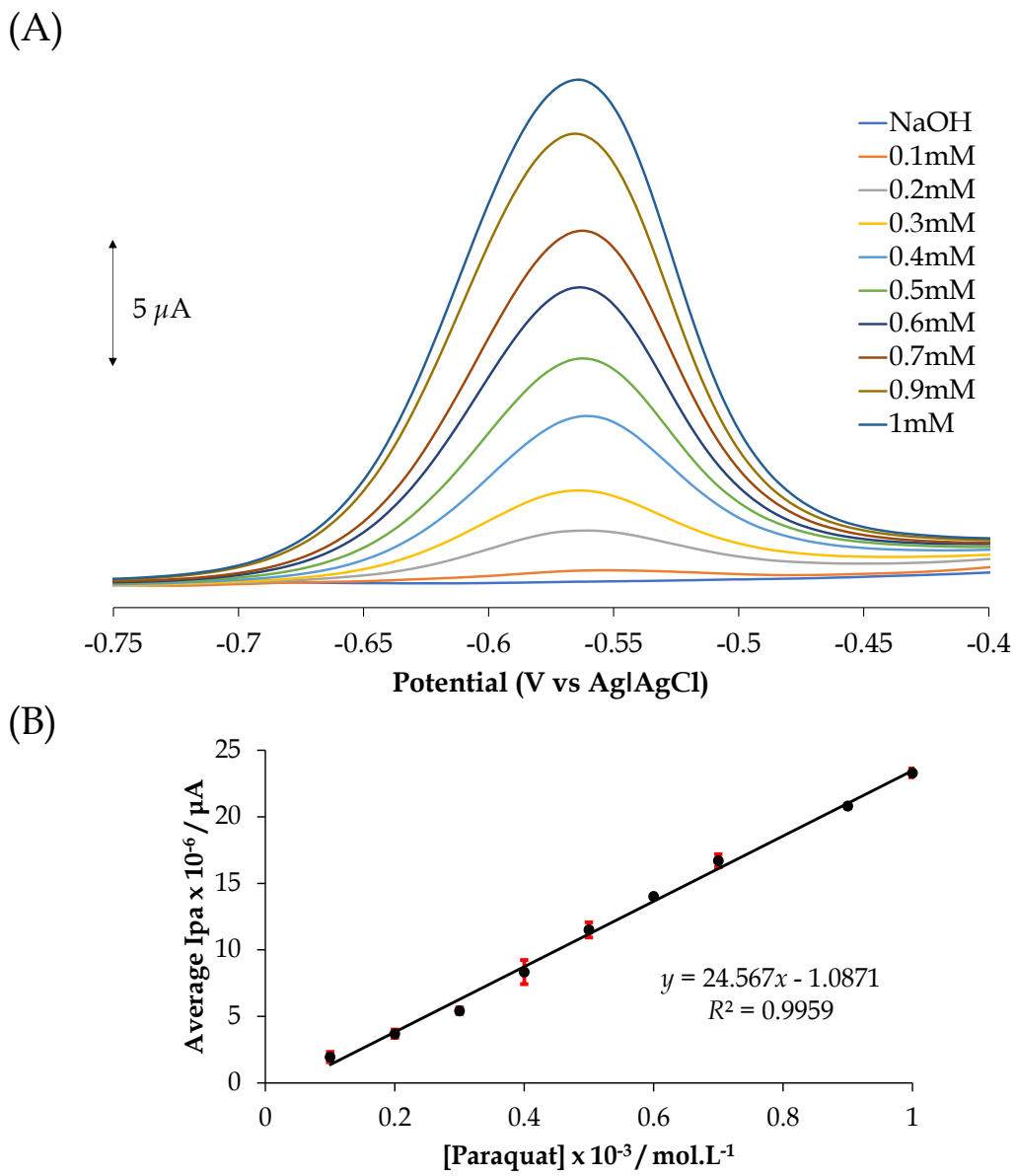

Figure 3.13: *(A) Variation in the DPV current responses with increasing [PQ] in 0.1 M NaOH measured using a CoPc-cou-f-MWCNT/3-HT | Au, (B) Calibration current vs [PQ]. The average %RSD for each data point was below 5%*

.

Table 3.2 : *Compilation of data to compare the performance of different electrodes used for the detection of PQ.*

Electrodes	Method of detection	Limit of detection, (µM)	Linear range (µM)	References
AuNPs/DNA | GE[a]	DPV	1.30	0-1200	63
Chit | CPE[b]	SWASV	0.00782	0.0015-10	96
CoPc | OPG[c]	SWV	0.144	0.5–29.1	97
CCDs | GCE[d]	DPV	0.064	0.1-10	98
CoPc-cou-f-MWCNT/3-HT | Au	DPV	0.193	0.584-1000	This Work
HPLC-MS	-	124	374-1000	This Work

[a] Gold nanoparticles DNA-modified gold electrode.

[b] chitin-modified carbon paste electrode.

[c] Cobalt phthalocyanine-modified ordinary pyrolytic graphite electrode.

[d] carboxylate pillar,

[e] arene-coated nitrogen-doped carbon dots modified glassy carbon electrode

3.3.5. HPLC-PDA/MS analysis of PQ

3.3.5.1. Instrument Calibration and Validation

The calibration standards of PQ were prepared in ultra-pure water within the range of 0.1 - 1 mM. Ten microlitres of each standard were injected into a 4.6 mm x 150 mm C18 reverse phase column set at 35 ^{o}C. PQ was eluted through a gradient protocol of 20 mM. NH_4HCO_2 in UPW and 20 mM NH_4HCO_2 in ACN from 90:10 to 30:70 over 20 mins with a 5 min re-equilibration time. The LC- PDA flow rate, injection volume and wavelength were optimized to be 0.1 mL/min, 10 μL and 258 nm, respectively.[99-101] Ammonium formate (NH_4HCO_2) was utilized to induce the formation of in situ ion-pair adducts with the aqueous PQ di-cations.[102] These adducts are relatively non-polar and therefore improved the problem of peak tailing and reduced the retention time of the analyte. PQ was detected by scanning the photodiode array (PDA) detector in the full wavelength range or on the interfaced mass spectrometric detector.

The calibration curve (peak area *vs* [PQ] of the LC-MS is shown in **Figure 3.14**. A sensitivity of 28.9 M^{-1} in the linear range of 0.1 - 1.0 mM (R^2 = 0.9722) was attained. The LOD and LOQ for PQ were estimated to be 124 μM and 375 μM, respectively. Noticeably, the precision of our CME is better than that using the LC-MS due to the higher correlation coefficient of the former. Moreover, the LOD and LOQ of the CME are significantly lower than those for the HPLC-MS indicating that the CME has a higher sensitivity for PQ.

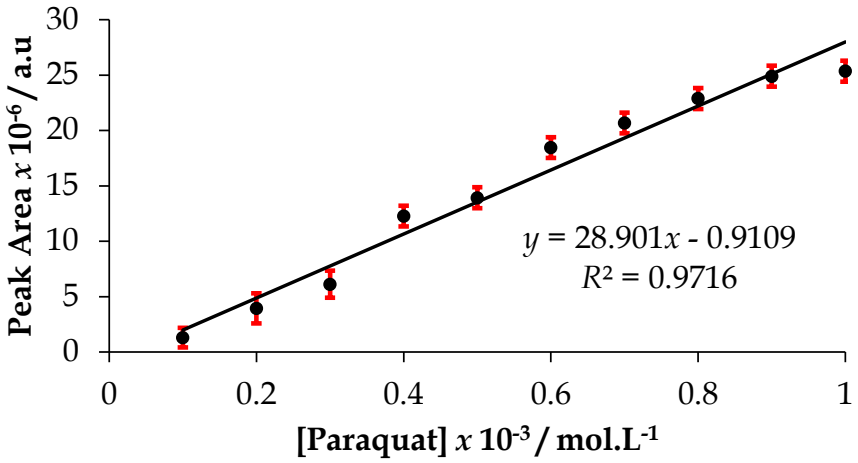

Figure 3.14: *Calibration curve (peak area vs PQ concentration) of PQ using LC-PDA/MS.*

Before HPLC-MS analysis of PQ in the real sample, the analyte was pre-extracted and concentrated by mSPE on a column packed with a Strata-X or strata-XC mSPE stationary phase. The four steps of conditioning, loading, washing and elution were optimized following the generic method initially reported by Wang.[103] Strata-X comprises polarizable cyclic amide (lactam) groups which are weaker cationic exchangers and are only suitable for the retention and preconcentration of polar compounds. Unlike Strata-X, the Strata-XC stationary phase contains strong organo-sulfonyl functional groups (cation exchange sites) that can differentially partition and retain (separate) a mixture of PQ and other cationic groups found in the sample matrices with good resolution. The SPE sample work-up steps were essential to reduce the complexity of the real sample matrices. Subsequently, this would ensure the attainment of more intense and well-resolved HPLC peaks, thus leading to good percentage recoveries for PQ.

The Strata-X stationary phase was pre-conditioned with methanol (ca. 3.0 mL) followed by loading the aqueous solution of PQ (ca. 3.0 mL) on the cartridges. Chloroform (ca. 3.0 mL) was used to wash polar organics from the loaded samples due

to their high solubility in the solvent. Finally, PQ is more soluble in aqueous media than most organic media, it was eluted using 3.0 mL of ultrapure.

Extract from the Strata-X did not result in detectable PQ peaks either on the PDA or mass spectrometer detectors at this volume. To avoid saturating the cartridges with excessive amounts of PQ (spiked samples), the steps for the Strata-X mSPE protocol were carried out at a lower loading volume of 1.5 mL and the volumes used for the other steps were accordingly scaled down by the same factor. It was assumed the Strata-X phase had poor retention of PQ and thus the analyte was lost into the wash solvent in the third step of the procedure The main steps for the Strata-X mSPE were then used on the Strata-XC mSPE protocol as illustrated in **Figure 3.15**. Extracts of the real water sample from Strata-XC mSPE did not yield detectable peaks. However, the spiked water sample gave detectable PQ peaks on the PDA/MS peaks from which the % recovery of the analyte could be calculated.

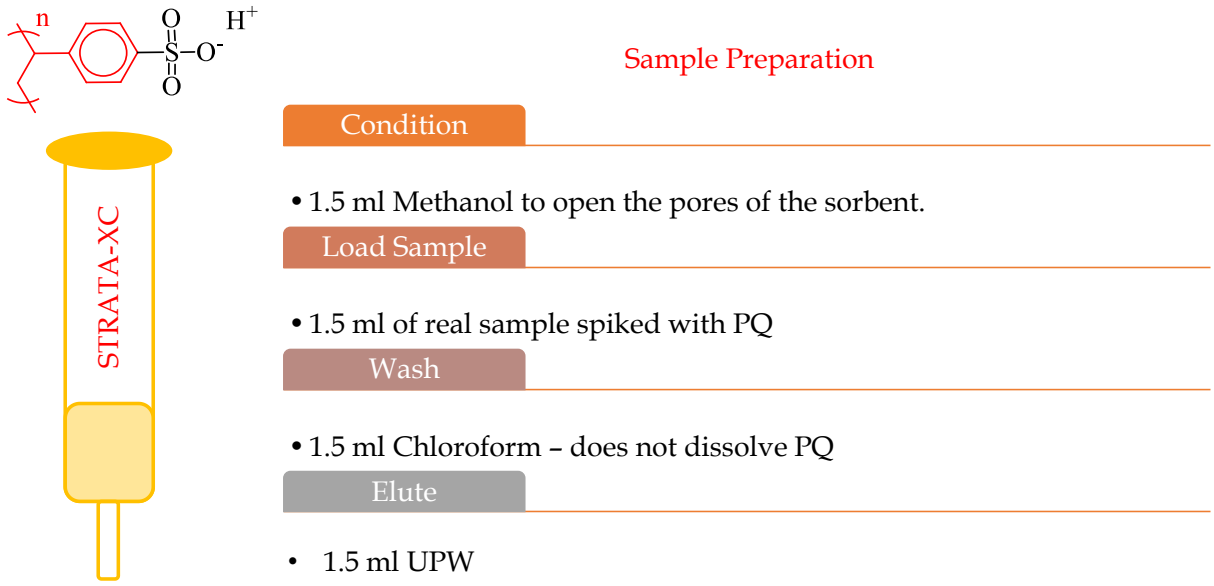

Figure 3.15: *Illustration of the Strata-XC mSPE sample preparation steps used to extract and preconcentrate PQ before its HPLC-PDA/MS analysis.*

3.3.7. Comparative real sample analysis using the CoPc-cou-f-MWCNT/3-HT/Au modified electrode and HPLC-PDA/MS.

The CoPc-cou-*f*-MWCNT/3-HT Au modified electrode was thereafter probed in real samples to determine its practical use for the analysis of paraquat in samples collected from the Umhlanga Lagoon, which was presumably polluted post the arson attack on the warehouse in Cornubia. The concentration of PQ in the sample was below the LOD of the CME, therefore the standard addition technique was employed to determine the % recovery to provide insight into the applicability of the CME sensor. As displayed in **Figure 3.16**, 1 mM standard of PQ was added to the real samples in increments of 1 mL, the percentage recovery was determined to be 86% ± 14 with a %RSD of 9.55 %. This can be attributed to the fouling on the surface of the electrode due to multiple interfering species in the real sample given the water was heavily contaminated with a cocktail of other chemicals in unknown quantities. However, as shown in **Figure 3.16**, the CME did display fairly good reproducibility despite the effects of fouling.

For comparison, the same water sample was spiked with six incremental volumes (1.0 mL) of the 1 mM standard of PQ and pre-extracted and concentrated using the outlined Strata-XC mSPE protocol (vide supra) for subsequent analysis using HPLC-MS. The standard addition plot of the data is shown in **Figure 3.17**. The percentage recovery of the spiked PQ using the optimized sample preparation method was calculated to be 97%. Direct analysis of PQ in the water, sample without pre-extraction, and concentration of PQ by Strata-XC mSPE did not yield detected peaks of PQ. This emphasized the significant improvement in HPLS-PDA/MS signals for the PQ in the water samples if it was purified and concentrated by the mSPE before quantitative analysis. Strata-XC mSPE efficiently removed species in the water sample which could have contributed to fouling of the CoPc-cou-*f*-MWCNT/3-HT|Au in the electrochemical analysis of PQ.

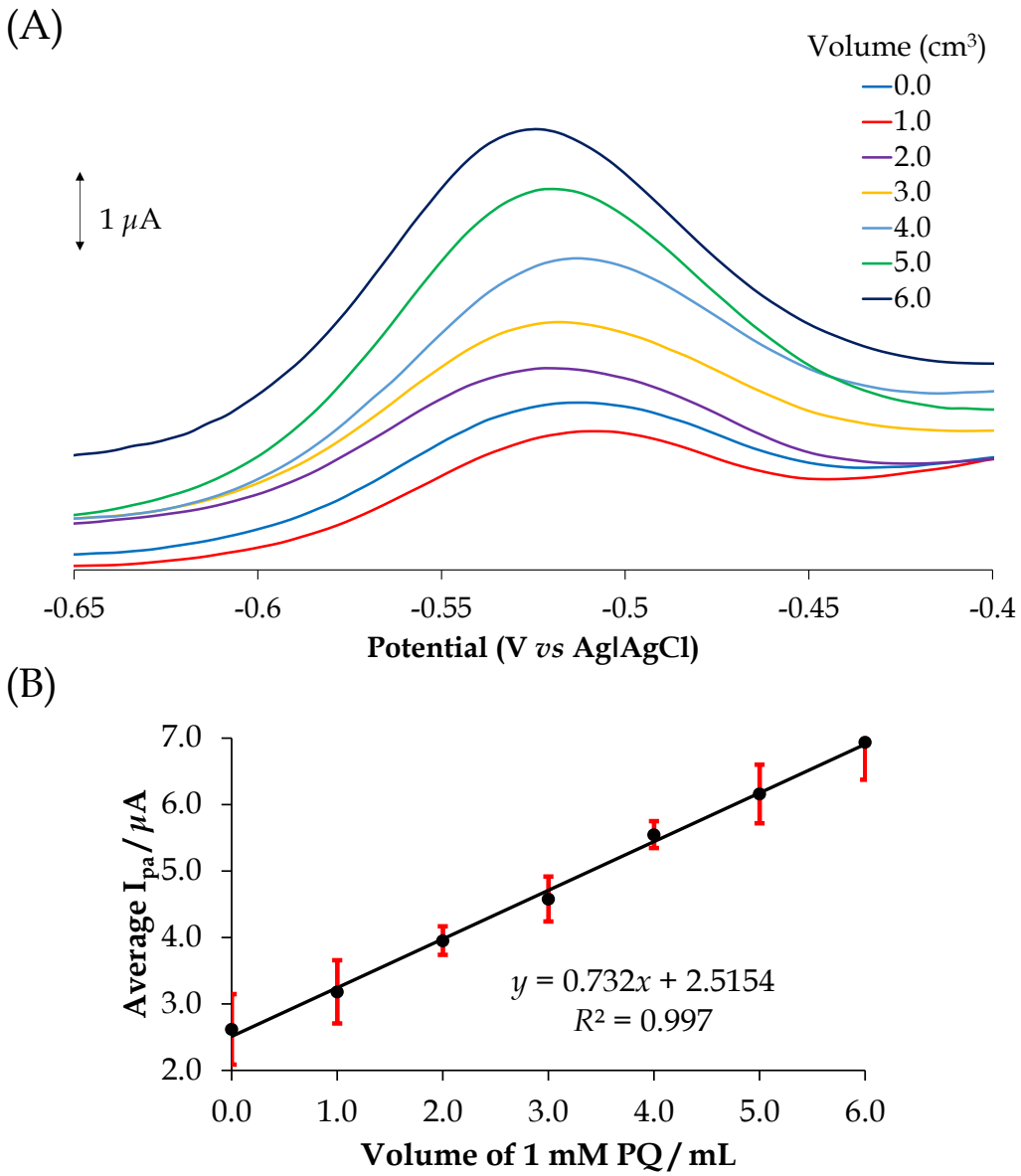

Figure 3.16: *(A) Overlay DPVs of the real water sample spiked with incremental volumes (1.0 mL) of the 1 mM standard of PQ at the CoPc-cou-f-MWCNT/3-HT | Au collected from the Umhlanga Lagoon, (B) The standard addition calibration plot.*

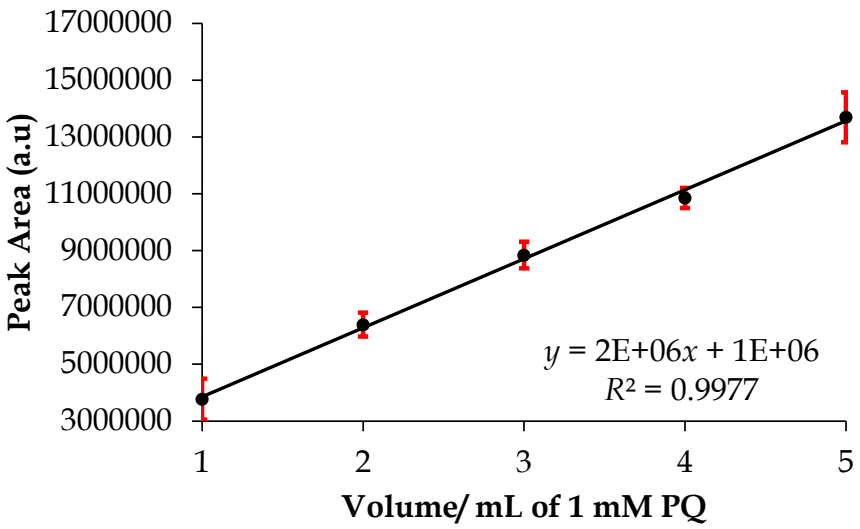

Figure 3.17: *Standard addition plot of pre-treated real samples using HPLC-MS.*

CHAPTER FOUR

Immobilization of cobalt phthalocyanine-imbedded electrospun nanofibers on a gold electrode for the electrocatalytic detection of mercury(II)

4.1. Introduction

Several provinces within the Republic of South Africa (RSA) have recently been inundated with various cases of water pollution. One of the main culprits for the water woes of the RSA has been failing local municipal infrastructure caused by poor maintenance and poor urban planning as well as uncharacteristic climate change-related serve storms. In addition, secondary sources of water pollutions arise from the leaching of industrial and farming fertiliser-based effluents into fresh- and salt-water bodies.[104, 105]

These effluents and sewage-spills contains a host of toxic pollutants of which the environmentally persistent heavy metal, mercury is typically among them. Mercury is a neurotoxin which has associated with serious health effects such as seizures, memory loss and renal dysfuction.[7] Traditional methods used for the qualitative and quantitative determination of mercury, such as inductively coupled plasma–optical emission spectrometry (ICP-OES), inductively coupled plasma–mass spectrometry (ICP-MS) and direct mercury analyser (DMA), provides accurate detection at low concentrations.[106] However, these techniques are unsuitable for real-time on-site analysis as they are expensive and stationary instruments which requires skilled technician to operate.

Furthermore, the procedures for sample preparation is time-consuming and complex.[107, 108]

Within the RSA's context and in other developing and third-world countries, there is a need for an inexpensive miniaturized system that can reliably and remotely detect mercuric species within real water samples. In fact, the Hg-electrocatalytic activities of MPcs and their nanoarchitectures immobilized on various substrates have been widely documented.[19, 109] These chemically modified electrodes (CMEs) display distinctive Hg signals with good reproducibility and precision. Currently, greater emphasis is placed on limiting the leaching of MPc redox mediators from the modifier layer and limiting surface fouling through the inclusion of them into conductive electrospun nanofibers.[110]

The electrocatalytic activities of electrospun nanofibers (ENFs) and their nanocomposites are currently being widely investigated for applications in fuel cells, supercapacitors and detectors.[111-113] ENFs are versatile nanostructures that can be easily functionalized with the covalent attachment of organic, inorganic and composite materials making them highly favourable with respect to altering their physical, chemical and mechanical properties for the relevant application.[114] Advantageously, ENFs have a higher surface area than their bulk polymer which in turn translates into higher effective electrocatalytic areas on chemically modified electrodes.[115] In addition, ENFs can interact with metallic substrates through directional bonding of their functional groups rendering stabile CMEs.[116] In contrast, to CMEs containing adsorbed electro-active dopants, the incorporation of electro-active dopants within the polymeric ENF matrix negates the leaching of these dopants from electrodes containing ENFs-dopants electron-mediating layers.[117] Polyaniline (PANI) is an electrically conductive polymer widely utilised due to it being inexpensive, easy to synthesise and its exceptional redox behaviour.[118, 119] Furthermore, polyvinyl alcohol (PVA) has a high water content aiding the ease of formation of electrospun nanofibers while retaining properties of non-toxicity and limited restrictions on diffusion.[120]

During this study, the nanofabrication and characterization of CoPc-cou-ENFs will be demonstrated and its functioning as an electrocatalyst on an Au substrate was examined. It was foreseen that the synergistic effects of the ENF constituents would enhance the electron-mediating effects and also encourage selective uptake of Hg(II) cations where they can undergo electrocatalytic transformations. Beside the electrical conductivity, the complementary interactions between the functional groups of the polymers will induce strong intermolecular interactions between themselves and the CoPc-cou molecules and Au substrate affording anti-leaching effects and CME stability. The CoPc-cou-ENFs adhesion layer of the modified Au electrode was sealed using an ion-permeable and negatively charge Nafion (Nf) which will entrap the heavy metal cation within its cavities prior to their diffusion to the adhesion layer. The CME CoPc-cou-ENFs-Nf|Au was applied in percentage recovery studies of mercury using a real water sample attained from Umhlanga lagoon and method validation was affirmed by its close correlation with the same real water samples re-analysed by Inductively Coupled Plasma Optical Emission spectroscopy (ICP-OES).

4.2. Experimental

4.2.1. Materials

The following chemical reagents: 4-nitrophthalonitrile, 7-mercapto-4-methyl coumarin, cobalt(II) chloride, potassium carbonate, mercury(II) sulfate, potassium ferricyanide, sodium sulfate, copper sulfate and sodium chloride were purchased from Merck-Sigma Aldrich and were used for the synthesis of ligand, complexes as well as for the electrochemical experiments. Polymeric constituents such as polyaniline, polyvinyl alcohol and Nafion were sourced from Capital Research Distributors (CRD). The synthesis of ligand and metal complex, CoPc was synthesised according to literature[54, 55] discussed in detail in Chapter 3. All mercury-containing standards and samples were handled according to laid down standard operating procedures (SOPs) for handling and

disposal of hazardous wastes to ensure a safe working environment and containment of downstream pollution.

4.2.2. Fabrication of CoPc-cou electrospun nanofibers (CoPc-ENFs)

A viscous polymer blend was formulated from the vigorous stirring of 0.10 g of polyvinyl alcohol (PVA) in 10 mL of ultrapure water at 80 ^{o}C until a consistently blended emulsion was attained. Thereafter, 0.05 g of CoPc-cou and 0.05 g of PANI were added to the mixture and then it was stirred at 30 ^{o}C overnight to form the homogenous PVA-PANI-CoPc-cou bulk polymer blend. Subsequently, this bulk polymer blend was transferred into a 5 mL syringe, which was fitted to the syringe driver of the Inovenso nanospinner 24 electrospinning instrument. Afterwards, the polymer nanofibers were fabricated under the following optimized instrument parameters included 35.0 kV, a spinneret ejection flow rate of 0.60 mL/h and a sheet of aluminium foil fitted flat onto the collector unit which was automatically placed at a distance of 10 cm from the spinneret.

4.2.3. Electrode modification

The bare gold (Au) electrode was cleaned by repeated immersions in a hot Piranha solution (*i.e.* a mixture of concentrated hydrogen peroxide and sulphuric acid in a 3:1 volume ratio) for 30 seconds at a time. Then it was rinsed repeatedly in ultrapure water to avoid damage to the plastic housing of the bare electrode. This was followed by polishing the Au electrode surface on a Buehler felt pad loaded with a 0.5 μm alumina paste. Finally, the electrode was ultrasonicated in acetone for 5 minutes before rinsing with ultrapure water to ensure any adsorbates that may have remained on the electrode surface were removed. Afterwards, the CoPc-cou-ENFs suspension in DMF was drop cast onto the electrode surface and thereafter immobilised by thermal annealing of Nafion in the oven (30 ^{o}C) to afford the modified electrode, CoPc-cou-ENFs-Nf|Au.

4.2.4. Parameters of ICP-OES

A Shimadzu ICPE-9820 was used to analyze mercury samples at a radio frequency of 1.2 kW. Argon gas was used as a cooling, auxiliary and nebulising/carrier gas at 9.99, 0.60, 0.70 L min^{-1}, respectively and to purge the system under a pressure of 417.96 kPa. The spray chamber was set at a temperature of 38° C in axial measurement mode. The peristaltic pump was used under low settings with a rotation speed of 20 r.p.m.

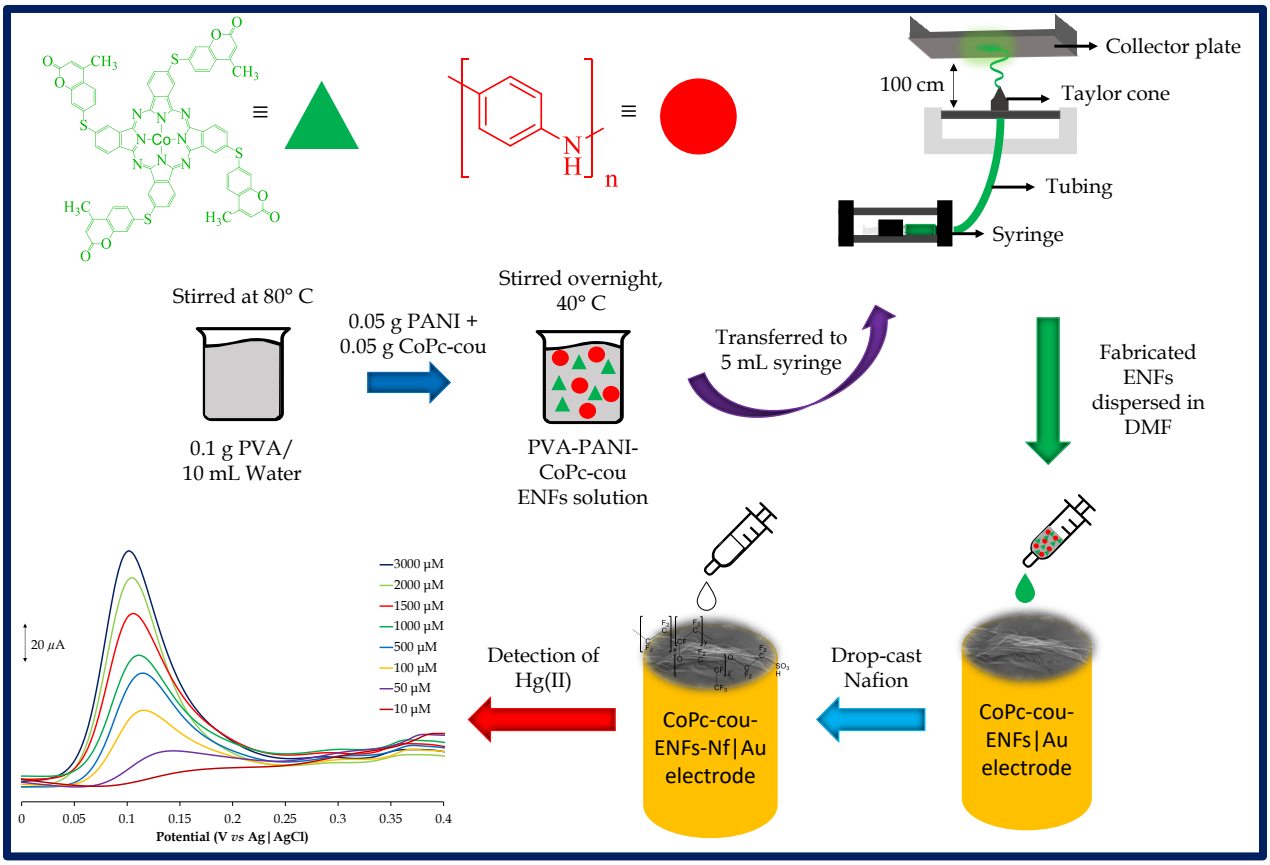

Scheme 4.1: *Illustration of the process of modification for the CoPc-cou-ENFs-Nf|Au.*

4.3 Results and Discussion

4.3.1. Nanofabrication and characterization of CoPc-cou-ENFs

Nanofabrication of the CoPc-cou-ENFs was performed by electrospinning a homogenous mixture of the bulk polymeric blend comprising of a conductive polymer,

PANI[121], an inorganic redox mediator, CoPc-cou and a stabilizing polymer, PVA[122] which aids to the processability of the ENFs by enhancing mechanical strength. The nanofabricated metal complex-ENFs initially accumulated as a well-dispersed nano-mat flat on the aluminium foil but later agglomerated as a spider-web microstructure on top of the nano-mat of ENFs, see **Figure 4.1**. This in turn emphasizes the importance of carefully controlling the solution and instrumental parameters to ensure the fabrication of monodispersed ENFs.

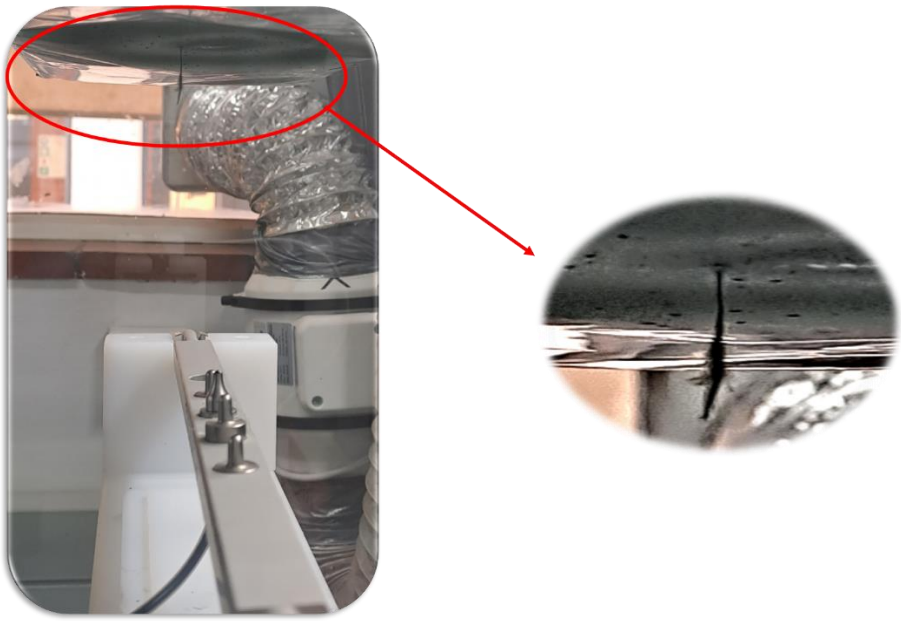

Figure 4.1: *Images of the CoPc-cou-ENFs collected on aluminium foil fitted to a flat collector plate.*

The morphological features and elemental composition of the CoPc-cou-ENFs were probed by SEM-EDX while the inclusion of the macrocyclic metal complex was affirmed through Powder X-ray diffractometry and Raman spectroscopy. The powder X-ray diffraction (PXRD) pattern for PANI displays typical peaks at 25.8°, 20.3° and 15.2° corresponding to the (200), (020) and (011) lattice planes.[123] Furthermore, the PXRD

spectrum of the CoPc exhibits broad but semi-coalescing peaks within the 2θ range of 13-27^{o} as well as a sharp spike at 19.1^{o} (104) and a peak at 26.7^{o} (026) that can be attributed to the diffraction planes of its CoPc's metal core and the sulphur atoms, respectively.[124, 125]

Noteworthy is that the PXRD pattern of the CoPc-cou-ENFs shows only one broad peak at a 2θ angle of 18.9^{o}. This broad peak predominately masks peaks associated with the PANI and CoPc but sharp peaks at 2θ = 21.4 ^{o} and 23.7 ^{o} suggest that the nanocomposite includes all the constituents. Furthermore, the broad and poorly resolved PXRD peak of the CoPc-cou-ENFs indicates the amorphous nature of the PANI polymer and the metal complex.

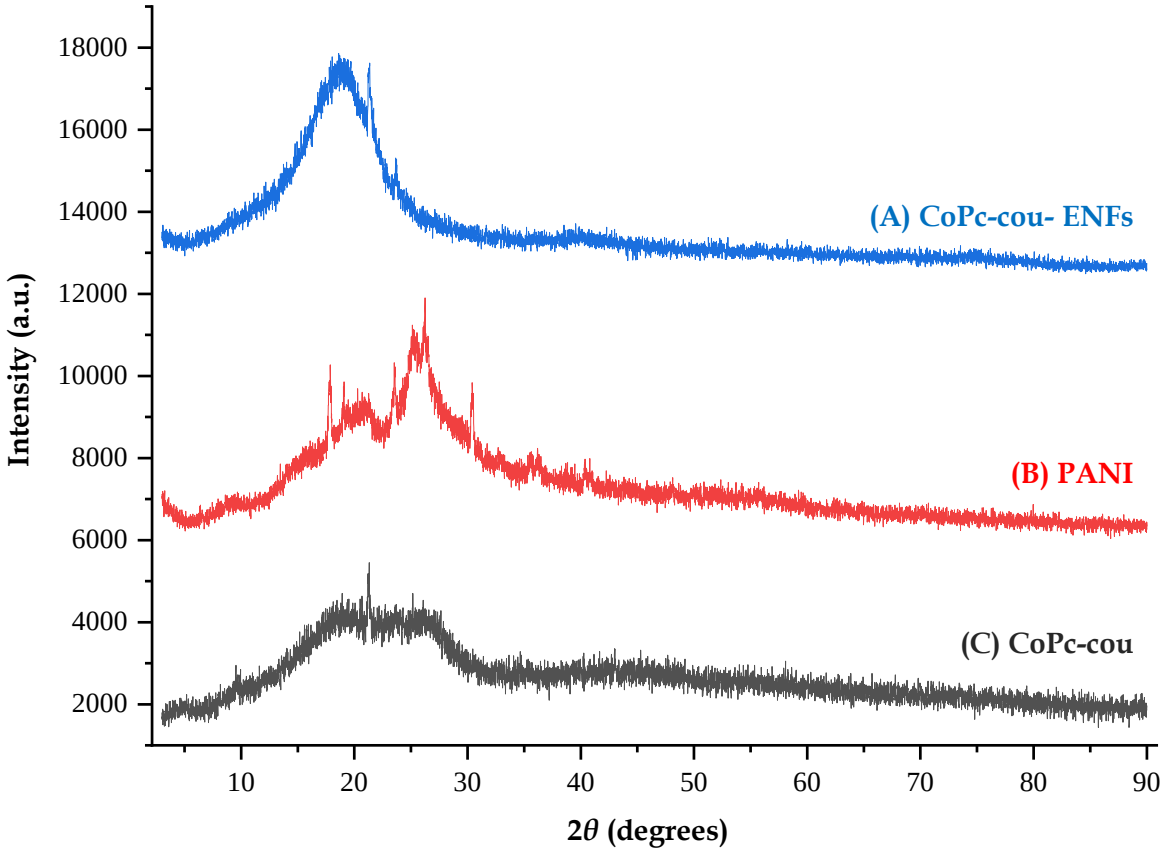

Figure 4.2: *PXRD patterns of (**A**) CoPc-cou-ENFs, (**B**) PANI and (**C**) CoPc-cou.*

In addition, Raman spectra of the constituent and CoPc-cou-ENFs were collected to ascertain functional groups within the nanofabrication (**Figure 4.3**). A broad peak at 1584 cm^{-1} appears in the spectra of the CoPc-cou and corresponds to the B_{1g} fundamental mode of vibration characteristic of vibrational deformations in the D_{4h} symmetry of the MPc.[126] This vibrational peak can be readily accounted to the stretching occurring within the C=N bonds within pyrrole moieties and is comparable to analogous signals of other symmetrical metalated phthalocyanines.[127] Furthermore, the Raman spectrum of PANI shows non-symmetrical broad peaks at 818, 1191 and 1615 cm^{-1} which corresponds to the out-of-plane deformations as a result of vibrations of amine and aromatic functional groups within the polymer chains.[128] Comparative Raman spectral analysis of the CoPc-cou-ENFs with those of PANI and the CoPc-cou indicate that the Raman spectrum of the nanocomposite has admixture character where it contains overlapping peak of the metal complex and the polymer. Thus, these spectral trends corroborate the nanoconjugation of the CoPc-cou with PANI *via* electrospinning.

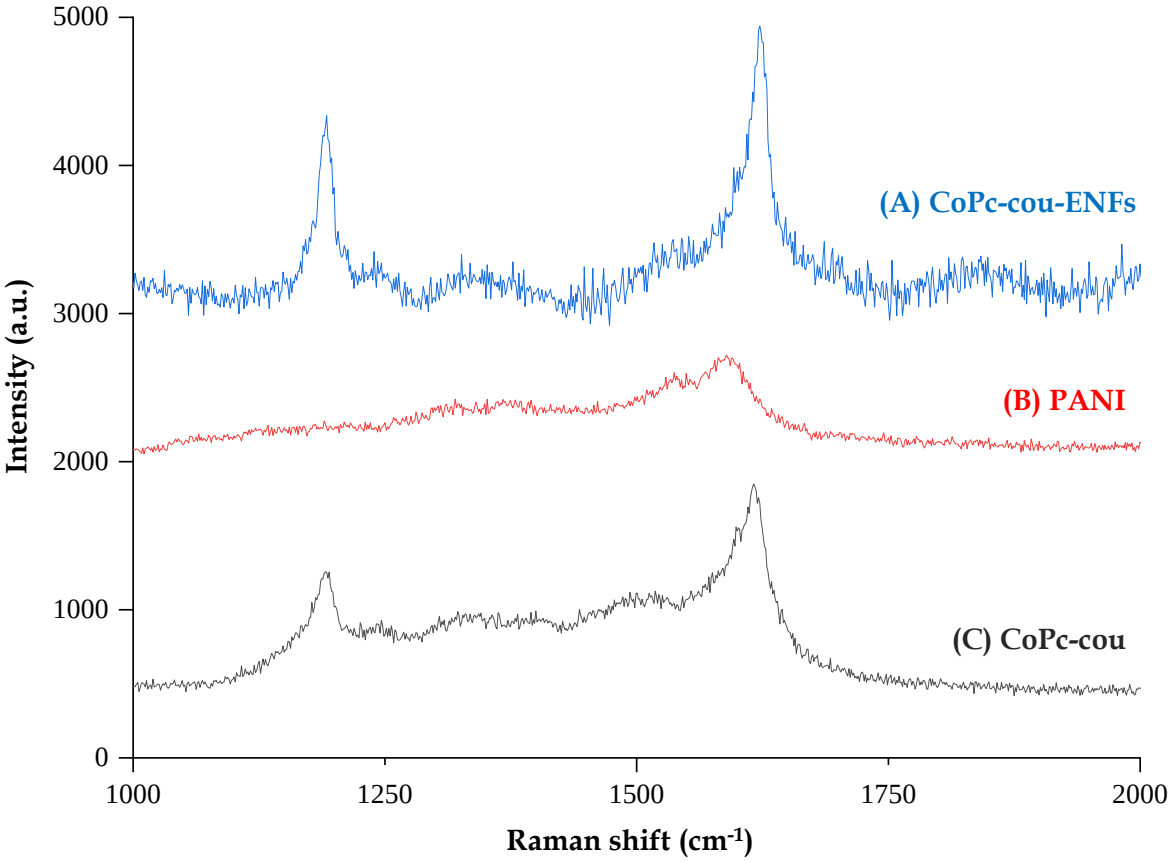

Figure 4.3: *Raman spectra of (**A**) CoPc-cou-ENFs, (**B**) PANI and (**C**) CoPc-cou.*

To visualize the surface morphology of the CoPc-cou-ENFs, scanning electron microscopy (SEM) was utilized. The SEM image of the CoPc-cou complex in **Figure 4.4A**, displays clustered nanostructures with interstitial irregular crevices which is characteristic of MPcs as they are prone to aggregation. Furthermore, the crevices make the surface rough and semi-porous leading to an increase in the effective surface area of the substrate if used as an electrode modifier nanomaterial.[129] In comparison, PANI exhibits a fibrillar morphology due to its polymerized chain structure[130] with a corresponding EDX spectrum containing only C and N atoms, see **Figure 4.4B**.

Unlike the constituents, the image of the CoPc-cou-ENFs shows a nanomaterial whose microstructure comprises thin and filamentous spider-web fibres, see **Figure 4.4C**.

According to the EDX spectrum, these ENFs contain the following elements, C, N, O, S and Co and the presence of these corroborates the incorporation of the individual constituents particularly the CoPc-cou complex into the ENFs. Furthermore, elemental contour mapping images confirms the presence of all elements directly on the surface of the CoPc-cou-ENFs with elemental compositions of S, N, O and Co, see **Figure 4.4D.**

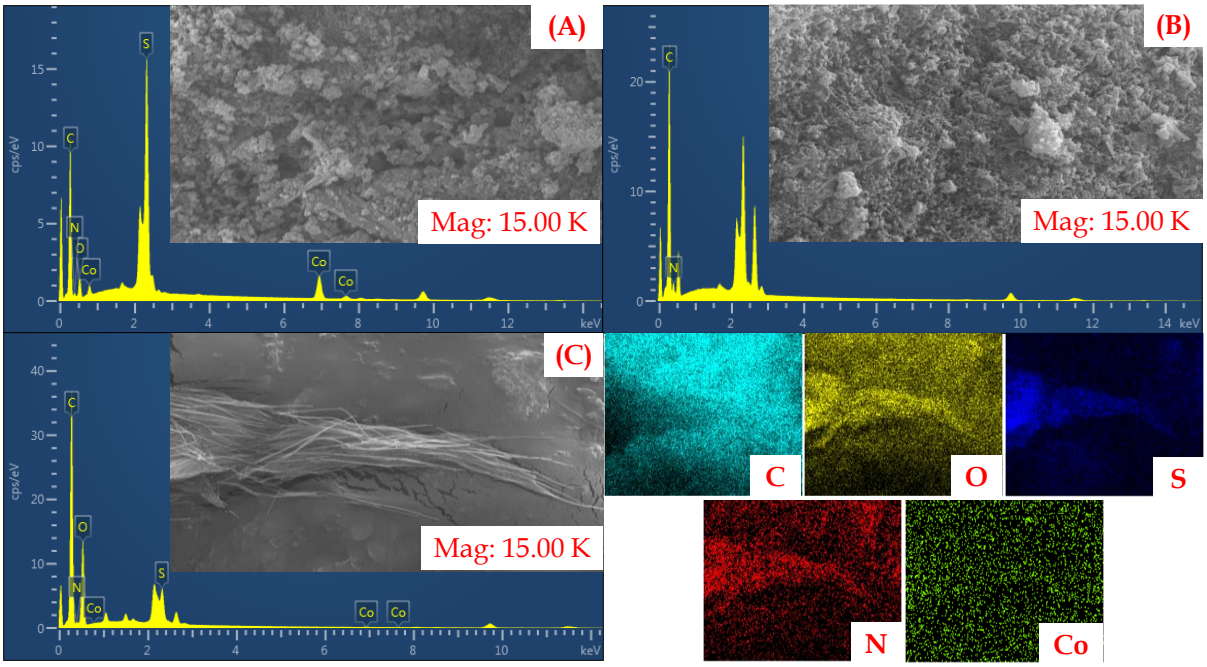

Figure 4.4: *SEM micrographs and EDX spectra of (**A**) CoPc-cou, (**B**) PANI-PVA-ENFs (**C**) and CoPc-cou-ENFs as well as the elemental mapping (viz. C, O, N, S and Co) of the CoPc-cou-ENFs.*

4.3.2. Comparative electron-transfer behaviours.

The influence of different redox mediators on the electron transfer behaviours of a standard redox probe, $K_3[Fe(CN)_6]$ was investigated using the bare Au and different CMEs (**Figure 4.5**). It was evident from the cyclic voltametric data that the immobilisation of PANI on the bare substrate led to a minor increase in the electron transfer rates ($\Delta E_{ferrocene}$ = 0.13 V for bare Au and 0.10 V for PANI | Au electrodes) and limited Fe(III) cation blocking effects. The CoPc-cou | Au electrode afforded the fastest electron transfer kinetics with a peak-to-peak potential difference of 0.05 V while its comparable peak

current suppression observed to the Nf | Au electrode relates to their electron-mediating films having a similar degree of Fe(III) permeability. The thin film of CoPc-cou-ENFs | Au electrode entirely passivates the substrate surface leading to no detectable redox signals which implies that this thin film is compact with essentially no effects.

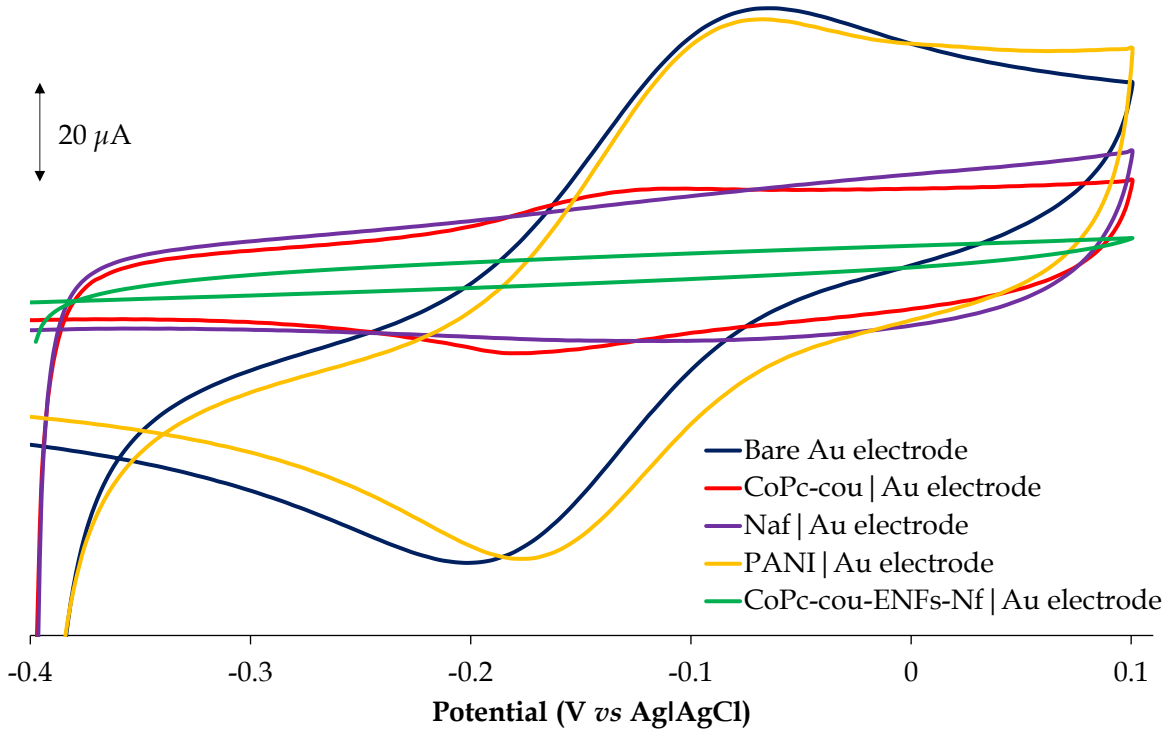

Figure 4.5: *Overlay CVs in a 5.00 mM $K_3[Fe(CN)_6]$ in 0.1 M KCl monitored at the bare Au, PANI | Au, Naf | Au, CoPc-cou | Au and CoPc-cou-ENFs | Au electrode surfaces.*

Similar trends were observed when examining the redox properties of the CoPc-cou-ENFs | Au electrode in other redox probe solutions, namely 1.00 mM solutions of Na_2SO_4 and $CuSO_4$ prepared in ~~a~~ pH 4 buffer (**Figure 4.6**). The current responses by the CoPc-cou-ENFs | Au electrode in both redox probe solutions are fully inhibited compared to that of the bare Au electrode, suggesting no ion-permeability within the ENFs film. This provides further confirmation that the electrode modifiers are a charge-passivating nanocomposite. This is not surprising given the bulk of the polymeric constituent in the

nanocomposite ENFs is PVA and it is inherently insulative. A consolation to this is the high catalytic loading of the CoPc-cou-embedded ENFs as shall be discussed ahead.

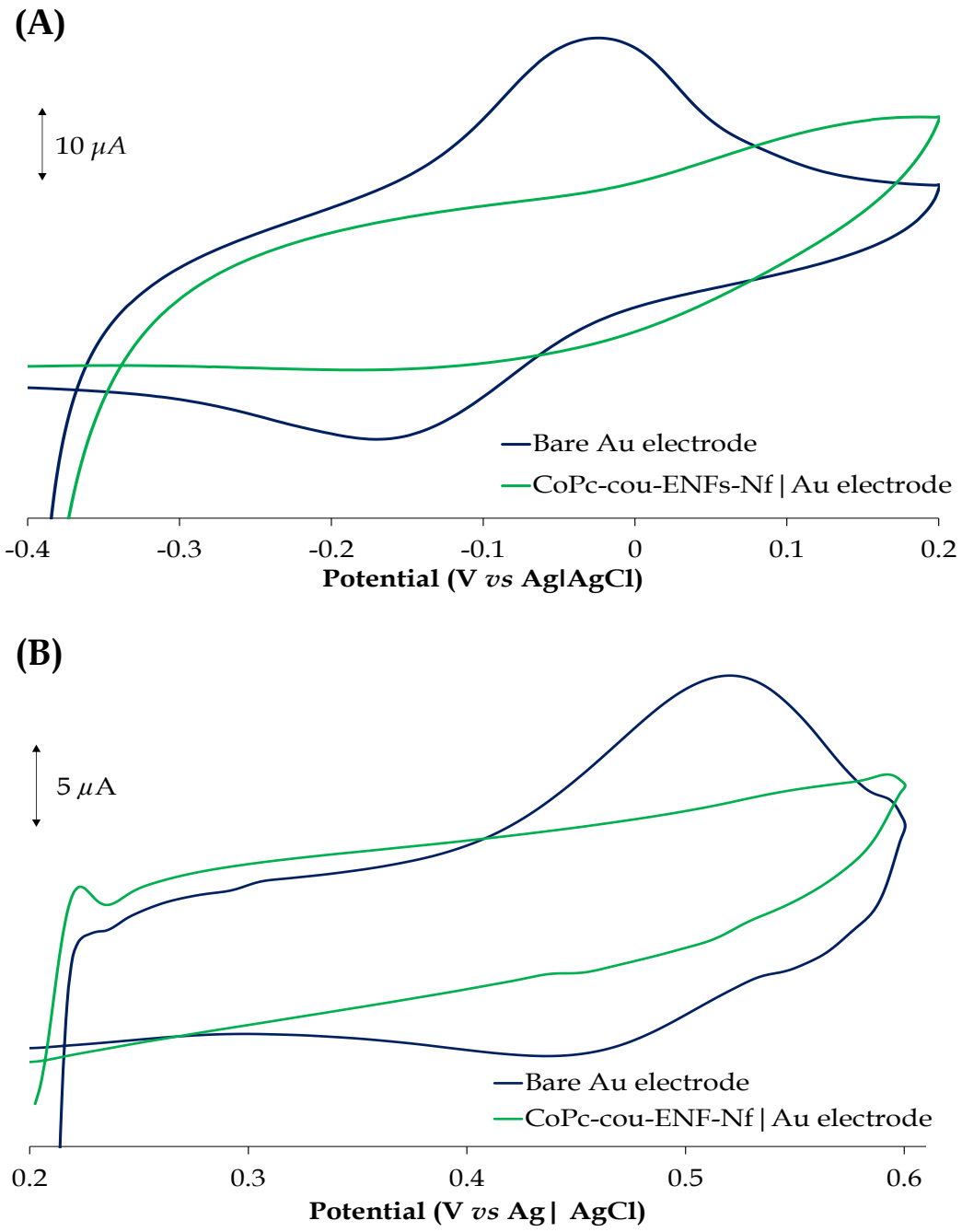

Figure 4.6: *Overlay CVs of 1 mM solutions of (**A**) $CuSO_4$ and (**B**) Na_2SO_4 in pH 4 buffer occurring at the bare Au and CoPc-cou-ENFs | Au electrode interfaces.*

4.3.3. Electrochemical impedance spectroscopy (EIS) of CMEs in 5 mM $K_3[Fe(CN)_6]$.

Electrochemical impedance spectroscopy gives insight into the electron transport characteristics displayed by the bare and modified electrodes. This can be deduced from the electron charge transfer resistance within a frequency range of 0.1 to 100 Hz. The experimental data was fitted to an equivalent circuit ([R(Q(RW))]) displaying the charge transfer resistance (R_{CT}), supporting electrolyte resistance (Rs), constant phased element (CPE) and the Warburg impendence (Zw). The CPE is introduced to model deviations from ideal capacitance behaviour that is associated with surface porosity and roughness due to the surface modifier.[131] Furthermore the Warburg impedance accounts for additional resistance due to redox species and diffusion of Fe(III) cations to the electrode surfaces.[131]

From the Nyquist plots depicted in **Figure 4.7**, it is evident that the CoPc-cou-ENFs|Au modified electrode limits charge transfer indicated by the semi-circular shape of the plot.[132] This is indicative of the passivation of the electrode towards the analyte which corroborates the CV data obtained. Additionally, **Table 4.1** indicates the quantitative data displaying the largest charge transfer resistance for the chemically modified electrode (Rct of 1.94 Ω) which implies that it is the least conductive. The CoPc-cou-ENFs|Au modified electrode can also be seen to have the highest CPE which is due to the high surface area that the ENFs occupy on the electrode surface.[133] Considering the value of CPE for the CME, as well as that a value of $n = 1$ indicates a homogenous, smooth surface, we can deduce that there is high surface roughness associated with the CoPc-cou-ENF|Au modified electrode, where $n = 0.683$.[134] The deviation from homogeneity for the bare Au electrode (n=0.903) can be attributed to surface roughness due to regeneration of the surface using a piranha solution as well as excessive cleaning of the bare electrode on polishing pads. Furthermore, the bode plots for the bare and modified Au electrodes (**Figure 4.8**) display angles less than 90 º indicating that the electrodes exhibit behaviour that deviates from an ideal capacitor, and thus are more conducive for charge transfer.[135]

Table 4.1: *Compilation of EIS data obtained in a 5 mM $K_3[Fe(CN)_6]$ solution using the bare and modified gold electrodes (with percentage errors indicated in brackets).*

Au Electrode	R_S (Ω)	R_{CT} (Ω)	Z_W (μMho)	CPE (μMho)	$^a n$
Bare (| Au)	100.7 (±0.4)	1.05 (±4.3)	196 (±2.1)	33.7 (±5.1)	0.903 (±1.2)
CoPc-cou | Au	129.4 (±2.4)	1.47 (±1.6)	376 (±4.3)	242 (±5.3)	0.701 (±2.2)
PANI | Au	85.9 (±1.8)	1.14 (±5.0)	522 (±1.5)	300 (±5.0)	0.697 (±1.8)
Naf | Au	177.4 (±1.2)	1.59 (±1.8)	206 (±4.1)	85.6 (±1.6)	0.884 (±0.7)
CoPc-cou-ENFs | Au	438.5 (±3.9)	1.94 (±7.4)	908 (±7.3)	672 (±7.2)	0.683 (±2.5)

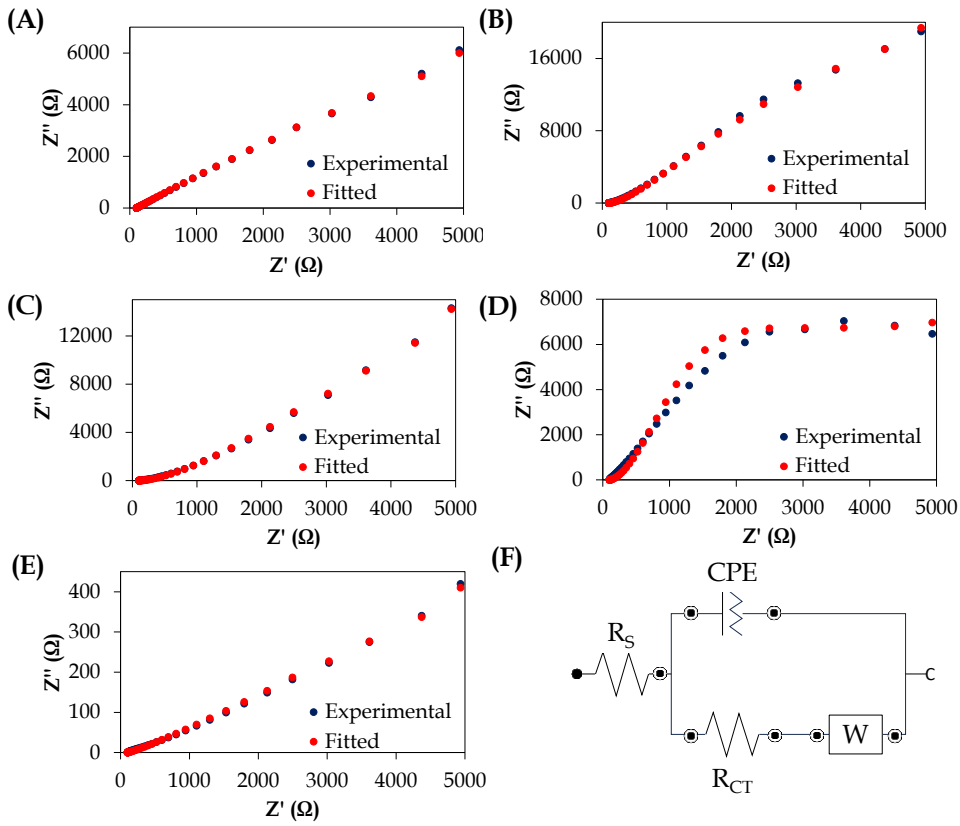

Figure 4.7: *Overlay experimental and fitted Nyquist plots obtained in a 5 mM $K_3[Fe(CN)_6]$ solution using the (**A**) bare, (**B**) CoPc-cou|Au, (**C**) Naf|Au, (**D**) PANI|Au, (**E**) CoPc-cou-ENFs|Au and (**F**) their corresponding circuits used to fit the EIS data.*

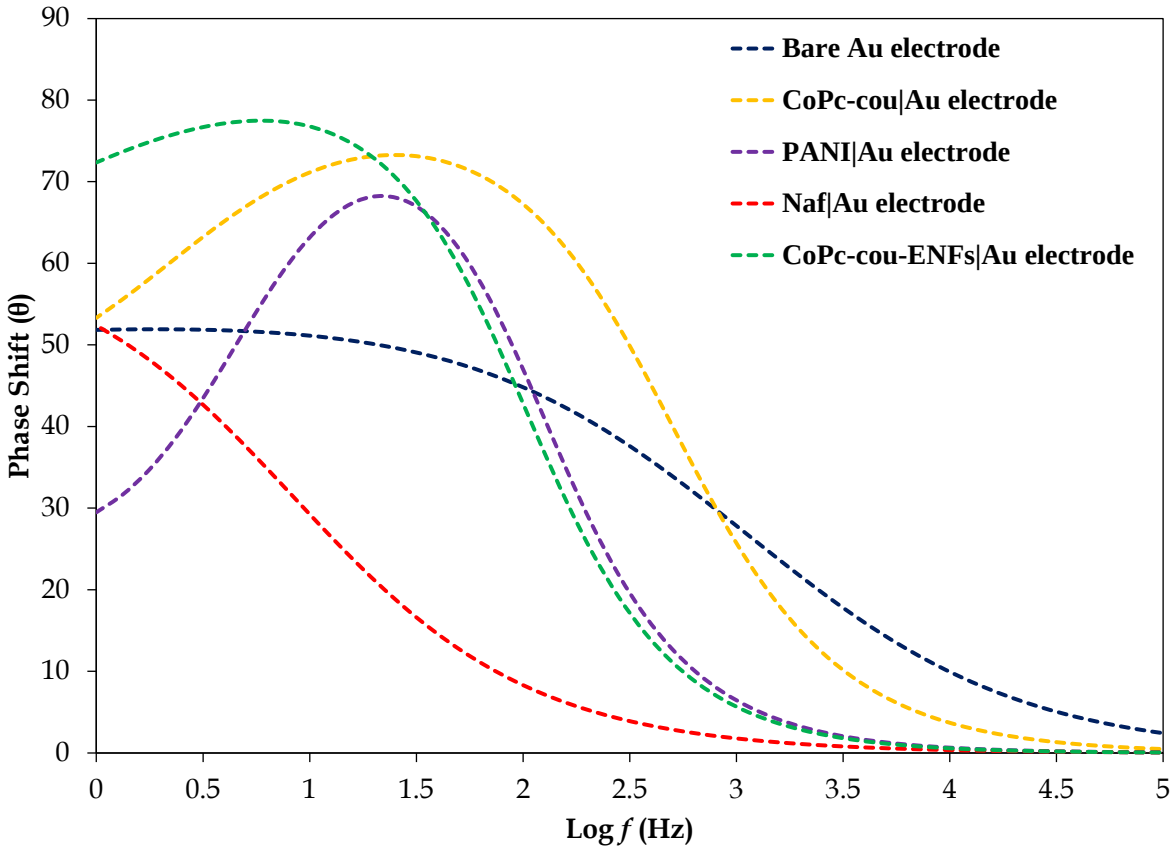

Figure 4.8: *Bode plots obtained using the bare Au and the respective chemically modified electrodes.*

4.3.4. Detection of Hg(II) at the CoPc-cou-ENF-Nf|Au.

4.3.4.1. Sensitivity of the CMEs towards Hg(II).

The electrocatalytic performance of the modified electrodes towards 1.00 mM Hg(II) solution in 0.1 M HCl and 0.4 M NaCl was evaluated using the differential pulse anodic stripping voltammetry (DPASV) technique and overlaid DPASVs are illustrated in **Figure 4.9**. From the DPASV overlays, it is evident that all except the Naf|Au electrode can detect Hg(II). Modifier films of CoPc-cou|Au or PANI|Au not only increased the electrode sensitivity towards Hg(II) but resulted in sharper respective Faradaic peak currents in comparison to the broad and smaller peak for the |Au electrode. The non-responsiveness of the Naf|Au is uncharacteristic however, this may be due to Hg(II) ions

being held tenuously by the sulfonyl groups of Nafion, thereby impeding fast charge transfer between the Hg(II) ions and the electrode surface. The current response of the CoPc-cou-ENFs|Au is the highest being 3 times larger than that of the |Au electrode, thereby showing the enhanced electrocatalytic detection of the CoPc-cou-ENF modifier film towards Hg(II). This can be attributed to the higher effective catalytic sites of the ENFs and the strong affinity between sulphur and Hg(II)-S interactions and therefore the associated selectivity. In addition, the high conductivity of PANI and hence enhanced charge permeability and relaying of PANI results in the enhanced detection of Hg(II). Thus, further evaluation of the analytical performance of the CMEs was restricted to the CoPc-cou-ENFs|Au. Chen *et. al.* also reported a noteworthy Au electrode modified with coumarin moieties for the detection of Hg(II) ions. It displayed a high selectivity, sensitivity as well low detection limits.[136]

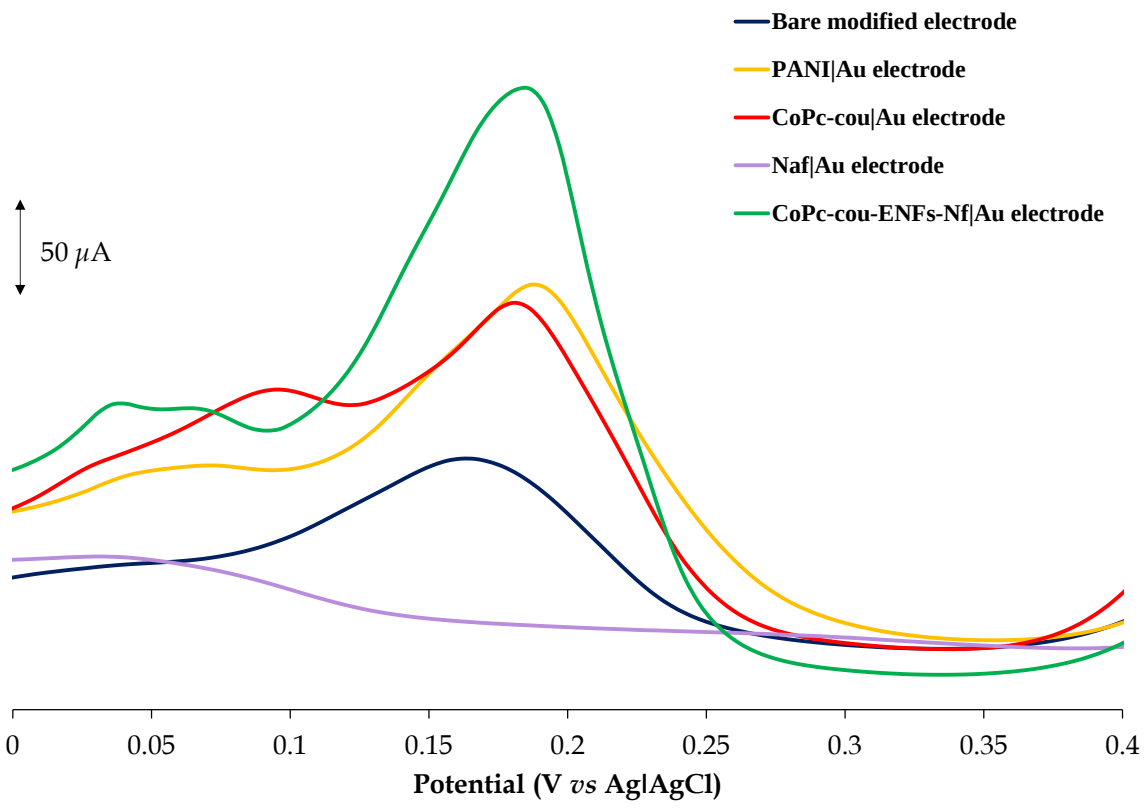

Figure 4.9: *Overlay DPASVs of 1.00 mM Hg(II) in 0.1 M HCl and 0.4 M NaOH at the |Au, PANI|Au, Naf|Au, CoPc-cou|Au and CoPc-cou-ENFs-Nf|Au electrodes.*

4.3.4.2. Mechanism of Hg(II) detection at the CoPc-cou-ENFs-Nf|Au.

A plausible mechanism founded on the high loading, dispersion and anchoring of the CoPc-cou as electrocatalytic sites on the ENFs, as synergistic factors promoting the facile reduction and accumulation of Hg(0) at the electrode surface. As shall be presented ahead, the CoPc-cou-ENFs-Nf|Au's CVs in the phosphate saline buffer (**Figure 4.10**) show an anodic current response (I_{pa}) due to the quasi-reversible oxidation of Co^{II} (mediator CoPc anchored on the ENFs) to electrogenerated Co^{III}, which will swiftly reduce Hg(II) to Hg(0). This happens despite the passivating nature of the CoPc-cou-ENFs-Nf|Au at the electrode surface area.

We proposed a transient catalytic cycle involving the anchored mediator ($PcCo^{II}$), the reduction auxiliary (mercaptocoumarin S donor atoms with a high affinity for Hg(II) ions) and the analyte ion to follow what we shall term a 3-centre $1e^-$ and $2e^-$ reduction which relays to swiftly produce Hg(0) that is stripped to afford the DPASV shown in **Figure 4.9**. Observations during experimentation lead to the deduction that ENFs aid the dispersion as well as anchor both the Co(II) and S donor atoms to stabilize the triangular catalytic cycle. **Figure 4.9** also shows that the cationic PANI modifier enhances the Hg(II) stripping current and thus it is a redox promotor constituent of ENFs by improving the conductivity of the modifier film. Furthermore, scanning negatively reduces the PANI polymer chain N donor atoms in a similar manner to the S atom on the CoPc substituents. The embedding of an S-bearing CoPc electrocatalyst in the ENFs is advantageous since the S atoms on the CoPc have a strong affinity for the target analyte Hg(II) and this would lead to the selective and electrocatalytic detection of the analyte at the CoPc-cou-ENFs-Nf|Au.[137] The synergistic effect of the CoPc-cou and PANI coupled with the stability endemic to the ENFs made this nanocomposite modifier exhibit the best electrocatalytic towards Hg(0) at the surface and its subsequent stripping.

4.3.5. Surface coverage of CoPc-cou-ENFs-NF|Au

Due to the passivating nature of the CoPc-cou-ENFs film the CoPc-cou-ENFs-Nf|Au and its effective surface area were probed, by measuring current in phosphate-buffered saline (PBS) solution (the reagent blank) and varying electrode scan rates as shown in **Figure 4.10A.** The anodic current responses (I_{pa}, due to the Co^{II}/Co^{III} oxidation redox couple) were plotted against the square root of the scan rate according to the Randles-Sevcik equation at increasing scan rates to calculate the effective surface area as shown in **Figure 4.10**

The surface coverage was calculated using the slope obtained in **Figure 4.10B** and **Equation 4:**

$$I_p = \frac{n^2F^2A\Gamma(v)}{4RT} \qquad (\mathbf{4})$$

where I*p* is the anodic peak current of the Co redox couple, *n* is the number of electrons, F is the Faradays constant (96 485 s.A.mol^{-1}), *A* is the effective surface area (0.0726 cm^2) of the CoPc-cou-ENFs-Nf|Au, R is the gas constant (8.314 J mol^{-1} K^{-1}) and T is the temperature (298 K).

The surface coverage was calculated to be 5.54 x 10^{-9} mol.cm^{-2} which is significantly larger than the reported values of planar CoPc molecules on the surface of the electrode (1x 10^{-10} mol cm^{-2}).[138] This could be due to the larger catalytic sites for loading the CoPc-cou made possible by the highly effective surface area of the ENFs.

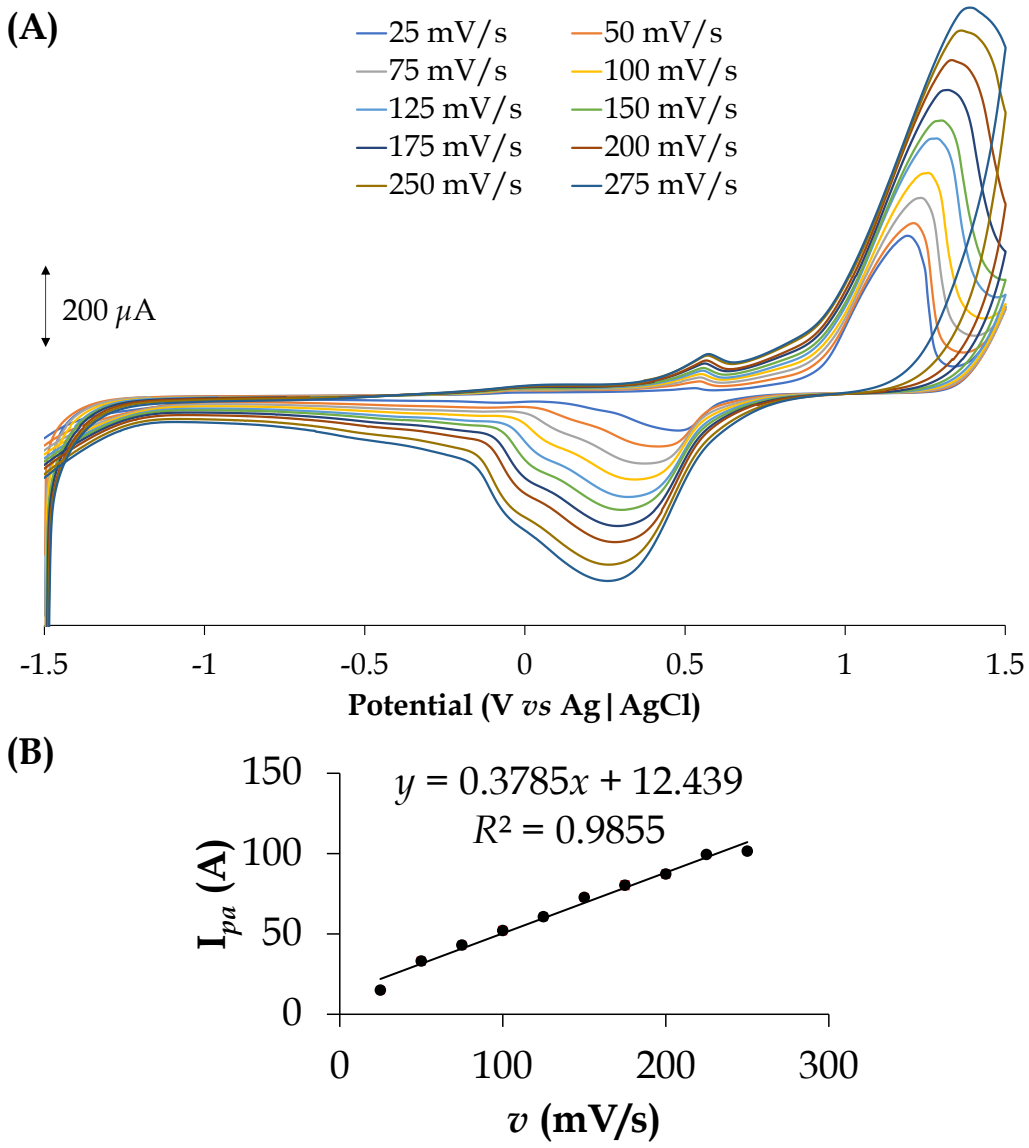

Figure 4.10*: (**A**) Overlay CVs in PBS at the CoPc-cou-ENFs-Nf|Au electrode for increasing scan rates and (**B**) Plot of the peak current vs scan rate.*

4.3.6. Optimising the parameters for Hg(II) detection

4.3.6.1. Supporting electrolyte

Previous reports on the voltametric determination of Hg(II) ions in aqueous solution have indicated dilute HCl (0.1 M) as the optimal supporting electrolyte at CMEs

modified with CoPc-nanoconjugates.[139] This was attributed to the aqueous stability of soluble mercuric complexes that form at a lower pH. Furthermore, the addition of NaCl shifts the reduction of Hg(II) towards negative potentials due to the formation of mercuric complexes which promotes oxidation. Therefore, in this study, a 0.1 M HCl /0.4 M NaCl (1:1) mixture was deemed the optimal electrolyte to reduce background currents and thus ensure the accurate detection of Hg(II). The detection of 3.00 mM Hg(II) ions in an equi-mixture of 0.1 M HCl / 0.4 M NaCl was compared with PBS and pH 4 as an electrolyte, using DPASV, and the former was proved to be a more effective electrolyte for the detection of Hg(II) in aqueous solutions.

4.3.6.2. Accumulation Potential

Accumulation potential has a direct influence on the sensitivity of the working electrode towards the detection of analytes, and thus, the DPASV current responses for a 3.00 mM Hg(II) were measured within the range of -1.0 V to 0 V. As depicted in **Figure 4.11A**, the peak current increased and peaked at a potential of -0.7 V as the applied potentials became more negative. The trend is attributed to Hg(II) being reduced completely as the working electrode becomes more negative leading to a facile transfer of electrons from the electrode surface to the analyte. Furthermore, the positive window of 0 – 1.0 V was investigated, however no conclusive results were obtained as the peak potential further decreased.

4.3.6.3. Accumulation Time

Accumulation time is an important electrochemical parameter that should be optimized to minimize electrode fouling effects associated with prolonged analyte accumulation. The accumulation time for Hg at the CoPc-cou-ENFs-Nf|Au was varied between 10 - 250 s and the DPASV current responses for a 3.00 mM Hg(II) standard were measured and graphed in **Figure 4.11B**. The peak current increased steadily, levelling in

the range of 75 – 125 s before its peak at 150 s. Thereafter, the response decreased which can be attributed to a combination of saturation of the active sites after 150 s of Hg(0) accumulation at the CoPc-cou-ENFs-Nf|Au microelectrode as well as concomitant adsorption of other non-electroactive that causes fouling and passivation of the CME. Hence an accumulation time of 150 s was used for further evaluative experiments.

4.3.6.4. Effect of pH

It is well known that the pH of the sample can drastically affect the current responses of the Hg(II) metal ions. Furthermore, research shows that Hg(II) ions are most stable at low pH values.[140] Therefore, the DPASV current responses for a 1.00 mM Hg(II) solution in different buffered pHs (1 – 9) were measured (under the optimized conditions of t = 150 s; E = -0.7 V) using the CoPc-cou-ENFs-Nf|Au. The obtained data (current response against pH) is graphed and illustrated in **Figure 4.11C.** The peak current decreases as the pH is increased. For pH of 7 and beyond, there was no measurable current due to the reduction of Hg(II) at the CME. A pH of 1.2 was considered the optimum electrolyte condition for the sensitive detection of Hg(II) due to the maximum current detected at this pH.

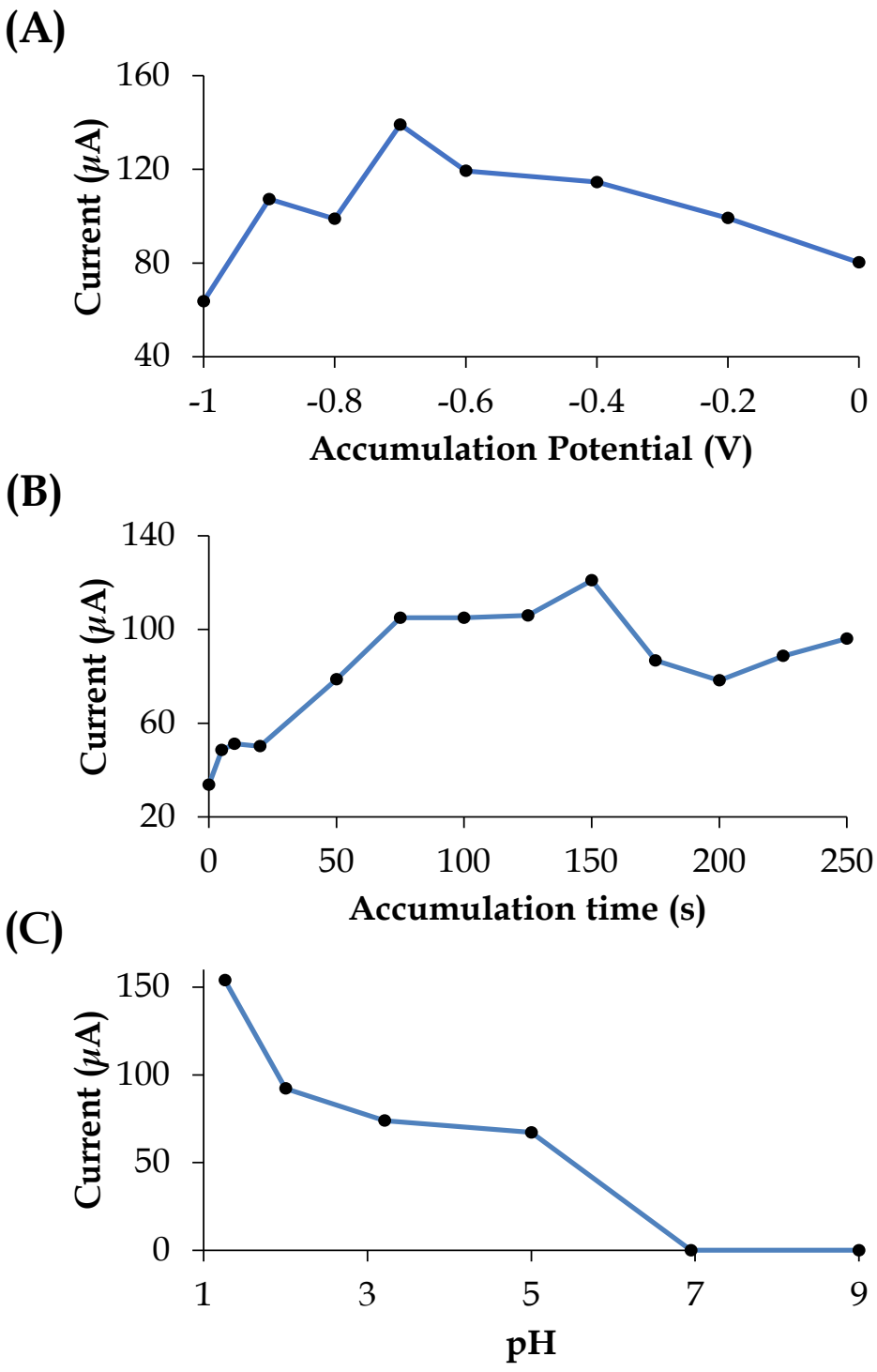

Figure 4.11: *Optimization of the DPASV parameters of the CoPc-cou-ENFs-Nf| Au using a 3.00 mM Hg(II) solution in 0.1 M HCl and 0.4 M NaCl as a function of (**A**) accumulation potential, (**B**) accumulation time and (**C**) pH.*

4.3.7. Electrocatalytic detection of Hg(II) using the CoPc-cou-ENFs-Nf|Au electrode

The CoPc-cou-ENFs-Nf|Au modified electrode was used to analyse increasing concentrations of Hg(II) to establish the linear response graph of the electrode as illustrated in **Figure 4.12A.** The calibration data was collected in triplicates to confirm the reproducibility of the electrode for the calibration process, see **Figure 4.12B.** The calibration precision is high as illustrated by the low error bar range and a high R^2 value of 0.97. The electrode has a moderate linear range of 10 – 3000 µM Hg(II), and a calibration sensitivity of 36.568 μA.mM^{-1}, with LOD and LOQ of 0.14 μM and 0.46 μM, respectively. However, there was a minor shifting of the peak maximum to more negative potentials as the concentration of the Hg(II) standards was increased (**Figure 4.12B)**. This shift is unexpected, given that the concentration of Cl^- ions in the electrolyte was fixed (0.1 M). Chloride variability in the electrolyte is one of the factors that cause drifts in the onset stripping potential of the accumulated Hg(II) owing to the mercury readily forming complexes with chlorine atoms.[141]

However, since the current response peak is symmetric (with no shoulders), and linearly correlated to Hg(II), it can be concluded that the CoPc-cou-ENFs-Nf|Au is selectively detecting the Hg^{2+} without interference from currents due to other stable mercuric species such as Hg_2^{2+} that may also form as an intermediate product of the initial reduction step. This would otherwise cause the broadening of the peaks which was not observed in these cases.

The performance of the CoPc-cou-ENFs-Nf|Au towards quantitative analysis of Hg(II) was compared with that reported for other CMEs. **Table 4.2** displays a wide range of literature-sited CMEs from which it is evident that the GCE/poly(CoTABImPc) is the best-performing electrode with an LOD of 0.038 μM and a linear range between 0.01-0.5 µM[142]. However, a comparison of the CoPc-cou-ENFs-Nf|Au towards quantitative analysis of Hg(II) with that of the SAMs-CoPc-fur|Poly(3-HT)-Au shows its embedment of the CoPc into nanometric ENFs drastically improves its detection capability and

sensitivity towards Hg(II). Furthermore, the CoPc-cou-ENFs-Nf|Au outperforms a vast majority of the other CMEs in **Table 4.2,** making it a promising and cost-effective sensor for the rapid and on-site analysis of Hg(II) in water samples.

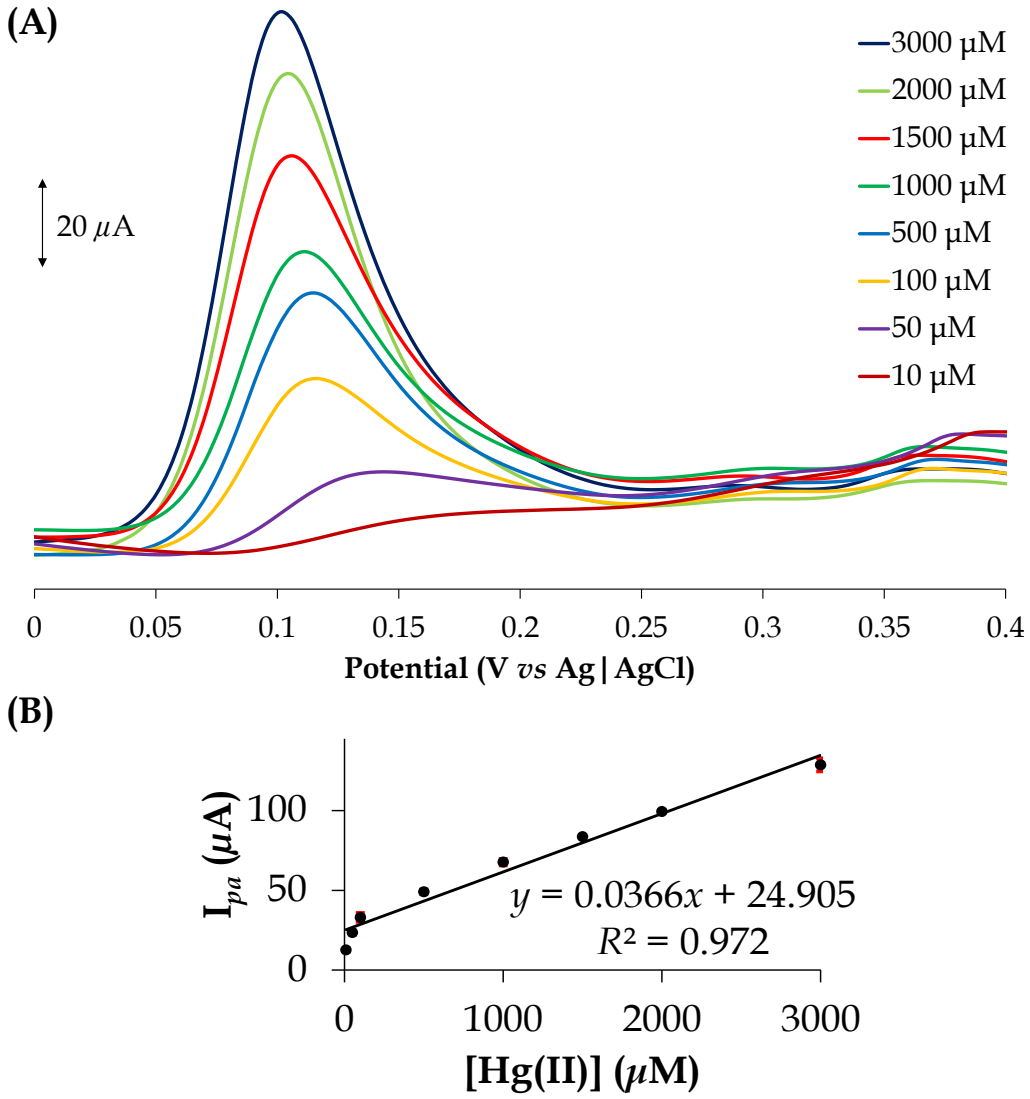

Figure 4.12: *(**A**) DPASVs of increasing concentrations of Hg(II) in 0.1 M HCl and 0.4 M NaCl at the CoPc-cou-ENFs-Nf|Au and (**B**) plot of the peak current against [Hg(II)].*

Table 4.2: *Comparison of calibration parameters of various modified electrodes for the electrocatalytic detection of Hg(II).*

Electrode	Detection method	Limit of detection (μM)	Linear range (μM)	References
Clicked-CoPc GCE [a]	DPSV	0.8194	0-30	143
SAMs-CoPc-fur | Poly(3-HT)-Au [b]	DPASV	14.8	42.1-3370	19
Gr-MnO_2/GCE [c]	CV	2	12.1-210.8	144
BTPSBA-MCPE [d]	DPASV	0.4	2-10	145
GCE/poly(CoTABImPc) [e]	DPV	0.038	0.01-0.5	142
EDTA_PANI/SWCNTs/SS [f]	DPV	0.68	2-20	146
GCE-SnO_2 [g]	CV	0.075	0.5-10	147
GC/rGO-SbNPs [h]	SWASV	0.0048	0.1-4.5	148
CoPc-cou-ENFs-Nf | Au	DPASV	0.14	10-3000	This work

[a] low symmetry alkyne terminated cobalt Phthalocyanine glassy carbon electrode, [b] self-assembled monolayers of cobalt-furan electropolymerized 3-hexylthiophene films, [c] graphene and MnO_2 glassy carbon electrode, [d] carbon paste electrode modified with SBA-15 silica organofunctionalised with 2-benzothiazolethiol, [e] cobalt(II) tetraamide benzimidazole phthalocyanine modified glassy carbon electrode, [f] ethylenediaminetetraacetic acid_polyaniline and singe walled carbon nanotubes nanocomposite stainless steel electrode, [g] Tin oxide particles modified glassy carbon electrode, [h] Glassy carbon reduced graphene oxide antimony nanoparticles

An important characteristic of a robust CME is the ability to be used repeatedly without compromising the modification on the surface. To ascertain the precision of reproducibility under similar experimental conditions, the CoPc-cou-ENFs-Nf|Au, current responses of 1.00 mM Hg(II) were measured repeatedly for 20 cycles as shown in **Figure 4.13** without rinsing nor replenishing the electrode between scans. The slight decreases in the current responses confirm the good stability of the CoPc-cou-ENFs modifier film as evidenced by a slight change in the detection fidelity for Hg(II). There is a noticeable decrease in the peak current only in the first 3 scans before the responses levelled off for the rest of the cycles. From this, we can further confirm that no adsorption-controlled processes are occurring as the analyte does not cause excessive fouling to the electrode surface. The percentage RSD was calculated to be 4.3% which indicates a statistically acceptable reproducibility.

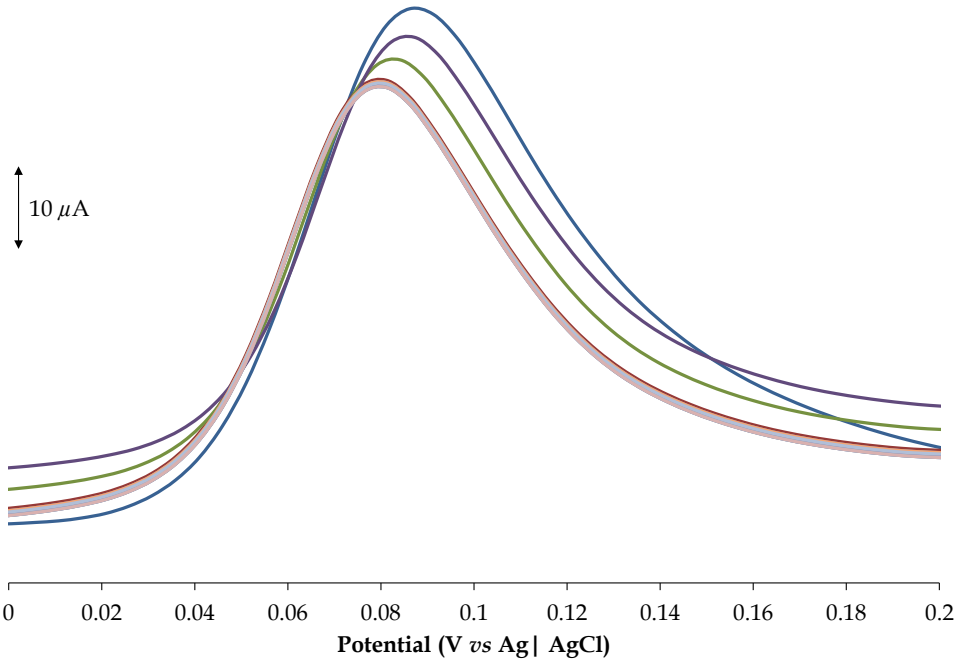

Figure 4.13: Replicated *CVs (20 cycles) of 1.00 mM Hg(II) in 0.1 M HCl and 0.4 M NaCl at the CoPc-cou-ENFs|Au.*

4.3.8. Interference studies

An essential attribute of chemically modified electrodes is selectivity towards the target analyte. Therefore, the current response of Hg(II) was measured in a sample containing 2.00 mM Pb(II), Cd(II) and Hg(II) provided by dissolving $Pb(NO_3)_2$, $Cd(NO_3)_2$ and $HgSO_4$ in 0.1 M HCl and 0.4 M NaCl. This was done to evaluate if the CME could still accurately detect and distinguish Hg(II) from other interferences. As shown in **Figure 4.14**, the CoPc-cou-ENFs-Nf|Au exhibits both high sensitivity and good selectivity towards Hg(II). Noteworthy is the unshifted and sharp stripping potential peak of Hg(II) at 0.07 V, is 3 and 10 times more intense than Cd and Pb respectively. Furthermore, the peak symmetry and resolution of the Hg(II) peak are much better than those previously reported for Hg(II) interference studies.[19] The presence of the other two ions in solution does not adversely affect the ability of the electrode to selectivity and accurately detect Hg(II). Furthermore, selective reduction, accumulation and detection of Hg(II) ions at the ENFs surfaces are rationalized by the high affinity of the benzothiazole S-donor atoms for Hg(II) compared to Pb(II) or Cd(II). The dispersion and anchoring CoPc's coumarin onto the ENFs improves the effectiveness of the electrocatalyst.

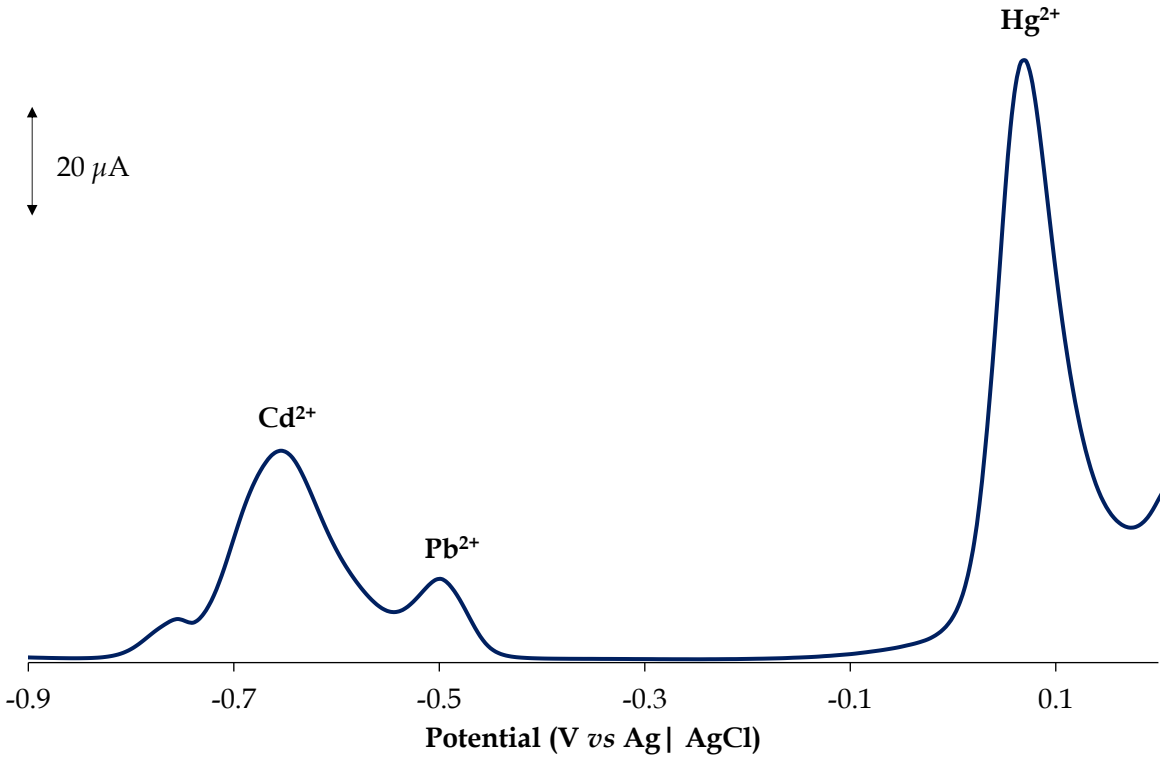

Figure 4.14: *DPASV scan of 1.00 mM of Hg^{2+}, Pb^{2+} and Cd^{2+} in 0.1 M HCl and 0.4 M NaCl using the CoPc-cou-ENFs-Nf|Au electrode.*

4.3.9. Hg(II) analysis in real water and spikes samples

4.3.9.1. Application of CoPc-cou-ENFs-Nf|Au

The CoPc-cou-ENFs-Nf|Au was then applied for the DPASV analysis of Hg(II) in a water sample (10.00 mL) collected from the Umhlanga Lagoon in Durban, South Africa to evaluate its practical applicability to environmental samples. As shown (in the first scan) **Figure 4.15A**, the CME could not detect Hg(II) in the water sample, hence the Lagoon water sample was pre-spiked to attain a concentration of 0.02 mM Hg(II). Although the LOD is higher than the acceptable level of Hg concentrations (0.001 ppm ≈ 5 nM[149]) in natural water, the results of the research study provide a basis for further

research and development to enhance the electrochemical sensitivities of MPc-based electrochemical sensors. While there is room for improvement with respect to the detection limits of the sensor, it is important to note that mercury contamination at any ultra-trace level is still toxic to the aquatic environment (plants and micro-organisms and animals) as well as human health. To assess the accuracy of Hg detection of the sensor, the lagoon water was further spiked with variable volumes (1.00 - 5.00 mL) of a 2.00 mM Hg(II) spike standard. From the standard addition plot of the current response of the Hg(II) spiked samples (**Figure 4.15B**), the percentage recovery for Hg(II) was determined to be 96% ± 8.34. This falls within the acceptable range of 80-120% for validating a new method for accuracy. The new CME did not require any pre-concentration or rinsing between runs, which is a desirable operational convenience that makes it easier to maintain during analysis. Furthermore, the modified electrode had a high correlation precision coefficient of $R^2 = 0.99$, and %RSD for the repeated data was 11%.

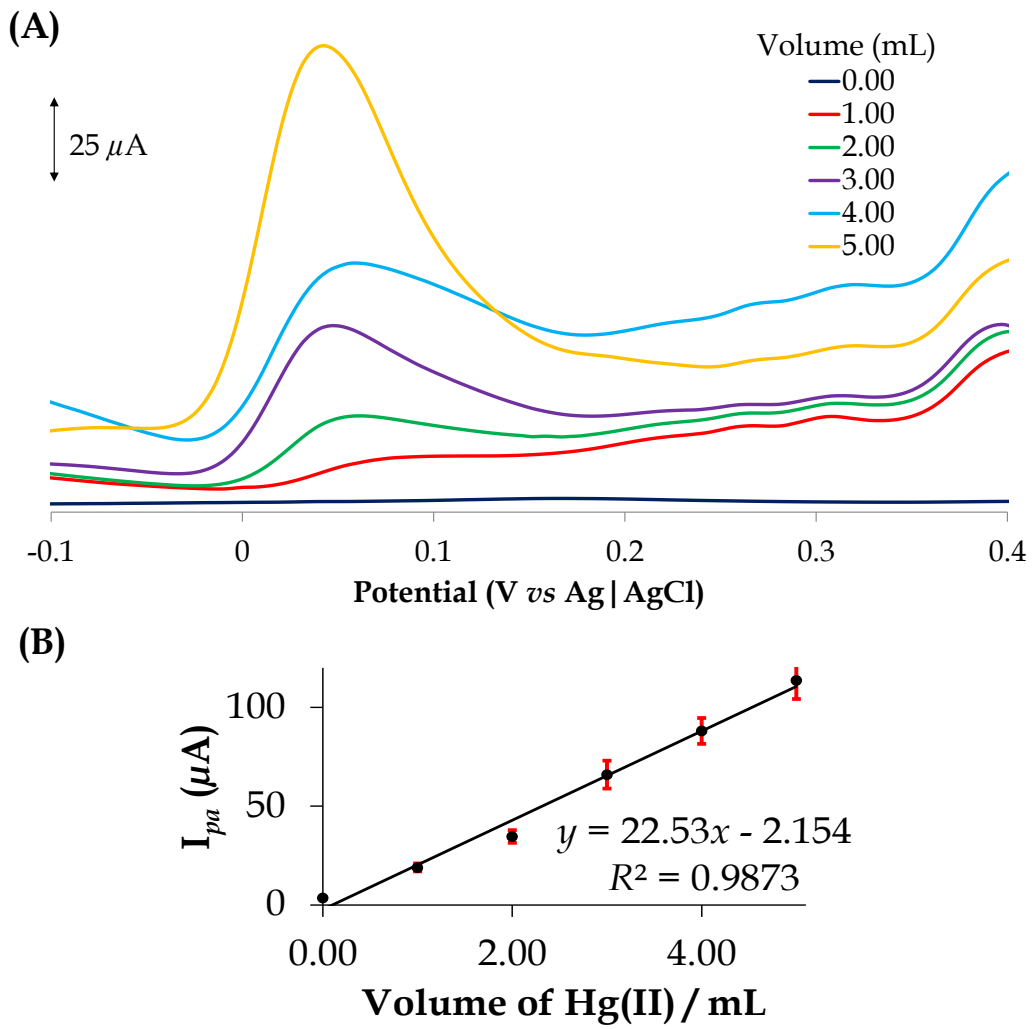

Figure 4.15: *(**A**) DPASV responses of the Umhlanga Lagoon water sample 10 mL) that was consecutively spiked with 2.00 mM Hg(II) at the CoPc-cou-ENFs-Nf|Au and (**B**) standard addition plot (spike current response versus volume of the 2.00 mM Hg(II) standards).*

4.3.9.2. Hg(II) analysis in real water using ICP-OES

To validate the performance of the CoPc-cou-ENFs-Nf|Au towards Hg(II), the water samples were also analysed using Inductively Coupled Plasma Optical Emission Spectroscopy. The ICP-OES was calibrated within the range of 0.3 μM – 0.7 mM (0.1 – 20 ppm) Hg(II) to generate **Figure 4.16**. Thereafter, the Umhlanga Lagoon water sample, with and without spiking (10 mL with 0.01 mM (5 ppm) standard) was analyzed for Hg(II). From the data, a percentage recovery of 98% was calculated and this value was

within the acceptable recovery range. Furthermore, an R^2 value of 0.9989 was obtained from the calibration curve, showing a high correlation precision.

The ICP-OES's Hg(II) percentage recovery compares well with that of the CoPc-cou-ENFs-Nf|Au value obtained (96%), we can deduce that the electrochemical sensor is a viable alternative for the detection of Hg(II). Furthermore, the portability of the sensor makes it advantageous for routine field measurements in needy areas such as natural water (dams, rivers and estuarine), wastewater in and out of integrated water treatment plants as well as effluent water from industrial processes generating mercury wastes.

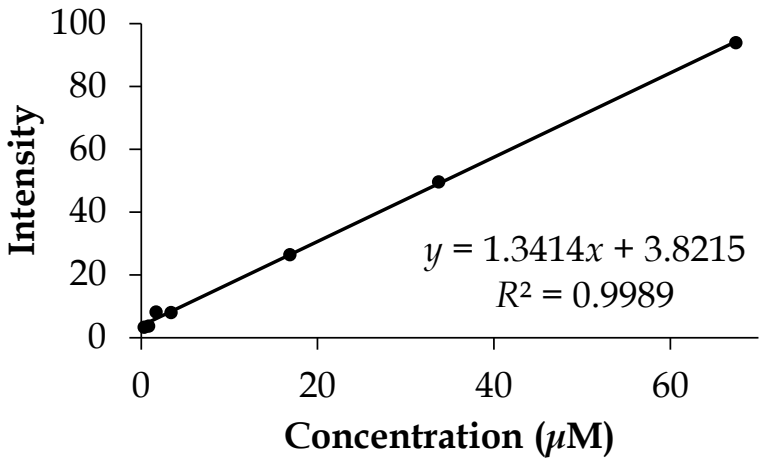

Figure 4.16: *ICP-OES calibration plot of emission intensity versus [Hg(II)].*

CHAPTER FIVE

Conclusions and future work

The current conundrum in water quality deterioration and sanitation within the Republic of South Africa requires innovative solutions such as rapid pollution screening and water remediation. This research project seeks to address the former national research imperative which is to discover smart materials that are functional electrochemical sensors in contaminated water bodies. The stark reality is that the rampant industrial and municipal water pollution cannot be exacerbated further since it will lead to more human fatalities related to diseases such as Cholera, deadly arbitrary infections from exposure to septic water containing antibiotic-resistant bacteria, heavy metal poisoning or elevated exposure of pharmaceutically derived water contaminates that counteracts chronic medication.[150-152] Thus, the continuous monitoring of industrial and municipal effluents and the fast detection of pollutants

In Chapter 3, Morphological features of the CoPc-cou-f-MWCNTs nanocomposite were probed by TEM where its micrograph shows nodal planes between the nanomaterial and metal complex constituents. The presence of these constituents within the CoPc-cou-*f*-MWCNTs nanohybrid was confirmed by Powder X-ray diffraction. SEM micrographs of the SAMs of CoPc-cou and its nanoconjugate, CoPc-cou-*f*-MWCNTs illustrate progressively enhanced surface modification when compared to the bare-gold coated glass. EDX analysis affirmed the presence of the elements of the metal complex within CoPc-cou SAM-modified Au-coated glass. The CoPc-cou-*f*-MWCNT/3-HT|Au electrode showed superior electrocatalytic activity towards PQ than the bare Au and the CoPc-cou-*f*-MWCNT|Au. The CoPc-cou-*f*-MWCNT/3-HT detected PQ selectively among other interfering pesticides, triclopyr (TCP) and atrazine (ATR). This chemically modified electrode (CME) electrochemically sensed PQ in ultrapure water with better

precision and sensitivity than LC-PDA/MS. However, LC-PDA/MS analysis of the spiked real water sample after a clean-up by mSPE afforded a percentage recovery of 99% for PQ. In contrast, the standard addition analysis of PQ by the CME in the lagoon water without prior sample clean-up afforded reproducible data with an 86% mean recovery. We speculate that the complexity of the sample matrix and unknown interferents may have contributed to the fouling of the CME electrocatalytic active sites thereby suppressing the Faradaic currents. Before the CME can be used as a portable device for conducting real-time, onsite analysis of PQ in water without any sample preparation, further development and optimization are required, including repurposing it for other unexplored analytes. This improvement can entail the immobilization of the CoPc-cou-*f*-MWCNT/3-HT| composite on a screen-printed electrochemical electrode and exploring its application as a photoelectrochemical sensor.

Chapter 4 describes the application of a CME, CoPc-cou-ENFs-Nf|Au electrode for the electrocatalytic detection of mercury(II). The CME was fabricated *via* a two-step modification process entailing the drop-casting of the PVA-PANI-CoPc-cou-ENF nanocomposite dispersed in DMF followed by thermal annealing of Nafion (Nf) on the adhesion layer. The resulting CME displayed superior electrochemical detection towards Hg(II) relative to bare Au electrodes and other CMEs which could be attributed to its higher effective surface area as well as the coordinative affinity of the thioether sulphur atoms of the coumarin.[17, 18, 153].Under optimised conditions the CoPc-ENF_Nf|Au modified electrode accurately detected Hg(II) within a linear range of 10 - 3000 µM with a limit of detection of 0.14 µM while displaying excellent stability and reproducibility. Furthermore, the fabricated electrode was able to sensitively and selectively differentiate between Hg(II), Pb(II) and Cd(II) in a standardized sample of these heavy cations. A percentage recovery of 96% was obtained using the CoPc-cou-ENFs-Nf|Au modified electrode in spiked real water samples which is comparable to the percentage recovery of 98% attained using the ICP-OES. This validates that the sensor has comparable detection capabilities with widely used laboratory-based analytical technique.

The chemically modified electrodes in this research study show enhanced detection limits and linear ranges for the detection of metals and pesticides in comparison to sensors modified solely with MPcs. However, there is room for improvement with respect to lower limits and simpler modification methods. The next phase of this research project can be the evolution to screen printed electrodes which opens up the avenue of developing multi-modal spectroelectrochemical sensors that may cross-reference qualitative and quantitative analyses across spectroscopic and electrochemical techniques.[154, 155] For real-time analysis to be realized, these dual spectroelectrochemical sensors should be embedded into continuous flow cells of industrial and municipal water treatment plants.[156] It is also foreseen that the formation of A_3B asymmetrical analogues of the CoPc-cou (where *A* are the coumarin substituents and *B* are the anchoring moieties for covalent attachment to nanomaterial or working electrodes), will render species with unique redox properties that can modulate the electrocatalytic activities towards specific antibiotic pollutant which are responsible for the manifestation of antibiotic-resistant bacteria.[157, 158]

REFERENCES

(1) Mohammed, A. S.; Kapri, A.; Goel, R. Heavy Metal Pollution: Source, Impact, and Remedies. In *Biomanagement of Metal-Contaminated Soils*, Khan, M. S., Zaidi, A., Goel, R., Musarrat, J. Eds.; Springer Netherlands, 2011; pp 1-28.

(2) Ali, H.; Khan, E.; Ilahi, I. Environmental Chemistry and Ecotoxicology of Hazardous Heavy Metals: Environmental Persistence, Toxicity, and Bioaccumulation. *Journal of Chemistry* **2019**, *2019*, 6730305. DOI: https://doi.org/10.1155/2019/6730305.

(3) Commoner, B. Rapid Population Growth and Environmental Stress. *International Journal of Health Services* **1991**, *21* (2), 199-227. DOI: https://doi.org/10.2190/B8RU-HA91-JJKW-PKUR.

(4) Ali, H.; Khan, E. What are heavy metals? Long-standing controversy over the scientific use of the term 'heavy metals' – proposal of a comprehensive definition. *Toxicological & Environmental Chemistry* **2018**, *100* (1), 6-19. DOI: https://doi.org/10.1080/02772248.2017.1413652.

(5) Rehman, K.; Fatima, F.; Waheed, I.; Akash, M. S. H. Prevalence of exposure of heavy metals and their impact on health consequences. *Journal of Cellular Biochemistry* **2018**, *119* (1), 157-184. DOI: https://doi.org/10.1002/jcb.26234.

(6) Martin, S.; Griswold, W. Human health effects of heavy metals. *Environmental Science and Technology briefs for citizens* **2009**, *15* (5).

(7) Budnik, L. T.; Casteleyn, L. Mercury pollution in modern times and its socio-medical consequences. *Science of The Total Environment* **2019**, *654*, 720-734. DOI: https://doi.org/10.1016/j.scitotenv.2018.10.408.

(8) Walters, C. R.; Somerset, V. S.; Leaner, J. J.; Nel, J. M. A review of mercury pollution in South Africa: Current status. *Journal of Environmental Science and Health, Part A* **2011**, *46* (10), 1129-1137. DOI: https://doi.org/10.1080/10934529.2011.590729.

(9) Rice, K. M.; Walker, E. M.; Wu, M.; Gillette, C.; Blough, E. R. Environmental Mercury and Its Toxic Effects. *Journal of Preventive Medicine & Public Health* **2014**, *47* (2), 74-83. DOI: https://doi.org/10.3961/jpmph.2014.47.2.74.

(10) du Plessis, A. Water Scarcity and Other Significant Challenges for South Africa. In *Freshwater Challenges of South Africa and its Upper Vaal River: Current State and Outlook*, du Plessis, A. Ed.; Springer International Publishing, 2017; pp 119-125.

(11) Agoro, M. A.; Adeniji, A. O.; Adefisoye, M. A.; Okoh, O. O. Heavy Metals in Wastewater and Sewage Sludge from Selected Municipal Treatment Plants in Eastern Cape Province, South Africa. In *Water*, 2020; Vol. 12.

(12) Davidson, C. M. Methods for the Determination of Heavy Metals and Metalloids in Soils. In *Heavy Metals in Soils: Trace Metals and Metalloids in Soils and their Bioavailability*, Alloway, B. J. Ed.; Springer Netherlands, 2013; pp 97-140.

(13) Keleş, T.; Akyüz, D.; Biyiklioglu, Z.; Koca, A. Electropolymerization of Metallophthalocyanines Carrying Redox Active Metal Centers and their Electrochemical Pesticide Sensing Application. *Electroanalysis* **2017**, *29* (9), 2125-2137. DOI: https://doi.org/10.1002/elan.201700249.

(14) Demir, F.; Yenilmez, H. Y.; Koca, A.; Bayır, Z. A. Metallo-phthalocyanines containing thiazole moieties: Synthesis, characterization, electrochemical and spectroelectrochemical properties and sensor applications. *Journal of Electroanalytical Chemistry* **2019**, *832*, 254-265. DOI: https://doi.org/10.1016/j.jelechem.2018.11.003.

(15) Zagal, J.; Páez, M.; Tanaka, A. A.; dos Santos, J. R.; Linkous, C. A. Electrocatalytic activity of metal phthalocyanines for oxygen reduction. *Journal of Electroanalytical Chemistry* **1992**, *339* (1), 13-30. DOI: https://doi.org/10.1016/0022-0728(92)80442-7.

(16) Bedioui, F.; Griveau, S.; Nyokong, T.; John Appleby, A.; Caro, C. A.; Gulppi, M.; Ochoa, G.; Zagal, J. H. Tuning the redox properties of metalloporphyrin- and metallophthalocyanine-based molecular electrodes for the highest electrocatalytic activity in the oxidation of thiols. *Physical Chemistry Chemical Physics* **2007**, *9* (26), 3383. DOI: https://doi.org/10.1039/b618767f.

(17) Ngororabanga, J. M. V.; Tshentu, Z. R.; Mama, N. A New Highly Selective Colorimetric and Fluorometric Coumarin-based Chemosensor for Hg2+. *Journal of Fluorescence* **2020**, *30* (5), 985-997. DOI: https://doi.org/10.1007/s10895-020-02542-x.

(18) Ngororabanga, J. M. V.; Tshentu, Z. R.; Mama, N. A highly selective and sensitive ESIPT-based coumarin–triazole polymer for the ratiometric detection of Hg2+. *New Journal of Chemistry* **2019**, *43* (30), 12168-12177. DOI: https://doi.org/10.1039/C9NJ01366K.

(19) Kantize, K.; Ngwenya, V.; Booysen, I. N.; Mambanda, A. Electrocatalytic determination of mercury cations at the interfaces of gold electrodes modified with self-assembled monolayers of cobalt phthalocyanines and electropolymerized 3-hexylthiophene films. *Polyhedron* **2021**, *203*, 115235. DOI: https://doi.org/10.1016/j.poly.2021.115235.

(20) Kasuga, K.; Tsutsuo, M. Some new developments in the chemistry of metallophthalocyanines. *Coordination Chemistry Reviews* **1980**, *32* (1), 67-95. DOI: https://doi.org/10.1016/S0010-8545(00)80370-7.

(21) Dent, C. E.; Linstead, R. P.; Lowe, A. R. 217. Phthalocyanines. Part VI. The structure of the phthalocyanines. *Journal of the Chemical Society (Resumed)* **1934**, (0), 1033-1039. DOI: https://doi.org/10.1039/JR9340001033.

(22) Simon, J.; André, J.-J.; Lehn, J. M.; Rees, C. W. Metallophthalocyanines. In *Molecular Semiconductors: Photoelectrical Properties and Solar Cells*, Simon, J., André, J.-J., Lehn, J. M., Rees, C. W. Eds.; Springer Berlin Heidelberg, 1985; pp 73-149.

(23) Shahrokhian, S.; Ghalkhani, M.; Amini, M. K. Application of carbon-paste electrode modified with iron phthalocyanine for voltammetric determination of epinephrine in the presence of ascorbic acid and uric acid. *Sensors and Actuators B: Chemical* **2009**, *137* (2), 669-675. DOI: https://doi.org/10.1016/j.snb.2009.01.022.

(24) Ogunsipe, A. Metallophthalocyanines: synthesis, properties and applications–a review. *Trends Food Sci. Technol.* **2018**, *3*, 669-681.

(25) Ünlü, S.; Yaraşır, M. N.; Kandaz, M.; Koca, A.; Salih, B. Synthesis, spectroscopy and electrochemical properties of highly soluble fluoro containing phthalocyanines. *Polyhedron* **2008**, *27* (13), 2805-2810. DOI: https://doi.org/10.1016/j.poly.2008.05.036.

(26) Akinbulu, I. A.; Nyokong, T. Syntheses and investigation of the effects of position and nature of substituent on the spectral, electrochemical and spectroelectrochemical

properties of new cobalt phthalocyanine complexes. *Polyhedron* **2010**, *29* (4), 1257-1270. DOI: https://doi.org/10.1016/j.poly.2010.01.004.

(27) Barrera, C.; Zhukov, I.; Villagra, E.; Bedioui, F.; Páez, M. A.; Costamagna, J.; Zagal, J. H. Trends in reactivity of unsubstituted and substituted cobalt-phthalocyanines for the electrocatalysis of glucose oxidation. *Journal of Electroanalytical Chemistry* **2006**, *589* (2), 212-218. DOI: https://doi.org/10.1016/j.jelechem.2006.02.009.

(28) Maree, S.; Nyokong, T. Electrocatalytic behavior of substituted cobalt phthalocyanines towards the oxidation of cysteine. *Journal of Electroanalytical Chemistry* **2000**, *492* (2), 120-127. DOI: https://doi.org/10.1016/S0022-0728(00)00281-3.

(29) Zagal, J. H. Metallophthalocyanines as catalysts in electrochemical reactions. *Coordination Chemistry Reviews* **1992**, *119*, 89-136. DOI: https://doi.org/10.1016/0010-8545(92)80031-L.

(30) Xu, H.; Xiao, J.; Liu, B.; Griveau, S.; Bedioui, F. Enhanced electrochemical sensing of thiols based on cobalt phthalocyanine immobilized on nitrogen-doped graphene. *Biosensors and Bioelectronics* **2015**, *66*, 438-444. DOI: https://doi.org/10.1016/j.bios.2014.12.011.

(31) Nyokong, T. Desired properties of new phthalocyanines for photodynamic therapy. **2011**, *83* (9), 1763-1779. DOI: https://doi.org/10.1351/PAC-CON-10-11-22.

(32) Zhu, T. C.; Finlay, J. C. The role of photodynamic therapy (PDT) physics. *Medical Physics* **2008**, *35* (7Part1), 3127-3136. DOI: https://doi.org/10.1118/1.2937440.

(33) Dube, E.; Oluwole, D. O.; Njemuwa, N.; Prinsloo, E.; Nyokong, T. Photophysicochemical and photodynamic therapy properties of metallophthalocyanines linked to gold speckled silica nanoparticles. *Photodiagnosis and Photodynamic Therapy* **2019**, *25*, 325-333. DOI: https://doi.org/10.1016/j.pdpdt.2019.01.019.

(34) Tong, Y.; Yan, X.; Liang, J.; Dou, S. X. Metal-Based Electrocatalysts for Methanol Electro-Oxidation: Progress, Opportunities, and Challenges. *Small* **2021**, *17* (9), 1904126. DOI: https://doi.org/10.1002/smll.201904126.

(35) Zhang, Z.; Li, P.; Feng, Q.; Wei, B.; Deng, C.; Fan, J.; Li, H.; Wang, H. Scalable Synthesis of a Ruthenium-Based Electrocatalyst as a Promising Alternative to Pt for

Hydrogen Evolution Reaction. *ACS Applied Materials & Interfaces* **2018**, *10* (38), 32171-32179. DOI: https://doi.org/10.1021/acsami.8b10502.

(36) Hebié, S.; Bayo-Bangoura, M.; Bayo, K.; Servat, K.; Morais, C.; Napporn, T. W.; Boniface Kokoh, K. Electrocatalytic activity of carbon-supported metallophthalocyanine catalysts toward oxygen reduction reaction in alkaline solution. *Journal of Solid State Electrochemistry* **2016**, *20* (4), 931-942. DOI: https://doi.org/10.1007/s10008-015-2932-6.

(37) Kumar, A.; Zhang, G.; Liu, W.; Sun, X. Electrocatalysis and activity descriptors with metal phthalocyanines for energy conversion reactions. *Journal of Electroanalytical Chemistry* **2022**, *922*, 116799. DOI: https://doi.org/10.1016/j.jelechem.2022.116799.

(38) Hanrahan, G.; Patil, D. G.; Wang, J. Electrochemical sensors for environmental monitoring: design, development and applications. *Journal of Environmental Monitoring* **2004**, *6* (8), 657-664. DOI: https://doi.org/10.1039/B403975K.

(39) Cranston, R. R.; Lessard, B. H. Metal phthalocyanines: thin-film formation, microstructure, and physical properties. *RSC Advances* **2021**, *11* (35), 21716-21737. DOI: https://doi.org/10.1039/d1ra03853b.

(40) Sivanesan, A.; John, S. A. Highly Sensitive Electrochemical Sensor for Nitric Oxide Using the Self-Assembled Monolayer of 1,8,15,22-Tetraaminophthalocyanatocobalt(II) on Glassy Carbon Electrode. *Electroanalysis* **2010**, *22* (6), 639-644. DOI: https://doi.org/10.1002/elan.200900443.

(41) Wu, H.; Chen, Z.; Zhang, J.; Wu, F.; He, C.; Wang, B.; Wu, Y.; Ren, Z. Stably dispersed carbon nanotubes covalently bonded to phthalocyanine cobalt(ii) for ppb-level H2S sensing at room temperature. *Journal of Materials Chemistry A* **2016**, *4* (3), 1096-1104. DOI: https://doi.org/10.1039/C5TA09213B.

(42) Darwent, J. R.; Douglas, P.; Harriman, A.; Porter, G.; Richoux, M. C. Metal phthalocyanines and porphyrins as photosensitizers for reduction of water to hydrogen. *Coord. Chem. Rev* **1982**, *44:1*. DOI: https://doi.org/10.1016/S0010-8545(00)80518-4

(43) Banoth, P.; Kandula, C.; Kollu, P. Introduction to Electrocatalysts. In *Noble Metal-Free Electrocatalysts: New Trends in Electrocatalysts for Energy Applications. Volume 2*, ACS Symposium Series, Vol. 1432; American Chemical Society, 2022; pp 1-37.

(44) Kang, D.; Wang, B.; Wang, X.; Li, Y.; Chen, Z.; He, C.; Wu, Y. Stably dispersed metallophthalocyanine noncovalently bonded to multiwalled carbon nanotubes for ammonia sensing at room temperature. *Sensors and Actuators B: Chemical* **2017**, *246*, 262-270. DOI: https://doi.org/10.1016/j.snb.2017.02.083.

(45) Vanaraj, R.; Arumugam, B.; Mayakrishnan, G.; Kim, I. S.; Kim, S. C. A Review on Electrospun Nanofiber Composites for an Efficient Electrochemical Sensor Applications. In *Sensors*, 2023; Vol. 23.

(46) Chen, K.; Chou, W.; Liu, L.; Cui, Y.; Xue, P.; Jia, M. Electrochemical Sensors Fabricated by Electrospinning Technology: An Overview. In *Sensors*, 2019; Vol. 19.

(47) Ghasemi, S.; Mousavi, M. F.; Shamsipur, M. Enhancement of electron transfer kinetics on a polyaniline-modified electrode in the presence of anionic dopants. *Journal of Solid State Electrochemistry* **2008**, *12* (3), 259-268. DOI: https://doi.org/10.1007/s10008-007-0386-1.

(48) Tamer, U.; Oymak, T.; Ertaş, N. Voltammetric Determination of Mercury(II) at Poly(3-hexylthiophene) Film Electrode. Effect of Halide Ions. *Electroanalysis* **2007**, *19* (24), 2565-2570. DOI: https://doi.org/10.1002/elan.200704013.

(49) Torma, F.; Kádár, M.; Tóth, K.; Tatár, E. Nafion®/2,2′-bipyridyl-modified bismuth film electrode for anodic stripping voltammetry. *Analytica Chimica Acta* **2008**, *619* (2), 173-182. DOI: https://doi.org/10.1016/j.aca.2008.05.004.

(50) Maduraiveeran, G.; Jin, W. Carbon nanomaterials: Synthesis, properties and applications in electrochemical sensors and energy conversion systems. *Materials Science and Engineering: B* **2021**, *272*, 115341. DOI: https://doi.org/10.1016/j.mseb.2021.115341.

(51) Ahammad, A. J. S.; Lee, J.-J.; Rahman, M. A. Electrochemical Sensors Based on Carbon Nanotubes. In *Sensors*, 2009; Vol. 9, pp 2289-2319.

(52) Balogun, S. A.; Fayemi, O. E. Recent Advances in the Use of CoPc-MWCNTs Nanocomposites as Electrochemical Sensing Materials. *Biosensors* **2022**, *12* (10), 850. DOI: https://doi.org/10.3390/bios12100850.

(53) Gökçeören, A. T.; Kaplan, E.; Arslanoğlu, Y. Electrochemical and morphological analysis on novel phthalocyanine grafted conductive polymeric nanofibers. *Journal of Electroanalytical Chemistry* **2014**, *729*, 87-94. DOI: https://doi.org/10.1016/j.jelechem.2014.07.018.

(54) Aslı Esenpınar, A.; Bulut, M. Synthesis and characterization of metal-free and metallo-phthalocyanines with four pendant coumarinthio/oxy-substituents. *Dyes and Pigments* **2008**, *76* (1), 249-255. DOI: https://doi.org/10.1016/j.dyepig.2006.08.037.

(55) Esenpınar, A. A.; Özkaya, A. R.; Bulut, M. Synthesis and electrochemistry of tetrakis(7-coumarinthio-4-methyl)-phthalocyanines, and preparation of their cinnamic acid and sodium cinnamate derivatives. *Polyhedron* **2009**, *28* (1), 33-42. DOI: https://doi.org/10.1016/j.poly.2008.09.021.

(56) Schwarzenbach, R. P.; Egli, T.; Hofstetter, T. B.; Von Gunten, U.; Wehrli, B. Global Water Pollution and Human Health. *Annu. Rev. Environ. Resour* **2010**, *35* (1), 109-136. DOI: https://doi.org/10.1146/annurev-environ-100809-125342.

(57) Abbaspour, S. Water Quality in Developing Countries, South Asia, South Africa, Water Quality Management and Activities that Cause Water Pollution. In *International Conference on Environmental and Agriculture Engineering* Singapore, 2011; IACSIT Press: Singapore, 2011; Vol. 15.

(58) Geldenhuys, K. Stay clear of disastrous hazmat incidents: they are dangerous. In *Servamus Community-based Safety and Security Magazine*, 2022; Vol. 115, pp 37-39.

(59) Comrie, S. UPL Cornubia catastrophe: Highly toxic cocktail of chemicals in smoke plume finally identified. *Daily Maverick: Our Burning Planet*, 2022. https://www.dailymaverick.co.za/article/2022-02-13-upl-cornubia-catastrophe-highly-toxic-cocktail-of-chemicals-in-smoke-plume-finally-identified/.

(60) Trager, R. Fire during riots exposes environmental impact of improperly stored agrochemicals. *Royal Society of Chemistry*, 2022.

https://www.chemistryworld.com/news/fire-during-riots-exposes-environmental-impact-of-improperly-stored-agrochemicals/4015102.article.

(61) Forum, T. U. M.-S. UPL still won't recognise community watchdog forum after Cornubia's catastrophic chemical spill. *Daily Maverick: Our Burning Planet*, 2022. https://www.dailymaverick.co.za/article/2022-05-08-upl-still-wont-recognise-community-watchdog-forum-after-cornubias-catastrophic-chemical-spill/.

(62) Barceló, D. Occurrence, handling and chromatographic determination of pesticides in the aquatic environment. A review. *Analyst* **1991**, *116* (7), 681-689. DOI: https://doi.org/10.1039/AN9911600681.

(63) Ribeiro, J. A.; Carreira, C. A.; Lee, H. J.; Silva, F.; Martins, A.; Pereira, C. M. Voltammetric determination of paraquat at DNA–gold nanoparticle composite electrodes. *Electrochim. Acta* **2010**, *55* (27), 7892-7896. DOI: https://doi.org/10.1016/j.electacta.2010.03.058.

(64) Kwaśniewska, K.; Gadzała-Kopciuch, R.; Cendrowski, K. Analytical Procedure for the Determination of Zearalenone in Environmental and Biological Samples. *Crit. Rev. Anal. Chem.* **2015**, *45* (2), 119-130. DOI: https://doi.org/10.1080/10408347.2014.896731.

(65) Akyüz, D.; Keleş, T.; Biyiklioglu, Z.; Koca, A. Electrochemical pesticide sensors based on electropolymerized metallophthalocyanines. *J. Electroanal. Chem.* **2017**, *804*, 53-63. DOI: https://doi.org/10.1016/j.jelechem.2017.09.044.

(66) Qi, P.; Wang, J.; Wang, X.; Wang, X.; Wang, Z.; Xu, H.; Di, S.; Wang, Q.; Wang, X. Sensitive determination of fenitrothion in water samples based on an electrochemical sensor layered reduced graphene oxide, molybdenum sulfide (MoS2)-Au and zirconia films. *Electrochim. Acta* **2018**, *292*, 667-675. DOI: https://doi.org/10.1016/j.electacta.2018.09.187.

(67) Şenocak, A.; Köksoy, B.; Akyüz, D.; Koca, A.; Klyamer, D.; Basova, T.; Demirbaş, E.; Durmuş, M. Highly selective and ultra-sensitive electrochemical sensor behavior of 3D SWCNT-BODIPY hybrid material for eserine detection. *Biosens. Bioelectron.* **2019**, *128*, 144-150. DOI: https://doi.org/10.1016/j.bios.2018.12.052.

(68) Karimi-Maleh, H.; Karimi, F.; Alizadeh, M.; Sanati, A. L. Electrochemical Sensors, a Bright Future in the Fabrication of Portable Kits in Analytical Systems. *Chem. Rec.* **2020**, *20* (7), 682-692. DOI: https://doi.org/10.1002/tcr.201900092.

(69) Mugadza, T. a. N., T. Synthesis, characterization and application of monocarboxy-phthalocyanine-single walled carbon nanotube conjugates in electrocatalysis. *Polyhedron* **2011**, *30* (11), 1820-1829. DOI: https://doi.org/10.1016/j.poly.2011.04.020.

(70) Altun, S.; Orman, E. B.; Odabaş, Z.; Altındal, A.; Rıza Özkaya, A. Gas sensing and electrochemical properties of tetra and octa 2H-chromen-2-one substituted iron(II) phthalocyanines. *Dalton Trans.* **2015**, *44* (9), 4341-4354. DOI: https://doi.org/10.1039/c4dt03301a.

(71) Chen, Z.; Zhao, Z.; Yang, J.; Gao, X.; Sang, X.; Khan, A.; Xu, R.; Feng, M.; Liu, L.; Liu, Q.; et al. Luminescent detection of pesticides by color changeable flexible coumarin-3-carboxylic acid/GdF3:Sm3+ composite film. *Spectrochim. Acta, Part A* **2021**, *261*, 120002. DOI: https://doi.org/10.1016/j.saa.2021.120002.

(72) Battison, A.; Schoeman, S.; Mama, N. A coumarin-azo derived colorimetric chemosensor for Hg 2+ detection in organic and aqueous media and its extended real-world applications. Research Square Platform LLC: 2022.

(73) Battison, A.; Schoeman, S.; Mama, N. A Coumarin-azo Derived Colorimetric Chemosensor for Hg2+ Detection in Organic and Aqueous Media and its Extended Real-world Applications. *Journal of Fluorescence* **2023**, *33* (1), 267-285. DOI: https://doi.org/10.1007/s10895-022-03065-3.

(74) Sankhla, M. S., Kumari, M., Sharma, K., Kushwah, R.S. and Kumar, R. Water contamination through pesticide & their toxic effect on human health. *IJRASET* **2018**, *6* (1), 967-970. DOI: http://doi.org/10.22214/ijraset.2018.1146.

(75) Helweg, A.; Bay, H.; Hansen, H. P. B.; Rabølle, M.; Sonnenborg, A.; Stenvang, L. Pollution at and below Sites used for Mixing and Loading of Pesticides. *Int. J. Environ. Anal. Chem.* **2002**, *82* (8-9), 583-590. DOI: https://doi.org/10.1080/03067310290009497.

(76) Tsai, W.-T. A review on environmental exposure and health risks of herbicide paraquat. *Toxicol. Environ. Chem.* **2013**, *95* (2), 197-206. DOI: https://doi.org/10.1080/02772248.2012.761999.

(77) Kantize, K.; Booysen, I. N.; Mambanda, A. Electrochemical sensing of acetaminophen using nanocomposites comprised of cobalt phthalocyanines and multiwalled carbon nanotubes. *J. Electroanal. Chem.* **2019**, *850*, 113391. DOI: https://doi.org/10.1016/j.jelechem.2019.113391.

(78) Ribeiro, F. W. P.; de Souza Lucas, F. W.; Mascaro, L. H.; Morais, S.; da Silva Casciano, P. N.; de Lima-Neto, P.; Correia, A. N. Electroanalysis of formetanate hydrochloride by a cobalt phthalocyanine functionalized multiwalled carbon nanotubes modified electrode: characterization and application in fruits. *Electrochim. Acta* **2016**, *194*, 187-198. DOI: https://doi.org/10.1016/j.electacta.2016.02.086.

(79) Adebayo Akinbulu, I.; Nyokong, T. Fabrication and characterization of single walled carbon nanotubes-iron phthalocyanine nano-composite: surface properties and electron transport dynamics of its self assembled monolayer film. *New J. Chem.* **2010**, *34* (12), 2875. DOI: https://doi.org/10.1039/c0nj00395f.

(80) Nwaji, N.; Mack, J.; Nyokong, T. An optical limiting study in aminophenoxy substituted phthalocyanine in the presence of semiconductor quantum dots. *J. Lumin.* **2018**, *203*, 247-256. DOI: https://doi.org/10.1016/j.jlumin.2018.06.044.

(81) Son, H.; Yang, M. H.; Mutyala, A. K.; Chang, D. W.; Park, J. S. Superior electrocatalytic performance of polyisobutylene-substituted metallophthalocyanines supported on single-walled carbon nanotubes for an oxygen reduction reaction. *Dyes Pigm.* **2019**, *162*, 662-670. DOI: https://doi.org/10.1016/j.dyepig.2018.10.065.

(82) Zhao, G.; Gao, Z.; Li, H.; Liu, S.; Chen, L.; Zhang, R.; Guo, H. Controlled assembly of Ag nanoparticles on the surface of phosphate pillar [6]arene functionalized single-walled carbon nanotube for enhanced catalysis and sensing performance. *Electrochim. Acta* **2019**, *318*, 711-719. DOI: https://doi.org/10.1016/j.electacta.2019.06.135.

(83) Ma, J.; Zhu, H.; Zheng, Y. Highly dispersed cobalt phthalocyanine on nitrogen-doped carbon towards electrocatalytic reduction of CO2 to CO. *Ionics* **2021**, *27* (6), 2583-2590. DOI: https://doi.org/10.1007/s11581-021-03960-y.

(84) Chohan, S.; Booysen, I. N.; Mambanda, A.; Akerman, M. P. Formation, characterization and electrochemical properties of novel tetrasubstituted cobalt phthalocyanines bearing tetrahydropyran, furan and coumarin moieties. *Inorg. Chim. Acta* **2016**, *447*, 183-191. DOI: https://doi.org/10.1016/j.ica.2016.04.021.

(85) Chohan, S.; Booysen, I. N.; Mambanda, A. Cobalt β-tetra(3-oxyflavone/2-(2-oxyphenyl)benzoxazole)phthalocyanines and their carbon nanotube conjugates: Formation, characterization and dopamine electrocatalysis. *Polyhedron* **2015**, *102*, 284-292. DOI: https://doi.org/10.1016/j.poly.2015.10.012.

(86) Kantize, K.; Booysen, I. N.; Mambanda, A. Electrocatalytic Determination of Nevirapine Using a Platinum Electrode Modified with a Polymeric CoPc-Nafion-carbon nanotube Composite. *Int. J. Electrochem. Sci* **2022**, *17* (2). DOI: https://doi.org/10.20964/2022.06.03.

(87) Nxele, S. R.; Oluwole, D. O.; Nyokong, T. Electrocatalytic activity of a push pull Co(II) phthalocyanine in the presence of graphitic carbon nitride quantum dots. *Electrochim. Acta* **2019**, *326*, 134978. DOI: https://doi.org/10.1016/j.electacta.2019.134978.

(88) Fomo, G.; Nwaji, N.; Nyokong, T. Low symmetric metallophthalocyanine modified electrode via click chemistry for simultaneous detection of heavy metals. *J. Electroanal. Chem.* **2018**, *813*, 58-66. DOI: https://doi.org/10.1016/j.jelechem.2018.02.016.

(89) Wachholz Junior, D.; Deroco, P. B.; Kubota, L. T. A copper-based metal-organic framework/reduced graphene oxide-modified electrode for electrochemical detection of paraquat. *Microchim. Acta* **2022**, *189* (8). DOI: https://doi.org/10.1007/s00604-022-05358-7.

(90) Dewald van Rensburg, S. C. UPL fire: Here's the full inventory of chemicals in the destroyed Cornubia warehouse. *amaBhungane: Centre for Investigative Journalism*, 2021. https://amabhungane.org/stories/210818-upl-fire-heres-the-full-inventory-of-chemicals-in-the-destroyed-cornubia-warehouse/.

(91) Mhammedi, M. A. E.; Bakasse, M.; Chtaini, A. Electrochemical studies and square wave voltammetry of paraquat at natural phosphate modified carbon paste electrode. *J. Hazard. Mater.* **2007**, *145* (1), 1-7. DOI: https://doi.org/10.1016/j.jhazmat.2007.02.054.

(92) Li, J.; Lei, W.; Xu, Y.; Zhang, Y.; Xia, M.; Wang, F. Fabrication of polypyrrole-grafted nitrogen-doped graphene and its application for electrochemical detection of paraquat. *Electrochim. Acta* **2015**, *174*, 464-471. DOI: https://doi.org/10.1016/j.electacta.2015.06.028.

(93) Riahifar, V.; Haghnazari, N.; Keshavarzi, F.; Ahmadi, E. A sensitive voltammetric sensor for methamphetamine determination based on modified glassy carbon electrode using Fe3O4@poly pyrrole core-shell and graphene oxide. *Microchem. J.* **2021**, *170*, 106748. DOI: https://doi.org/10.1016/j.microc.2021.106748.

(94) Zen, J. M.; Senthil Kumar, A.; Chang, M. R. Electrocatalytic oxidation and trace detection of amitrole using a Nafion/lead–ruthenium oxide pyrochlore chemically modified electrode. *Electrochim. Acta* **2000**, *45* (10), 1691-1700. DOI: https://doi.org/10.1016/S0013-4686(99)00327-8.

(95) Mustain, W. E.; Kepler, K.; Prakash, J. CoPdx oxygen reduction electrocatalysts for polymer electrolyte membrane and direct methanol fuel cells. *Electrochim. Acta* **2007**, *52* (5), 2102-2108. DOI: https://doi.org/10.1016/j.electacta.2006.08.020.

(96) El Harmoudi, H.; Achak, M.; Farahi, A.; Lahrich, S.; El Gaini, L.; Abdennouri, M.; Bouzidi, A.; Bakasse, M.; El Mhammedi, M. A. Sensitive determination of paraquat by square wave anodic stripping voltammetry with chitin modified carbon paste electrode. *Talanta* **2013**, *115*, 172-177. DOI: https://doi.org/10.1016/j.talanta.2013.04.002.

(97) Lopes, I. C.; De Souza, D.; Machado, S. A. S.; Tanaka, A. A. Voltammetric detection of paraquat pesticide on a phthalocyanine-based pyrolitic graphite electrode. *Anal. Bioanal. Chem.* **2007**, *388* (8), 1907-1914. DOI: https://doi.org/10.1007/s00216-007-1397-6.

(98) Zhang, H.; Huang, K.-T.; Ding, L.; Yang, J.; Yang, Y.-W.; Liang, F. Electrochemical determination of paraquat using a glassy carbon electrode decorated with pillararene-coated nitrogen-doped carbon dots. *Chin. Chem. Lett.* **2022**, *33* (3), 1537-1540. DOI: https://doi.org/10.1016/j.cclet.2021.09.002.

(99) Zou, T.; He, P.; Cao, J.; Li, Z. Determination of Paraquat in Vegetables Using HPLC–MS-MS. *J. Chromatogr. Sci.* **2014**, *53* (2), 204-209. DOI: https://doi.org/10.1093/chromsci/bmu041.

(100) Ruan, X.-L.; Qiu, J.-J.; Wu, C.; Huang, T.; Meng, R.-B.; Lai, Y.-Q. Magnetic single-walled carbon nanotubes–dispersive solid-phase extraction method combined with liquid chromatography–tandem mass spectrometry for the determination of paraquat in urine. *J. Chromatogr. B* **2014**, *965*, 85-90. DOI: https://doi.org/10.1016/j.jchromb.2014.06.016.

(101) Blake, D. K.; Gallagher, R. T.; Woollen, B. H. Improved methods for the analysis of paraquat in biological fluids. *Chromatographia* **2002**, *55* (S1), S183-S185. DOI: https://doi.org/10.1007/bf02493377.

(102) Lee, X.-P.; Kumazawa, T.; Fujishiro, M.; Hasegawa, C.; Arinobu, T.; Seno, H.; Ishii, A.; Sato, K. Determination of paraquat and diquat in human body fluids by high-performance liquid chromatography/tandem mass spectrometry. *J. Mass Spectrom.* **2004**, *39* (10), 1147-1152. DOI: https://doi.org/10.1002/jms.695.

(103) Wang, K.-C.; Chen, S.-M.; Hsu, J.-F.; Cheng, S.-G.; Lee, C.-K. Simultaneous detection and quantitation of highly water-soluble herbicides in serum using ion-pair liquid chromatography–tandem mass spectrometry. *J. Chromatogr. B* **2008**, *876* (2), 211-218. DOI: https://doi.org/10.1016/j.jchromb.2008.10.042.

(104) Zhou, Q.; Yang, N.; Li, Y.; Ren, B.; Ding, X.; Bian, H.; Yao, X. Total concentrations and sources of heavy metal pollution in global river and lake water bodies from 1972 to 2017. *Global Ecology and Conservation* **2020**, *22*, e00925. DOI: https://doi.org/10.1016/j.gecco.2020.e00925.

(105) Edokpayi, J. N.; Enitan, A. M.; Mutileni, N.; Odiyo, J. O. Evaluation of water quality and human risk assessment due to heavy metals in groundwater around Muledane area of Vhembe District, Limpopo Province, South Africa. *Chemistry Central Journal* **2018**, *12* (1), 2. DOI: https://doi.org/10.1186/s13065-017-0369-y.

(106) Hong, Y. S.; Choi, J. Y.; Nho, E. Y.; Hwang, I. M.; Khan, N.; Jamila, N.; Kim, K. S. Determination of macro, micro and trace elements in citrus fruits by inductively coupled

plasma–optical emission spectrometry (ICP-OES), ICP–mass spectrometry and direct mercury analyzer. *Journal of the Science of Food and Agriculture* **2019**, *99* (4), 1870-1879. DOI: https://doi.org/10.1002/jsfa.9382.

(107) Ashrafi, A. M.; Koudelkova, Z.; Sedlackova, E.; Richtera, L.; Adam, V. Review—Electrochemical Sensors and Biosensors for Determination of Mercury Ions. *Journal of The Electrochemical Society* **2018**, *165* (16), B824. DOI: https://doi.org/10.1149/2.0381816jes.

(108) Akbari Hasanjani, H. R.; Zarei, K. An electrochemical sensor for attomolar determination of mercury(II) using DNA/poly-L-methionine-gold nanoparticles/pencil graphite electrode. *Biosensors and Bioelectronics* **2019**, *128*, 1-8. DOI: https://doi.org/10.1016/j.bios.2018.12.039.

(109) Ngwenya, V.; Nelson, P. N.; Rhyman, L.; Ramasami, P.; Booysen, I. N.; Mambanda, A. Electrocatalytic performance of a nickel(II) phthalocyanine-carbon nanotube composite towards the detection of Hg2+ ions. *Journal of Applied Electrochemistry* **2024**. DOI: https://doi.org/10.1007/s10800-023-02049-w.

(110) Shoba, S.; Mambanda, A.; Booysen, I. N. Electrospun Nanofiber Composite Utilized as an Electrocatalyst for the Detection of Acetaminophen in Multifarious Water Samples. *ACS Omega* **2024**. DOI: https://doi.org/10.1021/acsomega.3c08432.

(111) Yu, S.; Xu, S.; Khan, R.; Zhao, H.; Li, C. Research developments in the application of electrospun nanofibers in direct methanol fuel cells. *Catalysis Science & Technology* **2024**. DOI: https://doi.org/10.1039/d3cy01509b.

(112) Li, X.-Y.; Yan, Y.; Zhang, B.; Bai, T.-J.; Wang, Z.-Z.; He, T.-S. PAN-derived electrospun nanofibers for supercapacitor applications: ongoing approaches and challenges. *Journal of Materials Science* **2021**, *56* (18), 10745-10781. DOI: https://doi.org/10.1007/s10853-021-05939-6.

(113) Mane, P. P.; Ambekar, R. S.; Kandasubramanian, B. Electrospun nanofiber-based cancer sensors: A review. *International Journal of Pharmaceutics* **2020**, *583*, 119364. DOI: https://doi.org/10.1016/j.ijpharm.2020.119364.

(114) Malara, A.; Fotia, A.; Paone, E.; Serrano, G. Electrospun Nanofibers and Electrochemical Techniques for the Detection of Heavy Metal Ions. In *Materials*, 2021; Vol. 14.

(115) Iftikhar, F. J.; Shah, A.; Wali, Q.; Kokab, T. Advancements in Nanofiber-Based Electrochemical Biosensors for Diagnostic Applications. In *Biosensors*, 2023; Vol. 13.

(116) Ragab, H. M.; Rajeh, A. Structural, thermal, optical and conductive properties of PAM/PVA polymer composite doped with Ag nanoparticles for electrochemical application. *Journal of Materials Science: Materials in Electronics* **2020**, *31* (19), 16780-16792. DOI: https://doi.org/10.1007/s10854-020-04233-6.

(117) Liu, Y.; Hao, M.; Chen, Z.; Liu, L.; Liu, Y.; Yang, W.; Ramakrishna, S. A review on recent advances in application of electrospun nanofiber materials as biosensors. *Current Opinion in Biomedical Engineering* **2020**, *13*, 174-189. DOI: https://doi.org/10.1016/j.cobme.2020.02.001.

(118) Jang, J. Conducting Polymer Nanomaterials and Their Applications. In *Emissive Materials Nanomaterials*, Springer Berlin Heidelberg, 2006; pp 189-260.

(119) Jang, J.; Ha, J.; Cho, J. Fabrication of Water-Dispersible Polyaniline-Poly(4-styrenesulfonate) Nanoparticles For Inkjet-Printed Chemical-Sensor Applications. *Advanced Materials* **2007**, *19* (13), 1772-1775. DOI: https://doi.org/10.1002/adma.200602127.

(120) Sapountzi, E.; Braiek, M.; Vocanson, F.; Chateaux, J.-F.; Jaffrezic-Renault, N.; Lagarde, F. Gold nanoparticles assembly on electrospun poly(vinyl alcohol)/poly(ethyleneimine)/glucose oxidase nanofibers for ultrasensitive electrochemical glucose biosensing. *Sensors and Actuators B: Chemical* **2017**, *238*, 392-401. DOI: https://doi.org/10.1016/j.snb.2016.07.062.

(121) Cho, S.; Lee, J. S.; Jun, J.; Kim, S. G.; Jang, J. Fabrication of water-dispersible and highly conductive PSS-doped PANI/graphene nanocomposites using a high-molecular weight PSS dopant and their application in H2S detection. *Nanoscale* **2014**, *6* (24), 15181-15195. DOI: https://doi.org/10.1039/c4nr04413d.

(122) Zhu, H.; Du, M.; Zhang, M.; Wang, P.; Bao, S.; Fu, Y.; Yao, J. Facile and green fabrication of small, mono-disperse and size-controlled noble metal nanoparticles embedded in water-stable polyvinyl alcohol nanofibers: High sensitive, flexible and reliable materials for biosensors. *Sensors and Actuators B: Chemical* **2013**, *185*, 608-619. DOI: https://doi.org/10.1016/j.snb.2013.05.062.

(123) Usman, M.; Adnan, M.; Ahsan, M. T.; Javed, S.; Butt, M. S.; Akram, M. A. In Situ Synthesis of a Polyaniline/ Fe–Ni Codoped Co3O4 Composite for the Electrode Material of Supercapacitors with Improved Cyclic Stability. *ACS Omega* **2021**, *6* (2), 1190-1196. DOI: https://doi.org/10.1021/acsomega.0c04306.

(124) Radhika, G.; Krishnaveni, K.; Subadevi, R.; Sivakumar, M. Investigations On Physical Properties Of Sulfur Based Composite Cathodes In Lithium Sulfur Battery Fabrication. *IRJET Journal* **2017**, 53-57.

(125) Ji, X.; Zou, T.; Gong, H.; Wu, Q.; Qiao, Z.; Wu, W.; Wang, H. Cobalt phthalocyanine nanowires: Growth, crystal structure, and optical properties. *Crystal Research and Technology* **2016**, *51* (2), 154-159. DOI: https://doi.org/10.1002/crat.201500244.

(126) Szybowicz, M.; Bała, W.; Fabisiak, K.; Paprocki, K.; Drozdowski, M. Micro-Raman spectroscopic investigations of cobalt phthalocyanine thin films deposited on quartz and diamond substrates. *Crystal Research and Technology* **2010**, *45* (12), 1265-1271. DOI: https://doi.org/10.1002/crat.201000331.

(127) Braik, M.; Dridi, C.; Ben Ali, M.; Ali, A.; Abbas, M. N.; Errachid, A. Investigation of structural, optical and electrical properties of a new cobalt phthalocyanine thin films with potential applications in perchlorate sensor. *Synthetic Metals* **2015**, *209*, 135-142. DOI: https://doi.org/10.1016/j.synthmet.2015.07.011.

(128) Zhao, J.; Lin, J.; Xiao, J.; Fan, H. Synthesis and electromagnetic, microwave absorbing properties of polyaniline/graphene oxide/Fe3O4 nanocomposites. *RSC Advances* **2015**, *5* (25), 19345-19352. DOI: https://doi.org/10.1039/c4ra12186d.

(129) Joya, K. S.; Ul Ain Babar, N.; Gilani, S. R.; Yasmeen, F.; Sarfaraz, M.; Ikram, S.; Colak, S. G.; Ocakoglu, K.; Ince, M. Heterogeneous Electrocatalysts for Efficient Water Oxidation

Derived from Metal Phthalocyanine. *ChemistrySelect* **2018**, *3* (40), 11357-11366. DOI: https://doi.org/10.1002/slct.201802089.

(130) Turczyn, R.; Krukiewicz, K.; Katunin, A.; Sroka, J.; Sul, P. Fabrication and application of electrically conducting composites for electromagnetic interference shielding of remotely piloted aircraft systems. *Composite Structures* **2020**, *232*, 111498. DOI: https://doi.org/10.1016/j.compstruct.2019.111498.

(131) Magar, H. S.; Hassan, R. Y. A.; Mulchandani, A. Electrochemical Impedance Spectroscopy (EIS): Principles, Construction, and Biosensing Applications. In *Sensors*, 2021; Vol. 21.

(132) B. Oliveira, S. C.; Oliveira-Brett, A. M. Voltammetric and electrochemical impedance spectroscopy characterization of a cathodic and anodic pre-treated boron doped diamond electrode. *Electrochimica Acta* **2010**, *55* (15), 4599-4605. DOI: https://doi.org/10.1016/j.electacta.2010.03.016.

(133) Gorduk, O.; Gencten, M.; Gorduk, S.; Sahin, M.; Sahin, Y. Electrochemical fabrication and supercapacitor performances of metallo phthalocyanine/functionalized-multiwalled carbon nanotube/polyaniline modified hybrid electrode materials. *Journal of Energy Storage* **2021**, *33*, 102049. DOI: https://doi.org/10.1016/j.est.2020.102049.

(134) Bredar, A. R. C.; Chown, A. L.; Burton, A. R.; Farnum, B. H. Electrochemical Impedance Spectroscopy of Metal Oxide Electrodes for Energy Applications. *ACS Applied Energy Materials* **2020**, *3* (1), 66-98. DOI: https://doi.org/10.1021/acsaem.9b01965.

(135) Khene, S.; Moeno, S.; Nyokong, T. Voltammetry and electrochemical impedance spectroscopy of gold electrodes modified with CdTe quantum dots and their conjugates with nickel tetraamino phthalocyanine. *Polyhedron* **2011**, *30* (12), 2162-2170. DOI: https://doi.org/10.1016/j.poly.2011.06.002.

(136) Chen, S.-Y.; Li, Z.; Li, K.; Yu, X.-Q. Small molecular fluorescent probes for the detection of lead, cadmium and mercury ions. *Coordination Chemistry Reviews* **2021**, *429*, 213691. DOI: https://doi.org/10.1016/j.ccr.2020.213691.

(137) Zhang, B.; Suo, Q.; Li, Q.; Zhu, Y.; Gao, X.; Lv, L.; Gao, Y.; Jia, H.; Wang, Y. New Sulfur-Containing Ferrocenylimidazo[4,5-b]pyridines: Multiresponsive Hg2+ Ion

Sensing and Structure-Sensing Correlation. *ChemistrySelect* **2022**, *7* (3), e202103565. DOI: https://doi.org/10.1002/slct.202103565.

(138) Chohan, S.; Booysen, I. N.; Mambanda, A.; Akerman, M. P. Formation, characterization and electrochemical properties of novel tetrasubstituted cobalt phthalocyanines bearing tetrahydropyran, furan and coumarin moieties. *Inorganica Chimica Acta* **2016**, *447*, 183-191. DOI: https://doi.org/10.1016/j.ica.2016.04.021.

(139) Jovanovski, V.; Hrastnik, N. I.; Hočevar, S. B. Copper film electrode for anodic stripping voltammetric determination of trace mercury and lead. *Electrochemistry Communications* **2015**, *57*, 1-4. DOI: https://doi.org/10.1016/j.elecom.2015.04.018.

(140) Caroli, S.; Forte, G.; Iamiceli, A. L.; Lusi, A. Stability of Mercury Dilute Aqueous Solutions: An Open Issue. *Microchemical Journal* **1996**, *54* (4), 418-428. DOI: https://doi.org/10.1006/mchj.1996.0119.

(141) Liang, R.; Wang, Q.; Qin, W. Highly sensitive potentiometric sensor for detection of mercury in Cl−-rich samples. *Sensors and Actuators B: Chemical* **2015**, *208*, 267-272. DOI: https://doi.org/10.1016/j.snb.2014.11.040.

(142) Palanna, M.; Aralekallu, S.; Keshavananda Prabhu, C. P.; Sajjan, V. A.; Mounesh; Sannegowda, L. K. Nanomolar detection of mercury(II) using electropolymerized phthalocyanine film. *Electrochimica Acta* **2021**, *367*, 137519. DOI: https://doi.org/10.1016/j.electacta.2020.137519.

(143) Fomo, G.; Nwaji, N.; Nyokong, T. Low symmetric metallophthalocyanine modified electrode via click chemistry for simultaneous detection of heavy metals. *Journal of Electroanalytical Chemistry* **2018**, *813*, 58-66. DOI: https://doi.org/10.1016/j.jelechem.2018.02.016.

(144) Lu, J.; Zhang, X.; Zhang, X.; Liu, N.; Li, H.; Yu, Z.; Yan, X. Electrochemical sensor for mercuric chloride based on graphene-MnO2 composite as recognition element. *Electrochimica Acta* **2015**, *174*, 221-229. DOI: https://doi.org/10.1016/j.electacta.2015.05.181.

(145) Cesarino, I.; Marino, G.; Matos, J. d. R.; Cavalheiro, É. T. G. Evaluation of a carbon paste electrode modified with organofunctionalised SBA-15 nanostructured silica in the

simultaneous determination of divalent lead, copper and mercury ions. *Talanta* **2008**, *75* (1), 15-21. DOI: https://doi.org/10.1016/j.talanta.2007.06.032.

(146) Deshmukh, M. A.; Celiesiute, R.; Ramanaviciene, A.; Shirsat, M. D.; Ramanavicius, A. EDTA_PANI/SWCNTs nanocomposite modified electrode for electrochemical determination of copper (II), lead (II) and mercury (II) ions. *Electrochimica Acta* **2018**, *259*, 930-938. DOI: https://doi.org/10.1016/j.electacta.2017.10.131.

(147) Lim, H. N.; Nurzulaikha, R.; Harrison, I.; Lim, S. S.; Tan, W. T.; Yeo, M. C. Spherical Tin Oxide, SnO2 Particles Fabricated via Facile Hydrothermal Method for Detection of Mercury (II) Ions. *International Journal of Electrochemical Science* **2011**, *6* (9), 4329-4340. DOI: https://doi.org/10.1016/S1452-3981(23)18331-3.

(148) Silva, M. K. L.; Cesarino, I. Electrochemical sensor based on Sb nanoparticles/reduced graphene oxide for heavy metal determination. *International Journal of Environmental Analytical Chemistry* **2022**, *102* (13), 3109-3123. DOI: https://doi.org/10.1080/03067319.2020.1763973.

(149) Kinuthia, G. K.; Ngure, V.; Beti, D.; Lugalia, R.; Wangila, A.; Kamau, L. Levels of heavy metals in wastewater and soil samples from open drainage channels in Nairobi, Kenya: community health implication. *Sci Rep* **2020**, *10* (1), 8434. DOI: https://doi.org/10.1038/s41598-020-65359-5.

(150) Haghighi, A. S. What effects does water pollution have on human health? *Medical News Today (Brighton, UK)*, 2020. https://www.medicalnewstoday.com/articles/water-pollution-and-human-health (accessed February 2024).

(151) Leonard, A. F. C.; Morris, D.; Schmitt, H.; Gaze, W. H. Natural recreational waters and the risk that exposure to antibiotic resistant bacteria poses to human health. *Current Opinion in Microbiology* **2022**, *65*, 40-46. DOI: https://doi.org/10.1016/j.mib.2021.10.004.

(152) Elumalai, V.; Brindha, K.; Lakshmanan, E. Human Exposure Risk Assessment Due to Heavy Metals in Groundwater by Pollution Index and Multivariate Statistical Methods: A Case Study from South Africa. *Water* **2017**, *9* (4), 234. DOI: https://doi.org/10.3390/w9040234.

(153) Hamukoshi, S.; Mama, N.; Schoeman, S.; Uahengo, V. A facile synthesis of a novel 4-hydroxyl-3-azo coumarin based colorimetric probes for detecting Hg^{2+} and a fluorescence turn-off response of 3CBD to Fe^{3+} in aqueous environment. *RSC Advances* **2023**, *13* (45), 31541-31553. DOI: https://doi.org/10.1039/d3ra04047j.

(154) González-Diéguez, N.; Colina, A.; López-Palacios, J.; Heras, A. Spectroelectrochemistry at Screen-Printed Electrodes: Determination of Dopamine. *Analytical Chemistry* **2012**, *84* (21), 9146-9153. DOI: https://doi.org/10.1021/ac3018444.

(155) Kagilev, A. A.; Gafurov, Z. N.; Kantyukov, A. O.; Mikhailov, I. K.; Yakhvarov, D. G. The power of in situ spectroelectrochemistry for redox study of organometallic and coordination compounds. *Journal of Solid State Electrochemistry* **2023**. DOI: https://doi.org/10.1007/s10008-023-05765-7.

(156) Duan, W.; Gunes, M.; Baldi, A.; Gich, M.; Fernández-Sánchez, C. Compact fluidic electrochemical sensor platform for on-line monitoring of chemical oxygen demand in urban wastewater. *Chemical Engineering Journal* **2022**, *449*, 137837. DOI: https://doi.org/10.1016/j.cej.2022.137837.

(157) Nkhahle, R.; Nyokong, T. Electrochemical Detection of Nitrite on Electrodes Modified by Click Chemistry Using Asymmetrical Co(II) and Mn(III) Phthalocyanines Containing Push-Pull Substituents. *Journal of The Electrochemical Society* **2021**, *168* (11), 117514. DOI: https://doi.org/10.1149/1945-7111/ac377f.

(158) Mgidlana, S.; Sen, P.; Nyokong, T. Dual action of asymmetrical zinc(II) phthalocyanines conjugated to silver tungstate nanoparticles towards photodegradation of tetracycline and inactivation of Staphylococcus aureus bacteria. *Journal of Photochemistry and Photobiology A: Chemistry* **2023**, *437*, 114444. DOI: https://doi.org/10.1016/j.jphotochem.2022.114444.